# X-linked Opitz Syndrome protein, MID1, and its effects on cell adhesion force and protein interactions

Catherine Koto

A dissertation

submitted in partial fulfillment of the

requirements for the degree of

Doctor of Philosophy

University of Washington

2015

Reading Committee:

Nathan J. Sniadecki, Chair

Susan W. Herring

Susan M. Parkhurst

Richard B. Presland

Program Authorized to Offer Degree:

Oral Biology

Catherine Koto

University of Washington

Abstract

# X-linked Opitz Syndrome protein, MID1, and its effects on cell adhesion force and protein interactions

Catherine Koto

Chair of Supervisory Committee:

Nathan J. Sniadecki

X-linked Opitz Syndrome (XLOS), which is caused by loss of function of Midline-1 (MID1), is a disorder characterized by developmental defects along the ventral midline, including hypospadias and cleft lip with or without cleft palate. MID1 is highly expressed in tissues affected in Opitz syndrome, such as orofacial epithelia that are destined to contact and fuse to form the lip. The formation of the lip involves fusion of freely projecting epithelial-covered tissue. The epithelia covering these tissue projections must undergo a complex series of changes in adhesion to facilitate the intact closure of the lip. Disruptions to this process lead to persistence of disjointed tissue projections that manifests as cleft lip with or without cleft palate. Understanding the cellular mechanisms controlling this epithelial behavior will provide insight into the pathologies that arise in XLOS as well as how MID1 may impact cellular adhesion during development. Recent studies not only highlight a role for MID1 in the regulation of cell adhesion, they show that loss of MID1 function can lead to defects in cell adhesion complexes. To this end, this thesis explores the role of MID1 and its

associated proteins in cell adhesion. Work presented here identifies that the MID1 paralog and binding partner, MID2, interacts with Plekstrin Homology Domain Family members 5 and 7 (PLEKHA5 and PLEKHA7). While PLEKHA7 is known to play a role in the regulation of cell-cell junctions, yeast-two hybrid and co-immunoprecipitation assays were used to show that PLEKHA5 also interacts with proteins involved in cell adhesion. To measure cell adhesion forces when MID1 function is disrupted, micropost arrays were used. In cells overexpressing a dominant negative MID1 mutation, cell-cell tugging forces and not cell-ECM traction forces contributed more significantly to decreased cell adhesion. Lastly, in this dissertation, to develop an in vitro model of XLOS, MID1 knockout epithelial cell lines were generated using CRISPR/Cas9 targeted against the N-terminal RING domain of MID1. MID1 wild type and MID1 knockout cell lines generated using this technique displayed phenotypic variability that depended on cell clone rather than specific genotype. However, this work identifies future strategies that will help to generate an in vitro model of XLOS that could be used to study the cellular functions of MID1.

Acknowledgements

The work presented here was made possible by all of those that supported me through this journey. Foremost, I'd like to thank my advisors, Dr. Tim Cox and Dr. Nathan Sniadecki. I am lucky to have been given the opportunity to work on an exciting project with two mentors from whom I have learned a great deal. I'd like to give special acknowledgement to Dr. Cox. Without his support, guidance, hard work, and time, this thesis would not have been possible. I am also especially grateful for Dr. Sniadecki. I am so lucky to have been welcomed into his lab to learn about cell mechanics; without Dr. Sniadecki's enthusiasm, scientific guidance, feedback, and support as a mentor I would have struggled to finish.

I am also incredibly thankful for the time, energy, feedback and given by the members of my committee, Dr. Richard Presland, Dr. Sue Herring, Dr. Susan Parkhurst, and Dr. Avina Paranjpe. I would like to give special appreciation to Dr. Presland for the opportunity to work and learn as a teaching assistant in his class, and additionally would like to thank him for the immeasurable amount of support he has contributed this thesis.

I am also incredibly appreciative of all of the amazing co-workers that have helped with useful suggestions, discussion, and feedback. I would like to give distinct gratitude for Yongzhao Huang. Not only is this work and offshoot of her research, but also, her guidance, knowledge, and friendship contributed significantly to the work presented here.

Beyond my lab mates, I am thankful for all the helpful discussion I've received from other scientist including Jamie Keck, Babette Saltzman, and future scientist Sarah Park. At home, I am supported by and would like to acknowledge my patient and encouraging partner, Erik Koto.

Table of Contents

List of Figures

Abbreviations

BME: 2-mercaptoethanol

bp: base pairs

BSA: bovine serum albumin

CIP: alkaline phosphatase, calf intestinal (New England Biolabs)

$CO_2$: carbon dioxide

CRISPR: clustered regularly interspaced short palindromic repeats

DMEM: Dulbecco's modified Eagle's medium

DMSO: dimethylsulfoxide

DNA: deoxyribonucleic acid

dNTP: deoxyribonucleoside triphosphate

DTT: dithiothreitol

EDTA: ethylene-diamine-tetra-acetic acid

FACS: fluorescence-activated cell sorting

FBS: fetal bovine serum

GFP: green fluorescent protein

HRP: horseradish peroxidase

IPTG: isopropyl β-D-thiogalactopyranoside

kDa: kilo Daltons

LB: Luria broth

MDCK: Madin-Darby canine kidney (cells)

mRNA: messenger RNA

nm: nanometers

NGS: normal goat serum

PBS: phosphate buffered saline

PBS-T: phosphate buffered saline with 0.1% Tween-20

PCR: polymerase chain reaction

PDMS: polydimethylsiloxane

PVDF: polyvinylidene difluoride

rpm: revolutions per min

RT: room temperature

SDS: sodium dodecyl sulphate

Silane: (tridecafluoro-1)-1,1,2,2,-tetrahydro-octyl)-1-trichlorosilane

TBS: tris buffered saline

TBS-T: tris buffered saline with 0.1% Tween-20

TE: tris-EDTA buffer

UV: ultraviolet light

V: volts

v/v: volume per volume

w/v: weight per volume

XLOS: X-linked Opitz syndrome

Y2H: yeast two-hybrid

Table 1: List of Primers

| Primer | Primer Sequence ( 5'-3)' |
|---|---|
| hPLEKHA7-stop | CATGCTGGGTCACGGGTCAGTC |
| hPLEKHA7-start | TCGGCGAACATGGCGGCGGCGA |
| hPLEKHA7-r2 | GCGAGGAAGCGTCTGGTCCAAG |
| hPLKEHA7-r1 | GTCCTCTGGGCTGTAGAGTTCG |
| hPLEKHA7-f2 | GGAATGCTGCCTGCCTCATATG |
| hPLEKHA7-f1 | CTGAAGCAGACCCTGCAGGAGC |
| hPLEKHA7-r3 | GAGGTAGCGAGATGAGGGCAGG |
| hPLEKHA7-f3 | CGAGAGCGCAAGAGGACACTGG |
| hPLEKHA7fixF | GATTCCAGGGTGGAGCTGCGGTCGTATGTCAGTGAG |
| hPLEKHA7fixR | CTGACATACGACCGCAGCTCCACCCTGGAATCCCCATTC |
| hPLEKHA6-stop | CTCAGACCCGCATGGTATAGCTG |
| hPLEKHA6-start | GAGATGGCCGATGAGATTGACTG |
| hPLEKHA6-r2 | CACGCGGATGTTGATGAGCTGG |
| hPLKEHA6-r1 | GGCTGATGTTGTCTGAGGGCTG |
| hPLEKHA6-f2 | ATGAGGCGATCCATCAGCTCC |
| hPLEKHA6-f1 | GCAACTCGCACAGCCCGCAAAG |
| hPLEKHA6-r3 | GCCTTGGTGACAGGTGCATTGG |
| | |
| hPLEKHA5-772f | CTGAGTAAACATAAGCAGCAAAG |
| hPLEKHA5-674r | TTAGCTGGCTGATAGCAAAGCTTG |
| hPLEKHA5-615f | ACGCTGTCACAAGATGAAGGTAG |
| hPLEKHA5-449f | CAGATTATGGCCCGCTACCCTG |
| hPLEKHA5-SiahMutR | ACCTCGTCTGACACCCGGTCCATTAGGATTCCTTTTAATTGAATTTG |
| hPLEKHA5-SiahMutF | AGGAATCCTAATGGACCGGGTGTCAGACGAGGTTGGCTTTATAAAC |
| PEPP2B-Kpn | GGGGTACCCTACACACACATGAAATGTGATCC |
| PEPP2F-v2 | CAGTCGACCATGGCGGCGGATCTAAAC |
| | |
| mPisp-start2 | GAAATGGACAACCGGATTCCC |
| mPisp-stop | CAAGTCTCTAGTGCACAGTCC |
| mSiah1a-start2 | ATGAGCCGCCAGACTGCTACAG |
| mSiah1b-start2 | ATGAGCCGTCAGGCTGCTACAG |
| mSiah1a/b-stop | GATTGCCGTTTCAACACATGG |
| mSiah2-start2 | ATGAGCCGCCCGTCCTCCAC |
| mSiah2-stop | GAGCCTCACTGACAGCATGTAG |
| mTrp53bp2-start2 | ATGCGGTTCGGGTCCAAAATGATG |
| mTrp53bp2stop | GTTTCAGGCCAAGCTCCTTTGTCTTGG |

| Primer | Primer Sequence ( 5'-3)' |
|---|---|
| MID2L146Q Mutant Construct | |
| h MID2 start | CTAAAGATGGAAACACTGGAGTC |
| hMID2-L146Qrev | GGTGCGTGGCCCGCTGGCAACGGTCACAG |
| hMID2-L146Qfor | CTGTGACCGTTGCCAGCGGGCCACGCACC |
| hMID2STOP | CTTAATGACAGGTTTTCATCCC |
| | |
| MID2-RFCC1 Construct | |
| HMID2-F | |
| GW2 (Invitrogen) | GTTGCAACAAATTGATGAGCAATTA |
| HM-MID6 (for sequencing) | |
| | |
| CRISPR | |
| he-cadREV | GCTGAGATTCAGTCCCAGACG |
| he-cadFWD | TGAGAAAGAAATCAGAGCACAAGG |
| he-cad(231)top | CACCGCACTTTGAATCGGGTGTCGA |
| he-cad(231)bottom | AAACTCGACACCCGATTCAAAGTGC |
| he-cad(173)top | CACCGAAGATTGCACCGGTCGACAA |
| he-cad(173)bottom | AAACTTGTCGACCGGTGCAATCTTC |
| dMID1 sgRNA Rev | CCCACTCACTGACGCTTTCT |
| dMID1 sgRNA Fwd | TGAGGACCCTCTCCTGCTAC |
| dMID1ex1R | CCCACTCACTGACGCTTTCT |
| dMID1ex1F | TGAGGACCCTCTCCTGCTAC |
| dMID1(134b)rev | CCCTCACCTTGACAACGCTA |
| dMID1(134b)fwd | GCGCCTAATCAGATCTCCCG |
| de-cadREV | ACAGTGTCCATGCTCTCACC |
| de-cadFWD | GACCACAATGGACAGTCCCTCTA |
| decad(271)top | CACCGTCAGAAACATAGGCTGTCCT |
| decad(271)bottom | AAACAGGACAGCCTATGTTTCTGAC |
| MID1 (134) Top | CACCGATGGACTCCACAGACTCGT |
| MID1 (134) Bottom | AAACACGAGTCTGTGGAGTCCATC |
| | |
| QPCR | |
| dRPS5rev | CCTGATTCACACGGCGTAG |
| dRPS5fwd | TCACTGGTGAGAACCCCCT |

## Chapter 1: Introduction

Regulation of epithelial adhesion is critical during embryonic development. The dynamic regulation of epithelial cell-cell adhesion allow tissues to respond to external cues in a coordinated manner, as well as undergo morphogenesis under tension to promote tissue growth and repair. Disruptions to cellular adhesion can therefore result in developmental pathologies such as cleft lip and palate (Cox, 2004). In the formation of the lip and palate, the regulation of epithelial behavior is thought to be under tight control as stereotypical morphological changes occur while the facial processes converge to form the lip and palate (Figure 1.1). When

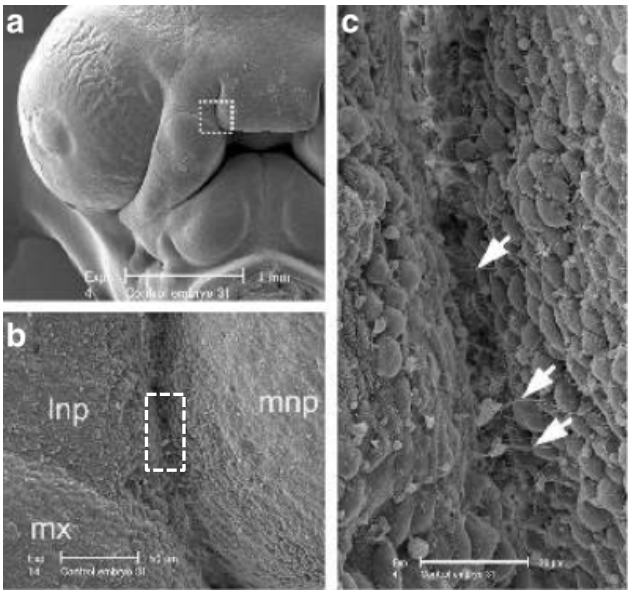


**Figure 1.1**. **Formation of lip and primary palate**. Image of facial development in the chick embryo from Cox, Clin. Genet. 2004. Panels highlight that cell-cell adhesion is dynamic at this time in development. A. Prior to fusion, the lip and primary palate are formed by the fusion of freely projecting facial processes. B. and C. Successive magnification at the site of fusion of the maxillary (mx) process, lateral nasal process (lnp), and medial nasal process (mnp). Image highlights changes in the prefusion epithelia where cells bulge as they lose cell-cell adhesions and form projections to adhere to opposing processes.

facial processes enlarge, the epithelia must also grow, but at the same time maintain cell-cell connections, which coordinate the growth of both the epithelium and underlying mesenchyme (Cox, 2004; Mossey et al., 2009). Then, as the facial processes approach each other, those epithelial cells destined to make contact (the pre-fusion contact zone epithelia) begin to bulge by weakening connections with adjacent cells (Figure 1.1). This process is thought to facilitate these epithelia becoming apically adhesive in preparation for fusion (Cox 2004). Fusion is then characterized by contralateral epithelial cells adhering to each other to form an epithelial seam between the processes. Through highly coordinated cell signaling events involving remodeling of cell-cell junctions, this seam disperses, possibly through a combination of radial movement, apoptosis and epithelial to mesenchymal transitioning, to enable replacement by a confluent layer of mesenchyme (Cox 2004). The goal of this thesis is to study how disruptions to the regulation of epithelial adhesion during this time in development might lead to pathologies such as cleft lip and palate. Specifically this project will address the role of *Midline-1* (*MID1*), a gene linked to cleft lip and palate, in the regulation of cell adhesion.

Opitz Syndrome

Optiz G/BBB syndrome is a congenital disorder that primarily affects ventral midline development. As such, patients with Opitz syndrome most commonly present with ocular hypertelorism and hypospadias (De Falco et al., 2003; Meroni, 2004). Additionally, patients may present with other ventral midline anomalies such as a broad nasal bridge, laryngotracho-esophageal defects, and cleft lip and/or

palate (De Falco et al., 2003; Meroni, 2004). Less common patient defects include imperforate anus, congenital heart malformations, developmental delays, and brain anomalies (De Falco et al., 2003; Meroni, 2004). Ventral midline defects found in X-linked Opitz syndrome have a common embryologic origin. During embryogenesis, structures of the ventral midline form from tissue outgrowth induced by the immigration of neural crest cells as well as epithelial-mesenchymal transition and programmed cell death that regulate the fusion of structures that form the ventral midline. Opitz G/BBB syndrome has both an autosomal dominant and a X-linked mode of inheritance, and the two are clinically indistinguishable (Robin et al., 1995). The autosomal locus is linked to 22q11.2 (Robin et al., 1995), whereas the X-linked form is associated with mutations in the MID1 gene at chromosome Xp22.2 (Quaderi et al., 1997).

MID1 Background

X-linked Opitz syndrome (XLOS) is caused by the loss of function of Midline-1 (MID1) (Cox et al., 2000). MID1 is a microtubule binding protein (Figure 1.2) that promotes microtubule stabilization (Berti et al., 2004; Cainarca et al., 1999; Schweiger et al., 1999; Short et al., 2006). Incidentally, the autosomal dominant form of Opitz G/BBB syndrome has been linked to SPECC1L (Sperm Antigen with Calponin Homology and Coiled-Coil Domains 1), a cytoskeletal protein that like MID1, binds to microtubules (Kruszka et al., 2015; Saadi et al., 2011). In the cell, SPECC1L stabilizes microtubules and it is believed to play a role in integrin mediated cell migration (Kruszka et al., 2015; Saadi et al., 2011). The association of

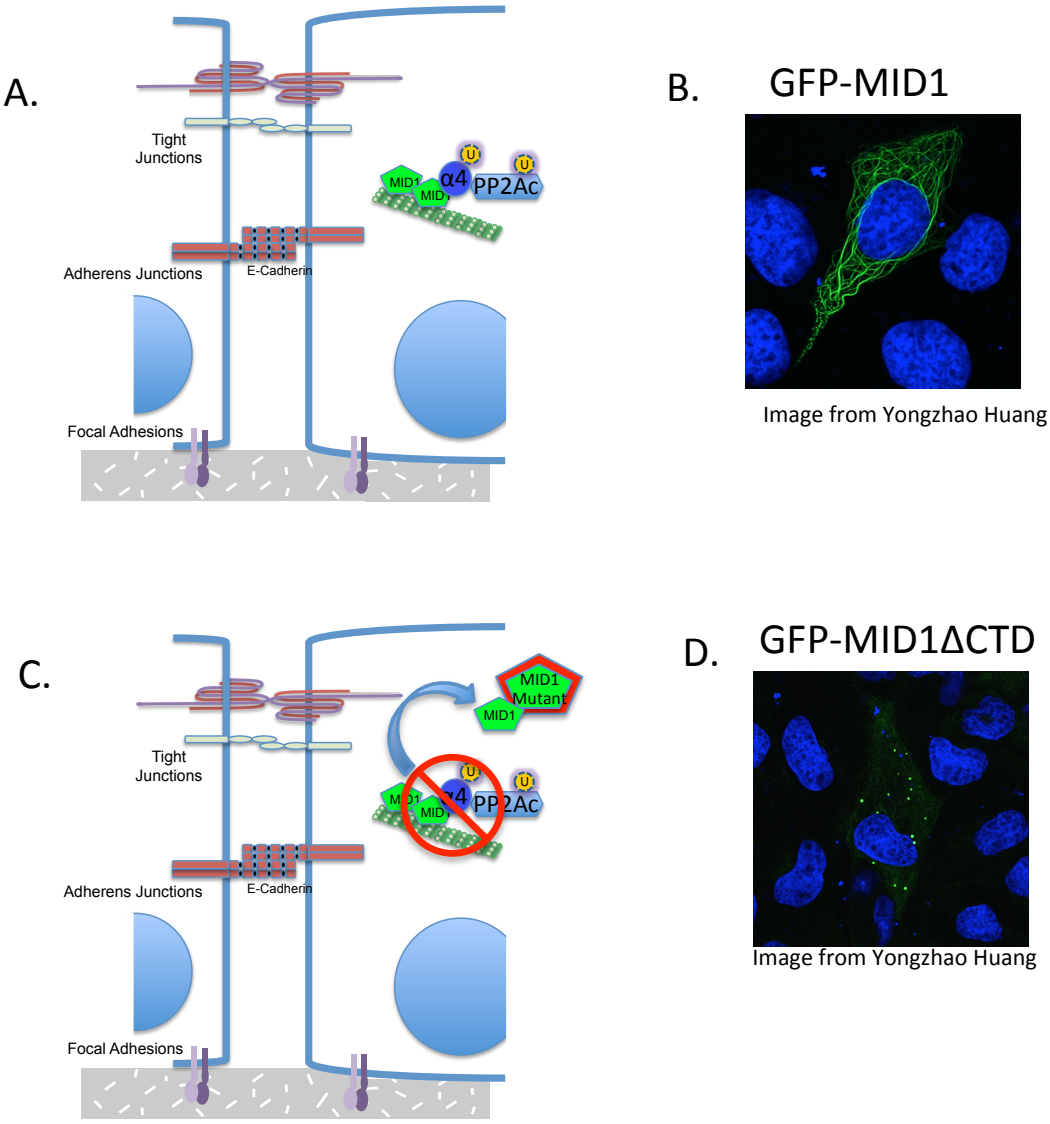


**Figure 1.2. MID1 binds microtubules and loss of MID1 function can disrupt its regulation of alpha4/PP2Ac as well as its localization along microtubules.** **A.** Cartoon showing MID1 binds microtubules and is thought to regulate alpha4/PP2Ac at this localization. **B.** Overexpression of GFP labeled MID1 shows distribution along microtubules (Image by Yongzhao Huang) **C.** Cartoon showing that loss of MID1 function can impact is localization as well regulation of alpha4/PP2Ac complex **D.** Overexpression of dominant negative MID1 construct, GFP-MID1ΔCTD, results in aggregates of mutant protein (Image by Yongzhao Huang).

MID1 with microtubules has been shown to be dependent on its phosphorylation, which is regulated by its association with alpha4 (Liu et al., 2001). Not only does MID1 binding to alpha4 affect its microtubule localization, but also, studies show

that the MID1/alpha4protein complex plays a key role in XLOS pathogenesis (Schweiger et al., 2003) (Figure 1.2). At its N-terminus, alpha4 binds to PP2Ac, the regulatory subunit of the important serine/threonine phosphatase PP2A, and at its C-terminus, alpha4 binds to MID1 (Liu et al., 2001). This heterotrimeric complex not only regulates MID1 association with microtubules (J. Liu et al., 2001), but it has also been shown that MID1 possesses E3 ubiquitin ligase activity that can target both alpha4 (Du et al., 2013; Han et al., 2011; Watkins et al., 2012) and PP2Ac (Boding et al., 2014; E. Liu et al., 2011; Trockenbacher et al., 2001) for proteasomal degradation (Figure 1.2A). As a result, mutations in MID1 are thought to elevate phosphatase activity of PP2A, and in support of this, an increase in microtubule associated proteins with low levels of phosporylation have been observed in XLOS patient fibroblasts (Trockenbacher et al., 2001). Moreover, the MID1-alpha4-PP2Ac complex has been shown to impact signaling in the mammalian Target of Rapamycin kinase complex 1 (mTORC1) pathway (Liu et al., 2011), which is a major regulatory pathway affecting epithelial cell-cell adhesion and nutrient-sensitive cell growth (Zoncu et al., 2011).

Loss of MID1 function leads to defects in epithelial morphology and adhesion.

Data in our lab demonstrate that adhesion defects occur in epithelia cells expressing a dominant negative, mutant MID1 protein termed MID1ΔCTD (Huang and Cox, unpublished data) (Figure 1.2D). Specifically, Mandin Darby canine kidney (MDCK) cells stably expressing MID1ΔCTD exhibit decreased activation of Rac1, a regulator of epithelial adhesion (Huang and Cox, unpublished data). Also, in polarized MDCKs, E-cadherin organization at the membrane is specifically disrupted

in cells expressing MID1ΔCTD ( Huang and Cox, unpublished data). In migration assays on a laminin substrate, MDCK cells, overexpressing dominant negative MID1ΔCTD protein, lose cell-cell contacts and as a result fail to migrate collectively (Huang and Cox, unpublished data). Similarly, in an adhesion assay, MID1ΔCTD expressing cells show decreased attachment to laminin, a phenomenon often seen following disruption of intercellular epithelial adhesion (Huang and Cox, unpublished data). Studies in which MID1 expression has been knocked down also support its role in regulation of epithelial adhesion. In Xenopus, knockdown of both MID1 and its paralog and binding partner Midline 2 (MID2), disrupted neuroepithelial adhesion and polarity as evidenced by abnormal cellular morphology, loss of basal lamina attachment, and disappearance of the apical actin adhesion belt (Suzuki et al., 2010). More recently, MID1 has been found to be necessary for polarized responses in cytotoxic T lymphocytes, which control exocytosis of lytic granules (Boding, Hansen, Meroni, et al., 2014), and moreover, when MID1 is knocked out in mice, *MID2* expression increases and plays a redundant role in the release of lytic granules in these cells (Boding et al., 2015). MID2, a binding partner of MID1, is structurally and functionally similar to MID1 but specifically interacts with proteins known to regulate epithelial adhesion.

To date, the majority of MID studies have focused on MID1, not MID2, although it is widely accepted that they play partially redundant roles (Boding et al., 2015; Buchner et al., 1999; Granata et al., 2005; Short et al., 2002; Suzuki et al., 2010). The MID1/2 proteins share 76% amino acid identity and 83% similarity (Buchner et al., 1999; Perry et al., 1999) (Figure 1.3). MID1 and MID2 also have overlapping

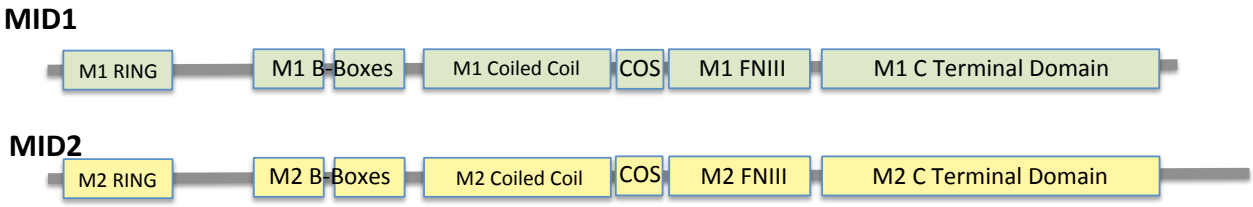


**Figure 1.3. MID1 and MID2 protein domains**. MID2 is structurally identical to MID1 and shares 76% amino acid identity and 83% similarity to MID1 (Buchner et al., 1999 and Perry et al., 1999).

expression patterns; both are expressed in pre-fusion facial epithelia (Buchner et al. 1999). In the developing chick, L/R asymmetry defects caused by knockdown of both MID proteins can be rescued by either MID1 or MID2 (Granata et al., 2003). In addition MID2, like MID1, binds to, and is thought to regulate the alpha4/PP2Ac complex (Short et al., 2002). Importantly, in Opitz syndrome, mutant MID1 loses its normal microtubule distribution and frequently forms cytoplasmic aggregates that also disrupt the normal distribution of MID2 (Short et al. 2002). Also, in skin fibroblasts derived from patients with Opitz syndrome, ectopically expressed wildtype MID2 is also directed to aggregates formed by endogenous mutant MID1 (Cox lab, unpublished data). Thus, mutant MID1 acts in a dominant negative manner to disrupt endogenous MID2 function (Short et al. 2002). The downstream consequences of MID2 mislocalization have not been determined, nor has a unique cellular role for MID2 been established. However, data from the Cox lab indicates that MID2 may also account for changes in epithelial adhesion observed in cells expressing mutant MID1. Specifically, work started by Yi Zou (Zou Y, 2004) and

research presented in this thesis identify plekstrin homology (PH) domain family members 5 and 7 (PLEKHA5 and PLEKHA7) as protein binding partners of MID2, but not MID1 (Zou, 2004) (Figure 1.4). Plekstrin homology domains are a common protein motif found in proteins with a wide range in function such as cellular signaling, membrane trafficking, and cytoskeletal reorganization, (Lemmon et al., 2002; Lander et al., 2001). PH domains can bind to phosphatidylinositol lipids, where they can may be involved in targeting of the protein to a membrane localization and signal transduction pathways (Scheffzek et al., 2012). While PLEKHA5 is implicated in controlling cell motility (Zou, 2004), PLEKHA7 has been shown to regulate cell-cell adhesion at adherens junctions (Meng et al., 2008) and promote tight junction maturation (Kurita et al., 2013; Meng et al., 2008; Pulimeno et al., 2011).

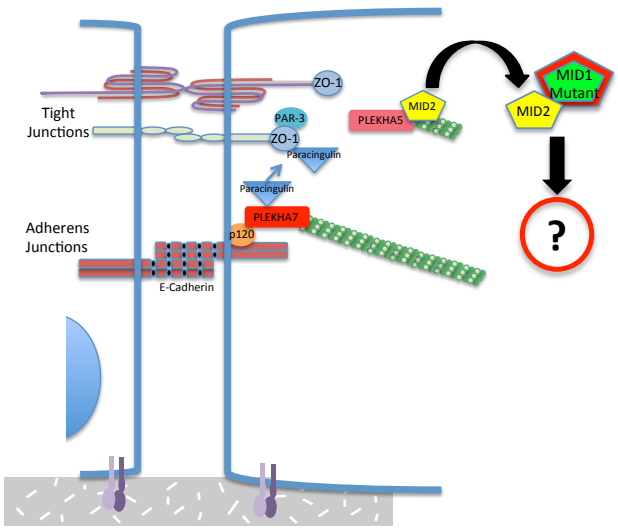


**Figure 1.4. Hypothesis: Loss of MID1 function can disrupt the normal localization of MID2 and consequently impact MID2 interactions in the cell**. MID2 has been shown to bind to PLEKHA5, a protein closely related to PLEKHA7, a known regulator of cell-cell adhesion.

Structure of MID1 and MID2.

MID1 (also known as FXY and TRIM18) and MID2 (also known as FXY2 and TRIM1) are both located on the X-chromosome. It is believed that MID1 and MID2 arose as a result of a gene duplication event in an early vertebrate ancestor; consequently, they share structural and functional characteristics (Buchner et al., 1999; Perry et al., 1998; Perry et al., 1999). While loss of MID1 function causes X-linked Opitz syndrome, Opitz patients present with highly variable phenotypes, and it is believed that the variation in Opitz presentation may be partially attributed to MID2 given its high degree of similarity and functional overlap with that of MID1 (Cox et al.,2000, Short et al., 2002, Granata et al., 2005, Suzuki et al., 2010, Bonding et al., 2015). The MID1 and MID2 protein domains are depicted in Figure 1.3. Both MID1 and MID2 are members of the C-I subclass of the TRIM/RBCC (TRI-partite motif/RING finger, B-box, coiled-coil domain) family of proteins (Buchner et al., 1999; Perry et al., 1999; Quaderi et al., 1997; Short and Cox, 2006). This subclass of TRIM/RBCC proteins possess a RING domain, two B-boxes, a coiled-coil region, a COS box, a fibronectin type III motif, and a C-terminal SPRY or B30.2-like domain (Cox, 2012).

RING domains are highly conserved, and a majority, including the domain in MID1 and MID2, exhibits E3 ubiquitin ligase activity (Budhidarmo et al., 2012; Deshaies and Joazeiro, 2009; Du et al., 2013; Napolitano et al., 2011; Trockenbacher et al., 2001; Watkins et al., 2012, Du et al., 2013, Du et al., 2014). E3 ubiquitin ligases confer specificity to the ubiquitin system by binding specific target substrates and facilitating the transfer of ubiquitin to its bound substrate. Ubiquitin modification is best known for its role in proteasomal degradation, but can also affect endocytosis, protein

localization, folding, and activity (Budhidarmo et al., 2012; Deshaies and Joazeiro, 2009). The MID1 RING domain catalyzes the monubiquitination of alpha4 (Du et al., 2013) and PP2Ac (Du et al., 2014). Tandem B-box domains lie adjacent to the RING domain lie, and they contribute to MID1 E3 ubiquitin ligase activity. B-box 1 of both MID1 and MID2 binds to alpha4 (also known as IGBP1), an important regulator of the serine-threonine phosphatase PP2A (Kong et al., 2009; Short et al., 2002; Trockenbacher et al., 2001). B-box 1 in tandem with the RING domain of MID1 has been shown to promote ubiquitin elongation of both PP2Ac as well as alpha4 (Du et al., 2013; Du et al., 2014).

The coiled-coil domain of MID1 and MID2 mediates protein interactions, and as such is required for the homo- and hetero-dimerization of MID1 and MID2 (Short et al., 2002). The MID coiled-coil domain also binds to MIG12, an interaction that promotes microtubule stability (Berti et al., 2004; Suzuki et al., 2010). Adjacent to the coiled-coil domain, the cos box (C-terminal subgroup one signature) was identified as the domain responsible for microtubule localization of the MID proteins (Short et al., 2006). No specific function has yet been attributed to the C-terminal domain. However while mutations in MID1 that result in X-linked Opitz occur throughout the length of the gene, many patient mutations are clustered within the C-terminal domain (Cox et al., 2000; Gaudenz et al., 1998).

Mutations found in the C-terminal domain result in a MID1 protein that no longer localizes along the length of the microtubule, but instead forms abnormal aggregates in the cytoplasm (Cox et al., 2000; Quaderi et al., 1997). Exogenous

expression of a mutant MID1 with a C-terminal deletion, MID1ΔCTD, mimics the mutant MID1 present in Opitz patient cells, which forms aggregates and acts in a dominant negative manner to affect both the function and localization of endogenous MID1 and MID2 (Du et al., 2013; Short et al., 2002) (Figure 1.2D).

Cell force when MID1 function is lost is unknown

Recent studies reveal that MID1 is involved in the regulation of epithelial cell adhesion (Huang and Cox, unpublished data; Suzuki et al., 2010), but how XLOS pathology arises from changes in epithelial adhesion remains unclear. Studies in mechanobiology demonstrate how forces in cell adhesion underlie developmental processes (Chen et al., 2004; Eyckmans et al. , 2011; Farge, 2011). Specifically, the dynamic regulation of cell adhesion allows tissues to respond to external cues in a coordinated manner as well as undergo morphogenesis under tension to promote tissue growth and repair. Cells connect to their external environment through transmembrane proteins such as integrins, which link cells to their extracellular matrix, or cadherins, which form connections between cells. Through these connections cells sense and transmit force. For instance, E-cadherin, a protein important for cell-cell junctions, has been linked to the transmission of force to the actin cytoskeleton, which can then trigger cellular responses through GTPase signaling pathways that impact cell behavior (le Duc et al., 2010; Liu et al., 2010). In other studies, the application of forces on cells can cause cytoskeletal reorganization and lead to transcriptional activation of genes involved in developmental patterning (Desprat et al., 2008; Weber et al., 2012). While it is known that components of cell

adhesion are disrupted when MID1 is lost, it is not yet known how these changes impact cellular forces.

This thesis quantifies changes in force that occur when MID1 is mutated. Additionally, protein-binding partners of MID1 and MID2 complex were evaluated to identify protein interactions that may contribute to force defects in cells where MID1 function is disrupted. Ultimately, work presented here gives insight into mechanisms that underlie Opitz pathology as well as cleft lip and palate malformations. **Hypothesis: MID1 loss of function can impact cell adhesion forces, and moreover the MID1 protein binding partner and paralog, MID2, may interact with proteins that contribute to regulation of cell adhesion.**

Specific Aims

**AIM1: Examine MID2 interactions with PLEKHA5, PLEKHA7, and Alpha4.**

Strategy: Yeast-two hybrid, co-localization, and co-immunoprecipitation assays were utilized to analyze MID2 binding to PLEKHA5 and PLEKHA7. To determine if alpha4 levels are affected by overexpression of MID2, a mutation was introduced in the B-box 1 domain of MID2 that disrupted its binding to alpha4. Western blot analysis was used to quantify alpha4 levels in the presence of overexpressed wild type and mutant MID2.

**AIM2: Measure cell traction and cell tugging forces in GFP-MID1ΔCTD cells.**

Strategy: Epithelial cells expressing a dominant negative MID1 mutation , GFP-MID1ΔCTD (generated by Huang and Cox, unpublished results) were seeded onto microposts. Cells were fixed and cell-ECM traction force and cell-cell tugging forces were measured in paired cells.

**Aim3: Knockout MID1 in epithelial cells to generate an accurate cell model of XLOS .**

Strategy: CRISPR/Cas9 technology was used to target the first coding exon of MID1. Clones were sequenced for indel mutations and clones that resulted in premature stop codons. The cell clones were also characterized morphologically and biochemically.

## Chapter 2: Role of MID2

### Introduction

Mutant MID1 exerts dominant negative effect on MID2

X-linked Opitz Syndrome (XLOS) is caused by the loss of function of the Midline-1 protein, MID1 (Cox et al., 2000). MID1 mutations that result in X-Opitz syndrome have been identified throughout the length of the gene (except the RING domain), and many types of mutations ranging from missense and nonsense mutations to whole gene deletions and duplications, have been found (Cox et al., 2000; De Falco et al., 2003; Fontanella et al., 2008; Gaudenz et al., 1998; Migliore et al., 2013; So et al., 2005). In general, the MID1 genotype does not correlate to phenotypic presentation (Migliore et al., 2013). Even sanguineous patients, harboring the same MID mutation, can present with variable clinical features (De Falco et al., 2003). It is not yet known what factors contribute to this wide range in clinical presentation, however it has long been suggested that MID2 may play a role in Opitz pathology (Granata et al., 2005; Short et al., 2002). As the paralog and protein binding partner of MID1, not only has MID2 been shown to possess overlapping functions to that of MID1, but also mutant MID1 can bind MID2 in a dominant negative manner, and thereby relocate MID2 from its normal distribution along the microtubules to cytoplasmic clusters instead (Short et al., 2002). To date, the consequence of this mislocalization of MID2 is unknown. Thus, the aim of this chapter was to elucidate the cellular role for MID2, which should ultimately help to clarify how MID2 may contribute to Opitz syndrome pathology.

MID1 and MID2 are similar in structure and function

MID1 and MID2 exhibit a high degree of structural and functional overlap (Boding et al., 2015; Buchner et al., 1999; Granata et al., 2005; Perry et al., 1999; Short et al., 2002; Suzuki et al., 2010). Structurally, extensive homology exists between *MID1 and MID2* (see Figure 1.3); both genes share 76% identity, possessing 9 coding exons of similar size and splice junction locations (Buchner et al., 1999; Perry et al., 1999). Moreover, both genes, which share 83% amino acid similarity, code for proteins with identical domains and organization (Buchner et al., 1999; Perry et al., 1999). Recent studies identify a role for MID1 in the regulation of microtubule stabilization, cell adhesion, and polarization (Berti et al., 2004; Boding, Hansen et al., 2014; Huang and Cox., unpublished; Suzuki et al., 2010), and MID2 has similar cellular functions that likely contribute to this role (Suzuki et al. 2010; Boding et al. 2015). In fact, functionally, studies demonstrate redundant roles for MID1 and MID2. MID2, like MID1, binds and is thought to regulate Alpha4, an important regulator of the phosphatase PP2A (Short et al., 2002). In the developing chick embryo, defects in L/R body axis are observed when both MID1 and MID2 are knocked out, and importantly, overexpression of either MID1 or MID2 can rescue the L/R asymmetry defects (Granata et al., 2003). In the developing neural tube of Xenopus, MID1 and MID2 stabilize microtubules, which impacts neuroepithelial morphology, polarity, and ultimately neural tube closure (Suzuki et al., 2010). In cytotoxic T-cells, both MID1 and MID2 facilitate the exocytosis of lytic granules to targeted cells, and when MID1 is knocked out, MID2 is upregulated to compensate for the loss of MID1 (Boding et al., 2015).

MID2 identity is not always shared by MID1

While studies support the notion that MID2 can compensate for MID1 loss of function, specific role(s) for MID2 are largely unknown. However, it has been shown that differences between MID1 and MID2 exist. In the developing mouse, *Mid2*, unlike *Mid1*, is not ubiquitously expressed and its expression tends to be at much lower levels than that of *Mid1* (Buchner et al., 1999). In addition, while *Mid1* expression in the heart is not detected in the mouse embryo (Buchner et al., 1999) or limited to weak expression detected only in the interventricular septum of the developing human heart (Pinson et al., 2004), *Mid2* transcripts are highly expressed in the developing heart (Buchner et al., 1999). More recently, a mutation in the microtubule binding domain of MID2 has been identified as the causal mutation for a family with X-linked Intellectual Disability (Geetha et al., 2014). The goal of this chapter is to identify the cellular role of MID2. This chapter confirms and explores MID2 binding to plekstrin homology domain family member 5 (PLEKHA5) and identifies a new MID2 binding partner, plekstrin homology domain family member 7 (PLEHA7). Interestingly, both PLEKHA5 and PLEKHA7 unite the MID1/ MID2 protein complex with the regulation of cell adhesion complexes. In addition, this chapter explores the binding of MID2 to alpha4.

## Materials and Methods

PLEKHA5, PLEKHA6 and PLEKHA7 constructs

Partial PLEKHA6 and PLEKHA7 clones were obtained from DNASU and Thermoscientific, respectively. Sequence specific primers were used to amplify partial sequences of PLEKHA7 (hPLEKHA7-start and hPLEKHA7-r3) and PLEKHA6

(hPLEKHA6-f1 and hPLEKHA6-stop). The missing sequences were synthesized and amplified using primers PLEKHA7-f3 and hPLEKHA7-stop to amplify the 3'region of PLEKHA7, and primers hPLEKHA6-start and hPLEKHA6-r3 to amplify the 5' region of PLEKHA6. To generate full-length clones, overlap extension PCR was performed. Full-length clones were incubated with Taq polymerase at 72˚C for 10 minutes to introduce 3' adenine to PCR amplifications and subsequently cloned into pCR8/GW/TOPO TA cloning vector (Invitrogen). Sequence orientation was determined by restriction digest. Full-length clones were verified by Sanger sequencing. PLEKHA5 was previously cloned in our lab (Zou, 2004).

PLEKHA5 interactors

Full length clones of mouse Siah1a, Siah1b, Siah2, PISP and TP53BP2 were previously cloned into pCR8/GW/TOPO TA vectors by Tim Cox and Brian Kellert, however, all clones were missing 1 base pair at the 5' end which rendered them incompatible with the Gateway cloning system (Invitrogen). Sequence specific primers (listed in Table 1) were ordered to amplify full length clones using high-fidelity polymerase and 3' adenine was added following amplification using Taq polymerase. PCR products were gel purified and cloned into pCR8/GW/TOPO TA (Invitrogen). Sequence orientation was determined by restriction digest and full-length clones were verified by Sanger sequencing.

Gateway Cloning

To generate protein expression constructs for use in yeast-two hybrid assays as well as protein expression for co-localization and co-immunoprecipitation studies, the Gateway cloning system (Invitrogen) was used. To generate expression constructs, donor vectors containing our sequence of interest were combined with the Gateway Destination vector desired (pDEST22 and pDEST32 for yeast-two hybrid assays, and pDEST-53 and pDEST-Myc for our labeled constructs) in a ratio of 50 ng:150 ng. Reactions were incubated in a total volume of 8 µL with 2 µL LR clonase for 1 hour at room temperature. Reactions were transformed into Top10 E.coli cells and plated on appropriate selection media. Clones were sequenced with a forward primer specific to the promoter to ensure all inserts were in the correct reading frame.

Transformation of Chemically Competent Escherichia Coli (E.coli) Cells

Chemically competent Top10 (Life Technologies) E.coli cells were transformed with plasmid DNA by heat shock. 50 µL of frozen competent Top10 cells were thawed on ice. Between 10 ng - 100 ng of plasmid DNA was added to thawed Top10 cells. Cells were flicked gently to mix and then incubated on ice for 10-20 minutes. Cells were heat shocked at 42˚C for 30 seconds, before returning to ice for 2 minutes. 250 µL S.O.C media was added to transformed cells and incubated at 37˚C for 1 hour. Following incubation, transformed cells were plated on LB Agar plates supplemented with antibiotic appropriate to antibiotic resistance encoded by

plasmid used in transformation (Ampicillin, 100 μg/mL, Kanamycin, 50 μg/mL, Spectinomycin, 100 μg/mL).

Plasmid DNA Preparations

Plasmid DNA was purified from transformed bacteria using QIAprep Spin Miniprep and Midiprep kits (Qiagen). Transformed bacterial cultures were grown overnight at 37˚C in LB Broth supplemented with appropriate antibiotic depending on antibiotic resistance encoded by plasmid. Plasmids were purified from bacterial cultures following the manufacturer's recommended protocol. Plasmid DNA concentrations and purity were determined by measuring absorbance of samples at optical densities of 260 nm and 280 nm using a NanoDrop- 1000 (NanoDrop Technologies).

Restriction Digests

Restriction digests were set up by mixing up to 1 μg of plasmid DNA with 1-5U of desired restriction enzyme(s) and its corresponding buffer. Reactions were incubated at 37˚C for 1 hour to overnight. Digests were visualized by DNA electrophoresis.

DNA Electrophoresis

Agarose gels were prepared by adding UltraPure Agarose (Invitrogen) to Sodium Borate buffer at a desired w/v ratio. For DNA visualization, Ethidium Bromide was added to a final concentration of 0.5 μg/mL. DNA diluted in loading

buffer was loaded into wells of casted gels and a voltage of 180-200 V was applied. A UV transilluminator was used to visualize DNA fragments.

Cloning MID2-RF/CC1 and MID1-RF/CC2

To generate MID2-RF/CC1, three cloning steps were required. First plasmid pCR8/GW TOPO PEPP2 3' kpn was digested with HindIII and KpnI and used as a vector. While plasmid pEGFP-C2-hMID2-CC1 (previously generated in the Cox lab by Blair Hopwood and Julie Zou), which contains a MID2 with the coiled-coil domain of MID1 was digested with HindIII and KpnI and used as an insert to generate a new plasmid. In the second step, using the new plasmid generated, forward primer H-MID2-F and reverse primer GW2 were used in PCR to amplify out a fragment containing a portion of MID2 surrounding the MID1 coiled-coil domain. PCR reaction was carried out using Prime Star polymerase (Takara). This PCR product was digested with XbaI and KpnI. This PCR product was submitted for Sanger sequencing to verify DNA sequence. Sequence verified PCR product was then ligated to a vector generated by digesting the plasmid, pEGFP-C2-hMID2-RF1 (previously generated in the Cox lab) with XbaI and KpnI (note this plasmid has 2 XbaI sites, but one site is dam methylated and remains uncut by XbaI) to generate plasmid that codes for a chimeric MID2 protein with MID1 RING and Coiled-coil domains (MID2-RF/CC1). To generate MID1-RF/CC2, two plasmids that were previously generated in the lab of Tim Cox by Blair Hopwood and Julie Zou were used (pEGFP-C2-hMID1 (BS/ES)-CC2 and pEGFP-C2-hMID1 (BS/ES)-RF2. pEGFP-C2-hMID1(BS/ES)-CC2 was digested with XbaI and KpnI (note there are 2 XbaI restriction sites but 1 site is dam methylated and remains uncut). From this digest,

the gel purified insert was used to ligate to the gel-purified vector that was generated by digesting pEGFP-C2-hMID1 (BS/ES)-RF2 with XbaI and KpnI). The new plasmid construct, MID1-RF/CC2, was verified by restriction digest.

Cloning PLEKHA5 Domain Deletion Constructs

Truncated PLEKHA5 expression plasmids were generated by PCR amplification using primers listed in Table1 to amplify regions from the plasmid, pCR8/GW PEPP2 5'3'kpn, which contained full length, sequence verified PLEKHA5. PCR products of PLEKHA5 domain deletions were submitted for DNA sequencing (Simple Seq by Operon, Eurofin Genomics) and sequence verified PCR products were A'tailed and ligated to a pCR8/GW/TOPO-TA cloning vector (Life technologies, Invitrogen). To generate expression clones of PLEKHA5 domain deletion constructs, gateway cloning was performed by combining the PLEKHA5-pCR8/GW/TOPO-TA plasmids with Gateway compatible expression plasmids. To generate PLEKHA5-ΔN449, primers hPLEKHA5-449f and PEPP2B-Kpn were used. To generate PLEKHA5-ΔN615, primers hPLEKHA5-615f and PEPP2B-Kpn were used. To generate PLEKHA5-ΔN772, primers hPLEKHA5-772f and PEPP2B-Kpn were used. To generate PLEKHA5-ΔCTD, primers PEPP2F-v2 and PLEKHA5-674r were used.

Yeast Two-Hybrid Assays (Y2H)

ProQuest™ Two-Hybrid System with Gateway® Technology (Invitrogen) was used to assay for protein-protein interactions. Single yeast colonies from transformed yeast cells, as well as yeast controls provided with the kit, were grown

in 2 mL of Synthetic Defined 2- and 3- amino acid dropout media (SD-Leu-Trp) (Sunrise Science). Cultures were incubated overnight at 30˚C with shaking. Culture density was measured on a Nandrop 1000 using $OD_{600}$. Cultures were diluted to an $OD_{600}$ of 0.1, then 3 μL of diluted culture was spotted onto selection plates. Plates were incubated at 30˚C for 48 hours and assayed for protein-protein interaction by 3 different methods for the induction of three reporter genes (URA3, lacZ, and HIS3 plus 3-amino-1,2,4-triazole (3-AT) at 50, 75 and 100 mM concentrations). All constructs were tested for self-activation and those constructs showing self-activation were not used to test protein-protein interactions. Controls for strong, weak, and non-interactors were provided in the ProQuest™ Two-Hybrid System with Gateway® Technology (Invitrogen).

Cell Culture

Cercopithecus aethiops kidney cells (Cos-1), Human embryonic kidney 293T cells (HEK 293T), and Madin Darby canine kidney cells (MDCK) were maintained in DMEM with sodium pyruvate (Cellgro) supplemented with 10% FBS (Cellgro), and 2mM GlutaMax (Gibco). Cells were plated in vented flasks or dishes treated for tissue culture and cultured at 37˚C with 5% $CO_2$. To maintain cells in culture, cells were passaged every 2-3 days. To passage cells, medium was aspirated from cells and cells were washed with 1X PBS without calcium and magnesium. TrypLE Express (Life Technologies) was added to cell culture dishes to ensure coverage of the cell monolayer. Cells were incubated at 37˚C until cells detached as observed using an inverted microscope. Detached cells were resuspended in pre-warmed

complete DMEM. Cells were pelleted by centrifugation at 200 g for 5 minutes. Cells were resuspended in complete DMEM and split to maintain lines. To freeze cell lines, cells were detached from plates as described above. Cells were pelleted by centrifugation (200 g, for 5 minutes) and resuspended in freezing media (95% Complete DMEM and 5% DMSO). Resuspended cells were alliquoted in cryovials and frozen overnight at -80˚C using Mr. Frosty freezing container filled with isopropyl alcohol. For long-term cell storage, cryovials were transferred to liquid nitrogen.

Cell Transfections

Twenty hours prior to transfection, cells were replated into culture dishes at a density that would allow them to reach ~80%-85% confluency at time of transfection. For transfections, Mirus TransIT-LT1 transfection reagent was used according to protocol by manufacturer (Mirus Bio LLC). On the day of transfection, purified plasmid DNA was mixed with TransIT-LT1 reagent and plated dropwise onto cultured cells. Cells were harvested 24 hours post transfection.

Cell Lysate Preparation

Cell lysate was collected from plated cells by washing cells 1X with ice cold PBS. Cells were lysed by rocking on ice with ice-cold RIPA buffer (Life Technologies, Inc.) prepared with protease inhibitor (1 μL/100 μL RIPA, Halt Protease Inhibitor Cocktail, Thermo Scientific). A cell scraper was used to further promote lysis and remove cells from plates. Lysates were transferred to microcentrifuge tubes and

centrifuged at 4˚C for 15 minutes at 14,000 x g. Supernatants were transferred to new tubes and stored at -80 ˚C for further analysis.

Protein Concentration Determination

Protein concentrations of cell lysates were determined using Bradford reagent (BioRad). Bradford reagent was warmed to room temperature for 20 minutes prior to use. Protein standards were made from serial dilutions of BSA at 2 mg/mL and used at a range of 0.125 mg/mL to 2 mg/mL. Unknowns were diluted 1:10 in $H_2O$. Samples were mixed with Bradford reagent at a ratio 1:50 and plated in triplicate on a microplate. Plates was incubated at room temperature for 20 minutes then absorbance was measured at 595 nm using a plate reader.

Western blots

Protein samples were prepared by diluting 20-30 µg of cell lysate in Laemmli –SDS loading buffer. To denature proteins, samples were heated at 95˚C for 5 minutes. Next, samples were loaded in wells of SDS-Page gel and run in BupH Tris-HEPES-SDS running buffer (Pierce) at 87 V for 1 hour. Proteins were transferred onto PVDF membrane by wet transfer. After transfer, membranes were blocked for 1 hour at room temperature in 5% non-fat dried milk dissolved in TBS-T (w/v). After blocking, blots were incubated in primary antibody solution made up as directed by the antibody manufacturer. Rabbit anti-MID1(Bioworld) was diluted 1:1000. Mouse-anti-cMyc [9E10] (Abcam) was diluted 1:1000. Rabbit anti-GFP (Abcam) was diluted 1:1000. Mouse anti-delta 1 catenin [6H11] was diluted to

1:10,000 (Abcam). After incubation with primary antibody, blots were washed 3X in TBS-T for 5 minutes/wash. Blots were then incubated with HRP-conjugated secondary antibody solution (1:10,000) for 30 minutes at room temperature. Blots were next washed 3X in TBS-T for 10 minutes/wash and signal was developed using a chemiluminescent reagent (West Pico from Pierce or Femto from Pierce diluted 1:5 in water). Chemiluminescence was detected through exposure to X-ray film. To quantify protein bands, X-ray films were scanned and bands were quantified using ImageJ.

c-Myc-tagged Immunoprecipitations and Co-immunoprecipitations

Cells overexpressing proteins tagged with c-Myc were immunoprecipitated using the Pierce c-Myc-tagged immunoprecipitation kit (Thermo Scientific), and immunoprecipitations were carried out as recommended by manufacturer. Briefly, cells overexpressing c-Myc tagged proteins were rinsed in cold TBS and lysed using M-PER lysis buffer prepared with protease inhibitor (1 µL/100 µL lysis buffer). Lysis was allowed to proceed for 5 minutes on ice. Lysis reactions including cell debris were transferred to cold microcentrifuge tubes and centrifuged for 15 mins X 14,000 rpm at 4˚C. Supernatants were transferred to clean tubes. Protein concentrations were determined by Bradford assay and 300-500 µg of total protein was combined with anti-c-Myc agarose beads in spin columns provided in the kit. Samples were incubated overnight at 4˚C with end-over-end mixing. Samples were pulsed centrifuged and flow through was saved for analysis. Anti-c-Myc agarose beads and proteins bound to beads were retained in spin columns and washed 3X

with cold TBS with 0.05% Tween-20. Proteins tagged with c-Myc and protein binding partners were eluted with 2X non-reducing sample buffer at 95˚C. After elution, 1.5 µL BME was added to sample to denature proteins. Proteins were separated on 8-16% SDS page gels, transferred to PVDF membrane, and analyzed by Western Blot.

Immunocytochemistry

Cells were grown on number 1.5 coverslips pre-treated as follows: Coverslips were acid washed and coated with poly-L-lysine (Sigma) overnight at 4˚C with rocking. Coverslips were next washed 10X in dd$H_2O$ then rinsed in 100% EtOH and allowed to dry in sterile incubator. Dried coverslips were stored at 4˚C for several months until needed. To prepare cells for imaging, coverslips were washed and fixed at RT for 15 minutes in 4% paraformaldehyde, 1% sucrose in PBS . Cells were permeabilized in 0.2% TritonX-100 and blocked in 10% NGS at RT in humid chamber for 1 hour. Primary antibodies were diluted according to manufacturer product sheet and incubated at RT for 1 hour, or O/N at 4˚C. Secondary antibody, diluted according to manufacturer recommendation, was applied for 30 minutes at room temperature. Cell nuclei were stained with DAPI (100 ng/mL diluted in PBS) for 5 minutes at RT in the dark. Coverslips were mounted on slides using Vectashield mounting medium with DAPI. Slides were imaged using 40X oil immersion lens on Leica TCS SP5 confocal system.

## Results

MID2 interacts with PLEKHA5 and PLEKHA7.

Previously in our lab, PLEKHA5 was identified as a binding partner of MID2 but not MID1 (Zou, 2004). To test if protein family members closely related to PLEKHA5 would also bind to MID2, PLEKHA6 and PLEKHA7 were cloned into Y2H expression vectors. While PLEKHA6 did not interact with MID2, PLEKHA7 appeared to be a possible binding partner, as indicated by weak growth of yeast plated on selection media (Figure 2.1A). The interactions of both PLEKHA5 and PLEKHA7 with MID2 were later confirmed by in vitro immunofluorescence and co-immunoprecipitation experiments. Overexpression of either PLEKHA5 or PLEKHA7 with MID2 altered the normal distribution of PLEKHA proteins. When expressed alone, PLEKHA7 is found predominantly on the plasma membrane, but occasionally, shows punctate regions of staining in the cytoplasm (Figure 2.1B). PLEKHA5 overexpression exhibits primarily cytoplasmic localization with some association on the plasma membrane (Figure 2.1B). However when either PLEKHA5 or PLEKHA7 is expressed with MID2, both co-localize with MID2 on the microtubules, although unlike the prominent expression of PLEKHA5 on the microtubules, the co-localization of PLEKHA7 on the microtubules was weak (Figure 2.1C and D). While PLEKHA7 maintains its prominent expression on the membrane while also co-localizing with MID2 on the microtubules, PLEKHA5 staining becomes focused on microtubules and its dispersed distribution throughout the cytoplasm is lost (Figure 2.1C).

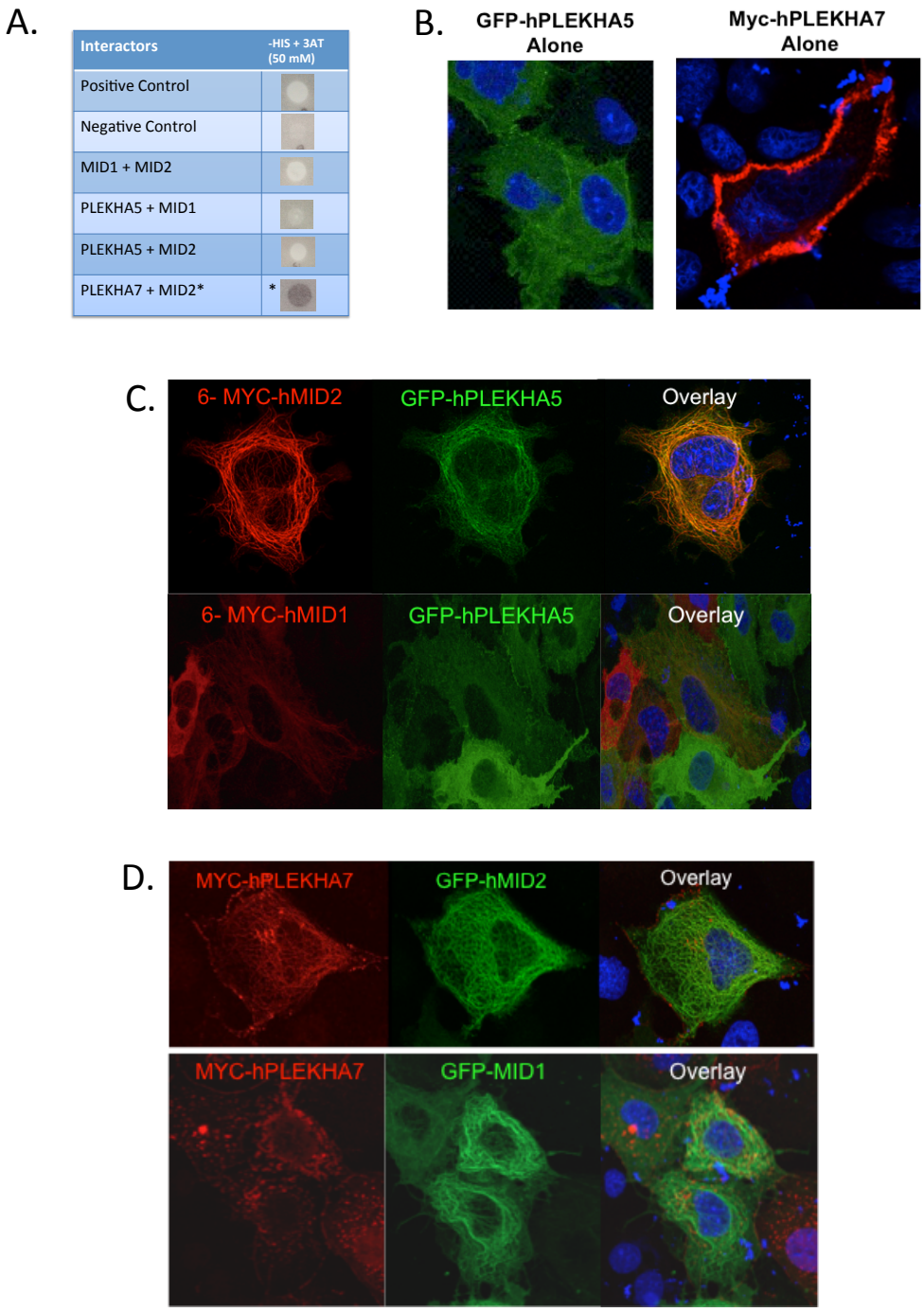


**Figure 2.1 MID2, but not MID1, interacts with PLEKHA5 and PLEKHA7. A.** Yeast Two-Hybrid assay where positive yeast growth on selection plate indicates that PLEKHA5 and PLEKHA7 interact with MID2 while MID1 does not interact with PLEKHA5. *Note testing of PLEKHA7 and MID2 done on a different plate using similar controls. **B.** Over expression of GFP-PLEKHA5 and Myc-PLEKHA7 alone. **C.** GFP-PLEKHA5 colocalizes with Myc-MID2 but not Myc-MID1. **D.** Myc-PLEKHA7 colocalizes with GFP-MID2, but not GFP-MID1.

In similar co-expression studies using MID1 instead of MID2, neither PLEKHA5 nor PLEKHA7 redistributed to the microtubules, which indicated that neither of the PLEKHA proteins co-localized with overexpressed MID1 (Figure 2.1C and D). However, some areas of PLEKHA5 expression seem to coincide with MID1 expression, which may be due to the diffuse cytoplasmic distribution of PLEKHA5 or may be an indication of an interaction, possibly through an indirect protein-binding partner (Figure 2.1C). It should be noted that these studies were conducted in Madin Darby canine kidney cells, which have undetectable levels of MID2 transcript as tested by RTPCR, and thus, MID2 is not present to facilitate an interaction between MID1 and PLEKHA5 (Figure 2.2A). Co-immunoprecipitation of Myc tagged -PLEKHA5 or -PLEKHA7 pulled down GFP tagged -MID2, confirming that MID2 interacts with both PLEKHA5 and PLEKHA7 (Figure 2.2B). Unexpectedly, in co-immunoprecipitation experiments where proteins were overexpressed in human 293T cells, both Myc tagged- MID1 and -MID2 pulled down GFP tagged -PLEKHA5 and -PLEKHA7 (Figure 2.2C). Since the yeast two-hybrid assay, which measures protein-protein interactions, showed that MID1 does not interact with PLEKHA5 (Figure 2.1A) nor PLEKHA7 (data not shown), this suggests that MID1 interacts with PLKEHA5 and PLEKHA7 indirectly, possibly through its binding to MID2, which is expressed in 293T cells (Figure 2.2A).

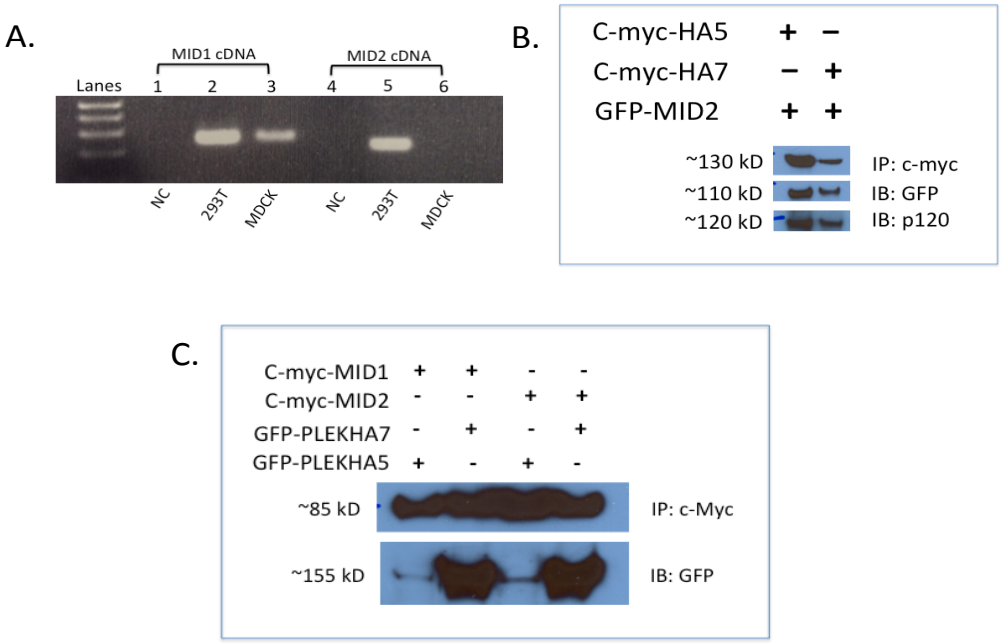


**Figure 2.2 PLEKHA5 and PLEKHA7 co-immunprecipitate with MID1 and MID2, suggesting MID1 may bind PLEKHA proteins indirectly.** **A.** RT-PCR showing that MID1 transcripts can be isolated from 293T and MDCK cells, while MID2 is present in 293T cells but not MDCK cells. **B.** Immunoprecipitation of Myc-PLEKHA5 and Myc-PLEKHA5 can pull down GFP-MID2 **C.** Immunoprecipitation of Myc-MID1 and Myc-MID2 can pull down both GFP-PLEKHA5 and GFP-PLEKHA5.

Identification of PLEKHA5 binding partners

Although PLEKHA5 was identified 15 years ago as a protein elevated in melanoma, only 3 publications have emerged since, and little is yet known about its cellular role. Previously in the lab, to help elucidate a role for PLEKHA5, a Y2H assay using full length PLEKHA5 as bait was performed. Several potential protein-binding partners were identified. To determine which proteins were bona fide PLEKHA5 binding partners, full-length clones of these putative binding partners were generated and tested by yeast-two hybrid assay. In this study 4 novel binding partners for PLEKHA5 were confirmed(Figure 2.3): 1. PDZ domain containing 11 (PISP), 2. seven in absentia 1b (Siah1b), 3. seven in absentia 2 (Siah2), and tumor protein p53 binding protein 2 (TP53BP2). These clones were also tested for their ability to bind PLEKHA7 in a subsequent yeast-two hybrid assay and it was found that PLEKHA7 could bind both PISP as well as TP53BP2. Since PLEKHA7 has been shown to interact with p120 catenin (Meng et al., 2008), both PLEKHA5 and PLEKHA7 were tested to see if either would interact with the full length clone of ARVCF (armadillo repeat gene deleted in velocardiofacial syndrome) which is a closely related homolog of p120 catenin. However, neither PLEKHA5 nor PLEKHA7 interacted with ARVCF in our yeast-two hybrid screen (figure 2.3).

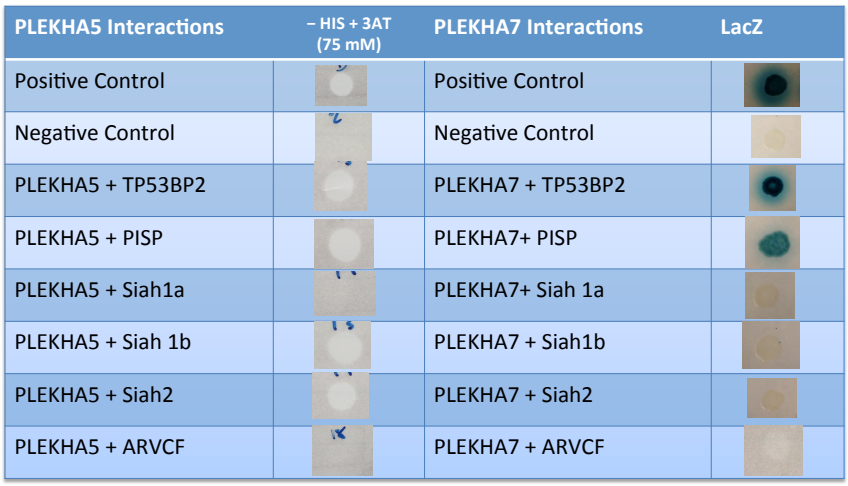


**Figure 2.3 PLEKHA5 binds other protein partners, two of which (ASPP2 and PISP) also bind PLEKHA7.** Full length clones of putative PLEKHA5 binding partners were generated and tested for their interaction with PLEKHA5. On the left columns, positive growth of of yeast on selection plate indicates binding interaction of PLEKHA5 with TP53BP2, PISP, Siah1b, Siah2. On the right columns, positive growth of yeast and B-galactosidase production indicates PLEAKH7 interaction with TP53BP2 and PISP.

Amino acids 688-772 of PLEKHA5 are necessary for co-localization to MID2.

To determine the regions of PLEKHA5 necessary for binding to MID2, several domain deletion constructs were generated (figure 2.4A). PLEKHA5 deletion constructs were fused to a GFP tag and overexpressed with Myc-tagged MID2 in Cos-1 cells to determine which regions of PLEKHA5 mediate its binding to MID2. Interestingly, the MID2 binding region of PLEKHA5 overlaps with the putative p120

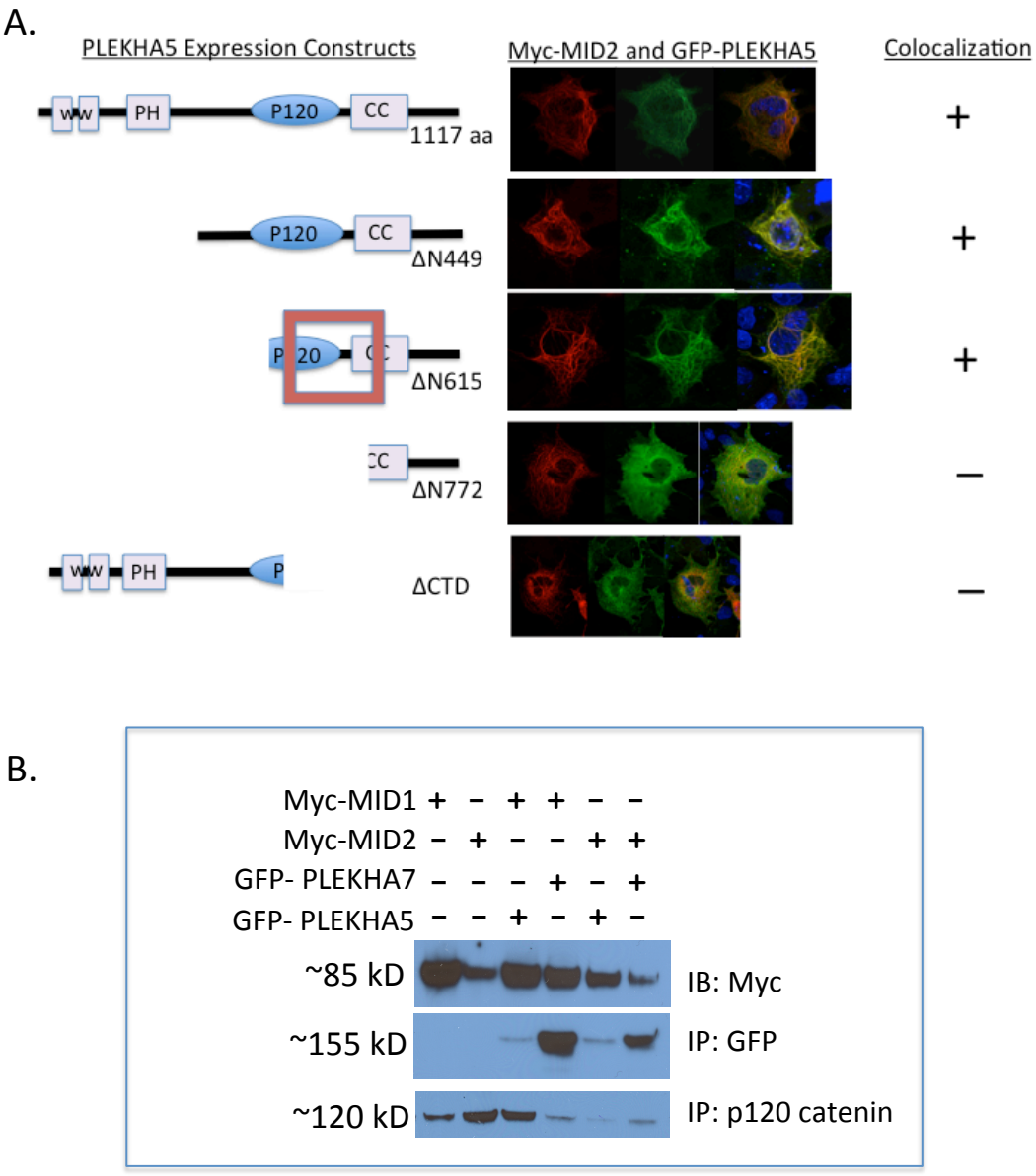


**Figure 2.4 Putative p120 binding region of PLEKHA5 necessary for interaction with MID2, and p120 co-immunoprecipitates with PLEKHA7, PLEKHA5, MID1, and MID2. A.** Amino acids 688-772 of PLEKHA5 are necessary for co-localization to MID2. **B.** Coimmunprecipitation shows that p120 can be immunoprecipitated with MID1, MID2, PLEKHA5, and PLEKHA7.

binding region of PLEKHA5, which is based on PLEKHA5 protein alignment to PLEKHA7 in conjunction with the published region of PLEKHA7 that mediates its interaction with p120 catenin (Meng et al., 2008). p120 catenin is known to bind the cytoplasmic, juxtamembrane region of the cell-cell adhesion protein E-cadherin to regulate E-cadherin stability at the plasma membrane (Yap et al., 1998). Moreover, PLEKHA7 binding to p120 at the adherens junctions stabilizes E-cadherin at apical cell-cell junctions (Meng and Takeichi, 2009). To determine if PLEKHA5 may also bind p120 catenin, Myc-tagged PLEKHA5 was overexpressed in 293T cells and immunoprecipitated using ProFound c-Myc Tag IP/Co-IP kit (Thermo Scientific #23620), and analyzed by Western blot using an antibody targeted against p120 catenin (Abcam, ab11508). Endogenous p120 co-immunprecipatated with Myc-tagged PLEKHA5, similar to that of Myc-tagged PLEKHA7 (Figure 2.4B).

Since the PLEKHA5 binding region for MID2 and p120 overlap, a co-immunoprecipatation experiment was carried out to determine if MID1 or MID2 immunoprecipitations could also pull down endogenous p120. Not only was it found that PLEKHA5/7 can immunoprecipitate both p120 and MID1/2, but also, immunoprecipatation of the MID proteins alone (without overexpression of PLEKHA5 or PLEKHA7) pulled down p120 (Figure 2.4B). This suggests that MID proteins may interact with p120 directly or indirectly.

<u>RING and Coiled-coil domains of MID2 are necessary for binding to PLEKHA5.</u>

Previously several, MID2 deletion constructs were tested by Julie Zou in yeast two-hybrid assays to determine that the RING and coiled-coil domains of

MID2 both interacted with PLEKHA5 (Cox, unpublished data). To verify this observation, chimeric MID1 and MID2 constructs in which the MID1 RING and coiled-coil domains were swapped with the MID2 RING and coiled-coil domains to generate two fusion constructs (MID1-RF/CC2 and MID2-RF/CC1) (Figure2.5). It was expected that MID1-RF/CC2, would confer MID1 binding to PLEKHA5, and conversely, it was anticipated that MID2-RF/CC1 would abrogate MID2 interaction with PLKEHA5. MID1-RF/CC2 and MID2-RF/CC1 were tagged with cMyc and tested by co-expression/co-localization with PLEKHA5-GFP. As predicted, MID1-RF/CC2 colocalized with PLEKHA5, while MID2-RF/CC1 lost its ability to interact with

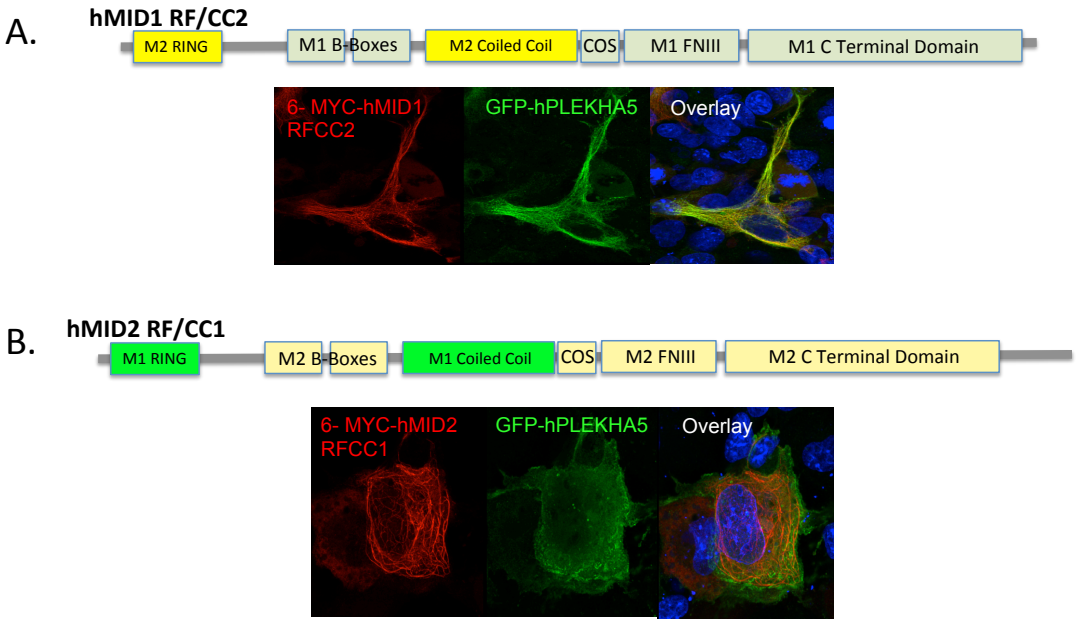


**Figure 2.5 Chimeric MID proteins with RING and coiled-coil domain swaps alters colocalizations with PLEKHA5. A.** A chimeric MID1 protein harboring the RING and coiled-coil domain of MID2 co-localizes with GFP-PLEKHA5. **B.** Conversely, a chimeric MID2 with MID1 RING and coiled-coil domains no longer co-localizes with GFP-PLEKHA5.

PLEKHA5 suggesting that the MID2 RING and Coiled-coil domains mediate MID2 binding to PLEKHA5 (Figure 2.5).

MID2 interacts with the protein alpha4

MID1 functions as an E3 ubiquitin ligase and its ubiquitin ligase activity has been shown to target both alpha4 and PP2Ac for degradation (Du et al., 2013; Liu et al., 2001; Trockenbacher et al., 2001). While MID1 has been shown to bind and regulate the alpha4/PP2Ac complex, MID2 binding, but not regulation, of alpha4/PP2Ac is suspected, but not yet demonstrated (Du et al., 2013; Liu et al., 2001; Short et al., 2002; Trockenbacher et al., 2001). Like its paralog MID1, MID2 is believed to function as an E3 ubiquitin ligase to regulate alpha4/PP2Ac (Short et al., 2002). To evaluate the involvement of MID2 in the regulation of the alpha4/PP2Ac complex, a MID2 construct with a Leucine to Glutamine amino acid substitution was generated, MID2L146Q (Figure2.6A). This construct was based on a MID1 L146Q mutant, which was shown to disrupt MID1 interaction with alpha4 (Du et al., 2013). The MID2L146Q-GFP overexpression construct was co-expressed with Myc-tagged alpha4 in MDCK cells. Protein localizations were determined by immunofluorescent microscopy (Figure 2.6B). Additionally, Myc-alpha4 was co-transfected with MID2 or MID2L146Q in 293T cells. One day (24 hours) post-transfections, cell lysates were collected and Myc-tagged proteins immunoprecipitated. In co-localization and co-immunoprecipitation studies, MID2L146Q prevented MID2 from interacting with alpha4 (Figure2.6B and Figure 2.7A). As expected, when overexpressing MID2L146Q with PLEKHA5 or an N-

terminal truncation of PLEKHA5 (PLEKHA5ΔN615), the MID2L146Q maintains its ability to co-localize with PLEKHA5 (Figure 2.6 C).

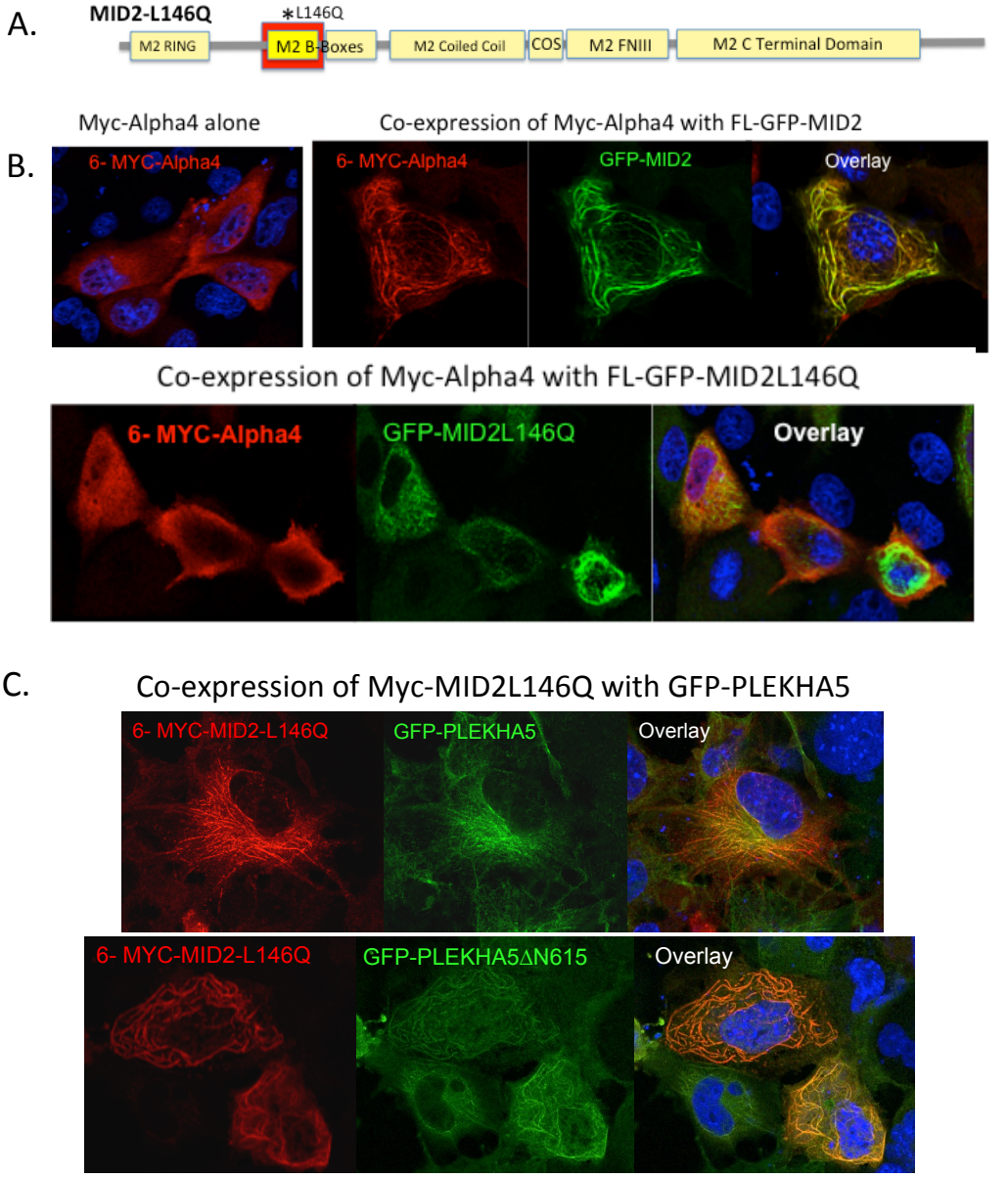


**Figure 2.6 Mutant MID2L146Q loses its ability to bind alpha4 and overexpression leads to increased levels of alpha4. A.** Cartoon schematic of MID2L146Q mutant construct. **B.** Immunocytochemistry shows that MID2L146Q, loses its ability to bind alpha4**. C** Myc-MID2L146Q maintains its ability to co-localize with GFP-PLEKHA5 and GFP-PLEKHA5ΔN615.

MID1 targets alpha4 for ubiquitin mediated degradation (Du et al., 2013). To assay if alpha4 levels would be affected by MID2, MID2 and MID2L146Q overexpression constructs were co-expressed with alpha4. One day (24 hours) post-transfection, cell lysates were collected, and proteins were separated on SDS-PAGE, and assessed by western blot. Alpha4 protein levels were then quantified relative to GAPDH control by western blot. Similar to alpha4 co-expression with MID1 versus MID1L146Q, it was found that alpha4 levels were higher when co-expressed with MID2L146Q than when co-expressed with MID2 (Figure 2.7B).

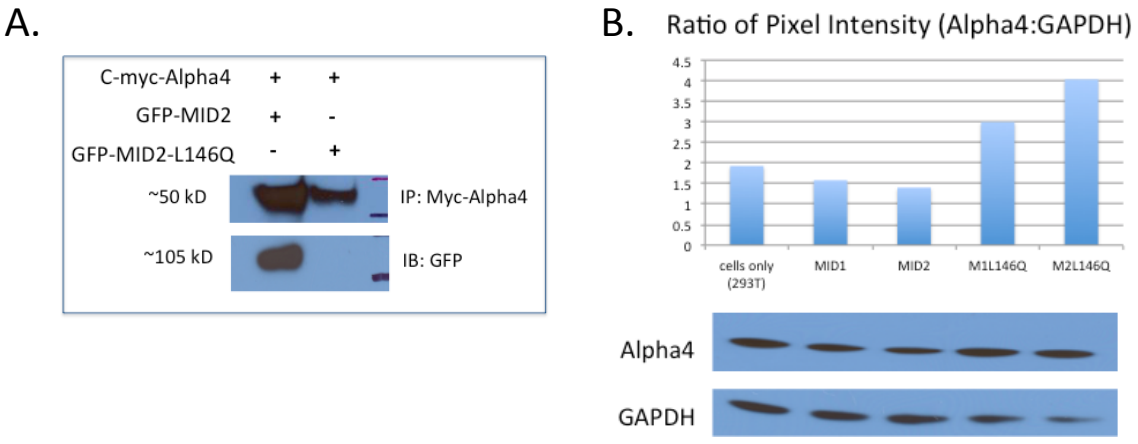


**Figure 2.7 MID2L146Q does not co-immunoprecipitate with Alpha4 and overexpression of MID2L146Q leads to increased levels of Alpha4 A.** MID2, but not MID2L146Q co-immunoprecipitates with Alpha4. **B.** Overexpression of either MID1L146Q or MID2L146 results in increased levels of Alpha4 relative to GAPDH.

## Discussion

MID2, like MID1, can impact Alpha4 levels

These studies highlight an emerging role for MID2 that will contribute to our understanding of the pathologies that arise in X-linked Opitz Syndrome (XLOS). To date, it remains unclear how MID1 mutations impact developmental processes that manifest as Opitz Syndrome. It is thought that MID1 functions at the microtubules to regulate the alpha4/PP2Ac complex (mTORC1) and because of the central role of PP2A phosphatase activity in the cell, it is thought that this contributes to the pathology observed in XLOS. Like MID1, MID2 has also been shown to bind to the alpha4/PP2Ac complex (Cox 2002), although it is unclear if this binding contributes to the degradation of either alpha4 or PP2Ac. When alpha4 is co-expressed with MID2, a decrease in alpha4 levels is observed, suggesting that MID2, like MID1, may impact alpha4 expression, perhaps through ubiquitin targeted degradation. However, it is also possible that MID2L146Q mutants exert a dominant negative effect on endogenous levels of MID1 and prevent it from regulating of alpha4. Future studies could address the E3 ubiquitin ligase activity of MID2 using in vitro studies as previously done for MID1 (Du et al., 2013). However this initial study suggests that disrupted MID2-alpha4 interactions may also contribute to the cell-cell adhesion defects that occur when MID1 function is lost.

MID2 may contribute to the cell adhesion defects observed with loss of MID1 function

While biochemical assays highlight a role for MID1 in the regulation of cellular phosphatase activity through its association with alpha4/PP2Ac, more recent work identifies MID1 as an important regulator of epithelial cell adhesion (Huang Cox and Cox, unpublished.; Suzuki et al., 2010). Suzuki et al. demonstrated that in Xenopus, knockdown of MID1, as well as MID2, not only disrupted neuroepithelial morphology and organization, but also resulted in marked decreases in the adhesion proteins, ZO-1, C-cadherin, β-catenin, and laminin (Suzuki et al., 2010). Research conducted by Huang and Cox corroborates an essential role for MID1 in epithelial cell adhesion. Huang and Cox found that MDCK cells overexpressing a dominant negative MID1 mutant showed defective cell migration due to loss of cell-cell contacts and weakened cell-ECM adhesion (Huang and Cox, unpublished data). Further, when these cells were polarized, markers of cell adhesion were impacted (Huang and Cox, unpublished data).

Until now, MID2 has mostly been defined through its association with MID1, but this chapter illuminates a new role for MID2 as a protein binding partner of PLEKHA proteins, which are linked to the regulation of cell migration and adhesion. *PLEKHA5* encodes a long form (1282 aa) and short form (1116 aa) protein with putative Trp-Trp (WW) and Plekstrin homology (PH) domains (Yamada et al., 2012). In lipid overlay assays, PLEKHA5 bound to PI3P, PI4P, PI5P, and PI(3,5)P2, the last of which is found in endosomal membranes (Yamada et al., 2012). In situ hybridization in mouse embryos demonstrated expression of PLEKHA5 mRNA

overlaps with that of MID2, with both showing a high level of expression in the developing CNS and heart (Buchner et al., 1999; Yamada et al., 2012). While little is known about PLEKHA5, initial studies indicate that it likely functions in membrane movement and cell motility (Lemmon et al., 2002; Yamada et al., 2005; Zou, 2004). Most recently, PLEKHA5 transcript levels have been shown to be elevated in melanomas that metastasize to the brain, and moreover, knockdown of PLEKHA5 in A735Br cells, which are representative of melanomas that metastasize, resulted in decreased cell growth and diminished transmigration through a membrane simulating the blood-brain barrier (Jilaveanu et al., 2014) .

Like PLEKHA5, PLEKHA7 binding to MID2 bridges the MID1/2 complex with proteins regulating cell morphology and membrane dynamics. Studies demonstrate that PLEKHA7, a protein which shares significant identity to PLEKHA5, is involved in regulation of apical adherens junctions, and also connects the apical junctions to microtubules (Kurita et al., 2013; Meng et al., 2008; Pulimeno et al., 2011). Formation of adherens junctions depends on PLEKHA7 binding to afadin, an important regulator of adherens junctions (Kurita et al., 2013). Also, at adherens junctions PLEKHA7 not only promotes the stability of E-cadherin, PLEKHA7 also connects the cell-cell adhesion protein E-cadherin to microtubules through direct binding to the E-cadherin juxtamembrane protein p120 and its interaction with the microtubule protein, Nezha (Meng et al., 2008). Additionally, PLEKHA7 interacts with paracingulin, a protein involved in Rho GTPase regulation of adherens junctions as well as tight junctions (Guillemot et al., 2008; Meng et al., 2008; Pulimeno et al., 2011).

Although a functional relationship between MID2 and PLEKHA proteins remains uncertain, these findings raise some interesting possibilities. Through my studies, I confirmed that both the MID2 RING and coiled-coil domain were necessary for its interaction with PLEKHA5. The MID2 RING has been shown to possess E3 ubiquitin ligase activity although its targets remain unknown (Napolitano et al., 2011). Binding of PLEKHA5 to the MID2 RING domain may indicate that PLEKHA5 is also a target of MID2 ubiquitin-mediated regulation or, alternatively, this interaction may inhibit the MID2 RING-dependent regulation of alpha4/PP2Ac at the microtubule-membrane interface. Another possibility is that MID2 may unite the PLEKHA proteins with alpha4/PP2Ac to direct the targeting of PP2A phosphatase activity to the PLEKHA proteins. Further, the requirement of the MID2 coiled-coil domain for its binding to PLEKHA5 also raises questions about the nature of its interactions with PLEKHA proteins. The coiled-coil domain of MID1 and MID2 is necessary for the homo and heterodimerization of MID1 and MID2 (Short et al., 2002). It also mediates the interaction between MID1/2 and the microtubule stabilization protein, MIG12 (Berti et al., 2004; Suzuki et al., 2010). It is not yet known if MID2 and PLEKHA interactions are inclusive or exclusive of the known MID2 biding partners, MID1 and MIG12. MID2 binding to PLEKHA proteins could increase in instances where MID1 is mutated, or just as likely, mutant MID1 could also indirectly bind PLEKHA proteins, through MID2, and result in the mislocalization of these proteins. Regardless, it is proposed that when MID1 is mutated, it directs MID2 mislocalization and consequently impacts the apical junctions directly through PLEKHA5/7 and/or alpha4/PP2Ac interactions.

PLEKH5 Protein Binding Partners

Although we do not yet know how MID2 might regulate PLEKHA5, this work indicates that several PLEKHA5 binding partners may be impacted should PLEKHA5's interaction with MID2 be disrupted. Yeast two-hybrid assays demonstrated that PLEKHA5 interacts with full length clones of PISP, Siah1b, Siah2, and TP53BP2. The significance of these interactions has yet to be explored. Interestingly, TP53BP2 is known for its interaction with apoptotic factor p53, but also binds p63, which is a well-known CLP gene (Bergamaschi et al., 2004; Cox, 2004). Additionally, TP53BP2 has been shown to regulate apical junction turnover and epithelial adhesion through direct binding to PARD3, an epithelial polarity protein necessary for formation of tight junctions (Cong et al., 2010). PISP has been shown to promote intestinal uptake of biotin (Nabokina et al., 2011), an essential cell micronutrient whose deficiency can result in neurological disorders and stunted growth (Pacheco-Alvarez et al, 2002). Siah proteins, like MID1 and MID2, possess a RING finger domain, a known protein motif that confers E3 ubiquitin ligase activity (Qi et al., 2013). Siah proteins have primarily been linked to the regulation of cellular stress responses such as hypoxia, which has a prominent role in cancer (Krämer et al., 2012; Qi et al., 2013). Notably, Siah2 has been found to interact and regulate the stability of TP53BP2 (aka Apoptosis Stimulating Proteins of p53 family member 2 or ASPP2) and ASPP1, which impacts tight junction integrity and cell polarity (Kim et al., 2013). Work by House et al. identified a Siah binding motif defined by amino acid residues PxAxVxP (House et al., 2003). PLEKHA5 contains amino acid residues PNAPVVR that likely confers its binding to the Siah proteins.

Interestingly, the homologus region of PLEKHA7 encodes amino acid residues PNVPVVVR, where the mostly conserved Siah binding residue, Alanine (House et al., 2003), is replaced by a valine.

## Conclusions

The work presented here links the MID1 protein complex to regulators of cell-cell adhesion, and surprisingly, in biochemical studies of MID1 or MID2 it was found that p120 catenin, a known regulator of adherens junction assembly and E-cadherin membrane stability (Keil et al., 2013), is also part of the MID protein complex. This work implicates a suggested role for MID2 in the pathology of XLOS that involves important regulators of cell adhesion.

## Chapter 3: Cell Adhesion Force in dominant negative MID1ΔCTD

### Introduction

The goal of this chapter is to evaluate if MID1 impacts cell-cell forces involved in mechanotransduction. Mechanotransduction is the study of how forces experienced by cells and tissues are translated into biochemical signals that elicit functional responses (Chen et al., 2004; Eyckmans et al. , 2011; Farge, 2011; Hoffman, Grashoff et al, 2011). Factors that regulate cell adhesion are key mediators of mechanotransduction. Cellular transmembrane receptors, such as integrins and cadherins, allow a cell to adhere, sense, and transmit the forces from its external environment to its internal cytoskeletal network, which can respond and in turn, generate force from within the cell (Chen et al., 2004; Farge, 2011; Gomez et al. 2011; Leckband et al. 2011; Schwartz et al., 2008). Through these forces, cells and tissues communicate with the surrounding environment to coordinate developmental processes such as proliferation, migration, and differentiation (Chen et al., 2004; Eyckmans et al., 2011; Goody & Henry, 2010). Recent studies show that MID1, a microtubule binding protein, is implicated in the regulation of cell adhesion (Huang and Cox, unpublished data; Suzuki et al. 2010), and moreover, loss of MID1 disrupts collective cell migration (Huang and Cox, unpublished data), a process coordinated by external and internal cell forces (Etienne-Manneville, 2014). Despite this, it is not yet known how MID1 impacts cell forces. This chapter will measure cell traction and tugging forces in epithelial cell lines overexpressing a dominant negative MID1 mutation (MID1ΔCTD) to quantify cell forces that might contribute to defects observed in X-linked Opitz syndrome.

Traction Forces and Development

Cellular traction force describes the force that exists between the cell and its extracellular matrix (ECM). Cellular transmembrane receptors such as integrins mediate extracellular and intracellular interactions that constitute and generate traction forces. Externally, transmembrane receptors adhere to the ECM, which provides important biochemical cues that regulate proliferation and differentiation (Goody et al, 2010; Schwartz et al., 2008). The ECM also provides mechanical cues such as substrate stiffness and shape (determining cell confinement) that can orchestrate internal cellular responses (Engler et al., 2006; Han et al., 2012; McBeath et al., 2004; Rodríguez-Fraticelli et al., 2012). Within the cell, integrins bind to cytoskeletal components such as actin and myosin II, which through Rho GTPase mediated signaling, can generate cytoskeletal tension (Geiger et al., 2001).

Traction forces have been shown to guide developmental processes such as cell proliferation, migration, and differentiation, and recent studies examining the role of MID1 in epithelial adhesion suggest that traction forces may play a role in the development of XLOS pathology. Loss of MID1 in neuroepithelial cells leads to decreased deposition of the basement membrane protein laminin (Suzuki et al., 2010), a ECM protein that binds cellular integrins to establish cellular apico-basal polarity (O'Brien et al., 2001; Rodríguez-Fraticelli et al., 2012; Yu et al., 2005). Additionally mutant MID1 cells expressing MID1ΔCTD show decreased adhesion on laminin, as well as activation of focal adhesion kinase, leading to increased actin stress fiber formation (Huang and Cox, unpublished data). Although focal adhesion kinase activation leading to actinomyosin contraction is a known signaling pathway

in mechanotransduction (Geiger et al., 2001), it is not yet known how MID1 might influence cell traction forces.

Tugging Forces and Development

Not only do cells sense forces at the ECM, cells also detect and transmit force to and from neighboring cells through cell-cell adhesions. Similar to the role of integrins in mechanotransduction, cadherins are also cellular transmembrane proteins that allow a cell to sense extracellular forces (Ganz et al., 2006; Ladoux et al., 2010; Z. Liu et al., 2010; Maruthamuthu et al., 2011) and respond internally to coordinate cytoskeletal changes that direct cellular processes important to development and disease (le Duc et al., 2010; Leckband et al., 2011; Smutny & Yap, 2010).

Significantly, in epithelial cells, the strength of tugging forces has been shown to directly depend on ECM traction forces (Maruthamuthu et al., 2011). MID1 may be a protein linking cell forces at the cell-ECM and cell-cell interface. Not only does MID1 impact cell-ECM interactions, but also, MID1 modulates cell-cell adhesion (Huang and Cox, unpublished data; Suzuki et al. 2010). Specifically, when MID1 is knocked down in Xenopus neuroepithelia, there is a loss of cell-cell adhesion proteins, C-cadherin, β-catenin, and zonula occludens-1 (Suzuki et al., 2010). In polarized MDCK cells over-expressing MID1ΔCTD, E-cadherin appears disorganized. Moreover, in migration studies using these cells, cells lose their cell-cell adhesion and as a result, fail to migrate collectively (Huang and Cox, unpublished data). Thus, to better understand the mechanical basis of XLOS pathology in patients with

mutations in MID1, in this chapter cell-ECM and cell-cell adhesion forces were examined in epithelial cells expressing a GFP-tagged MID1ΔCTD mutant (referred to in this thesis as MID1ΔCTD) that was generated by Yongzhao Huang (Huang and Cox, unpublished data).

Microposts Measure Traction and Tugging Forces

To measure and quantify cell traction and tugging forces in mutant MID1 cells, micropost technology was utilized. Microposts are arrays of elastomeric posts that form a surface onto which cells can be plated. Initially described as a "bed of microneedles" (Tan et al., 2003), under magnification, microposts might conjure the image of the coils that comprise a bed mattress. However, unlike the compression of coils, when cells are plated on microposts, they exert forces that bend the posts. This deformation can be tracked, and since microposts have a known length (L), diameter (D), and Young's modulus (E), the force that the cell exerts at the post tip can be quantified (Tan et al., 2003). Unlike traction force microscopy, where force calculations are complicated because cells are plated on a continuous surface in which forces generated at the cell surface impact adjacent forces, micropost deflections are independent from adjacent microposts. For this reason, micropost technology makes it possible to accurately track cell forces at each post-cell interface (Chen et al., 2004). Since their inception, microposts have made it possible to measure the nano Newton scale forces exerted by the cell on its environment, as well as track and identify traction and tugging forces involved in mechanotransduction (Chen et al., 2004).

## Materials and Methods

Generation of Stable MDCK Cell Lines

Stable Madin Darby canine kidney (MDCK) cell lines were generated by Yongzhao Huang (Cox Lab) as previously reported (Du et al., 2013). Briefly, MDCK cells were cultured at 37˚C with 5% $CO_2$. Cells were grown in DMEM (Thermo Scientific) supplemented with 10% fetal bovine serum (Thermo Scientific) and 1X GlutaMAX (Invitrogen). MDCK cells were transfected with either pEGFP-C2 or pEMID1ΔCTD expression constructs using TransIT-LT1 transfection reagent (Mirus Bio). Plasmids conferred resistance to geneticin. To generate stable cell lines, transfected cells were grown under selection using geneticin at 0.6 µg/mL (Invitrogen). Clonal lines were started from GFP-positive single cells grown in 96 well plates. Expression of GFP or GFP-MID1ΔCTD in clonal cell lines was verified by western blot probed with anti-GFP (ab290, Abcam) .

Microposts (Microfabricated-Post-Array-Detectors (mPADs))

Microposts were made by replica-molding using negative molds of posts. Negative molds were cast from a master silicone wafer of posts, which was previously found to generate posts with a stiffness of 32 nN/µm. To make negative molds, polydimethylsiloxane (PDMS) (Sylgard 184, Dow-Corning) was mixed with a ratio of 10 g of PDMS to 1 g curing reagent. PDMS was degassed under vacuum and poured over the silicone master and baked at 110˚C for 5 minutes. Negative molds were peeled from silicone master, oxidized in an air plasma for 90 seconds, then

silane-coated overnight by placing negative molds in a vacuum chamber with 25 µL silane ((tridecafluoro-1,1,2,2-tetrahydrooctyl)-1-trichlorosilane (United Chemical Technologies, Bristol, PA) dropped onto a glass slide inside a chamber. To fabricate posts, PDMS was made as described for negative molds. Posts were cast onto plasma treated, #2 glass slides by placing a small drop of PDMS (~200µL) onto the glass slide then placing a negative mold on top of the PDMS drop and allowing PDMS to flow into negative molds for 10-15 minutes at room temperature. Next, post castings were placed at 110˚C to cure overnight (16 hours). Cured posts were pulled gently away from negative molds immediately after removal from the oven. To functionalize the posts, tips of posts were coated in natural mouse laminin (Invitrogen). To do so, laminin-coated stamps were made by pouring a PDMS mixture of 30 g PDMS and 1 g cure over a flat silicone wafer and baking at 110˚C for 10 minutes to cure. Once cured, PDMS was pulled from wafer and cut into rectangular stamps to approximate the surface area of posts. Laminin was diluted in PBS to a final concentration of 5.8 µg/mL and added dropwise to the surface of stamps until stamps were completely coated. Laminin was adsorbed onto stamp for 1 hour at room temperature. Prior to coating posts with laminin, posts were ozone treated for 7 minutes in UV ozone cleaner to activate surface for protein absorption. Laminin stamps were then placed gently on top of posts to transfer laminin from stamps to post tips. Stamps were removed immediately after making contact between tips of posts and the laminin coating the stamps. Posts were washed 2X in DI water then cleaned in a series of baths (100% ethanol, 70% ethanol, then 2X DI water). Next, posts were stained in the dark at room temperature with a 1:1000

dilution of bovine serum albumin – Alexa Fluor 594 conjugate (Life Technologies). Posts were washed 1X in DI water then placed in 0.2% Pluronic F-127 diluted in PBS for 30 minutes at room temperature to render the sides of the posts hydrophobic.

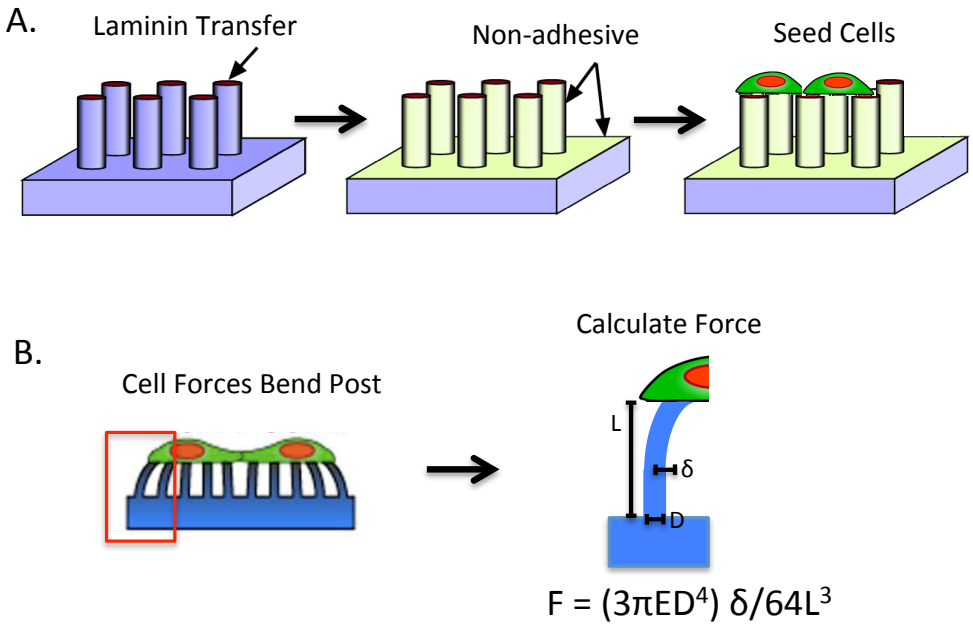


(Image adapted from Nathan Sniadecki and Liu et al., 2010)

**Figure 3.1 Microposts Protocol. A.** Tips of microposts are stamped with laminin and sides are rendered hydrophobic. Cells are seeded onto microposts and adhere to tips. **B.** Cells exert forces that bend the tips of the posts and this deflection is used to calculate force at each cell-post interface.

After treatment, posts were washed 2X in DI water and 1X in PBS (Figure 3.1A).

Seeding Cells Onto Posts

To seed cells onto posts, posts were placed in tissue culture dishes with pre-warmed complete DMEM. Cells were detached using TrypLE and diluted to desired concentration and added dropwise to culture dishes. Cells were grown on posts for

72 hours. At 16 hours prior to fixing, cells were serum starved by replacement of DMEM containing 10% FBS with DMEM containing 0.1% FBS (Figure 3.1A).

Immunofluorescence Microscopy and Image Analysis of Cells

To prepare for imaging, cells plated onto posts were first fixed and permeablized. Next, cells were blocked in 10% NGS at RT for 1 hour, incubated for 1 hour at RT with mouse IgG antibody against β-catenin diluted 1:400 in 10% NGS (Santa Cruz Biotechnology), washed, then stained in secondary antibody (1:200 dilution of goat anti-mouse IgG conjugated with Alexa Fluor 647 (Invitrogen)). Cell nuclei were stained using 1:1,000 Hoescht 33342. Cells were mounted onto #0 coverslips with Fluoromount-G (Southern Biotech). Images were captured by a Nikon Eclipse Ti inverted microscope using a 40X objective and type DF immersion oil (Cargille). The spread area of a cell was determined by GFP staining, which was ubiquitous throughout the cytoplasm. Cell junction length was determined by β-catenin staining and measured using ImageJ.

Force Measurements

To determine cell traction forces, micropost deflections were determined by comparing images of the original position of the posts, at bottom of the slides, to the images of the deflected posts, where the cells attached to the laminin-coated tips of the microposts. A custom MATLAB analysis program was used to determine post deflections (δ). Using the equation, $F=(3\pi ED^4)\delta/64L^{3,}$, the magnitude and direction of forces generated was calculated (Figure 3.1B). The net traction force underneath

cell pairs was determined by summing the traction force vectors across the cells, $\Sigma|F|$. Just as net traction force for single cells sums to zero, which indicates no net cell movement, the net traction force for cell pairs also sums to zero, indicating that each cell of the cell pair exerts an unbalanced traction force that is generated at the cell-cell junctions. Thus to determine cell-tugging forces between cell A and cell B ($F_{AB}$), cell-cell boundaries were first determined by β-catenin staining, the total traction force underneath each cell was calculated ($\Sigma|F_A|$ and $\Sigma|F_B|$), and the tugging force was measured as the absolute sum of the force divided by 2 ($F_{AB}= (\Sigma|F_A|+\Sigma|F_B|)/2$) as previously reported (Liu et al., 2010).

Statistical Analysis

Data presented here represents results from three replicate experiments and error bars show the standard error of the mean. Student t-test was performed using Stata (StatCorp).

**Results**

MID1ΔCTD cells generate less tugging force than control cells

In this study, microposts were used to measure the tugging force between pairs of cells. Specifically, stable MDCK cells expressing either GFP-MID1ΔCTD or GFP alone (generated by Huang and Cox, unpublished data) were seeded onto laminin-coated microposts arrays at a low density. Cells were allowed to adhere onto microposts, and develop cell-cell junctions over a time period of 72 hours. At

16 hours prior to fixing cells, cells were serum starved by replacement of cell culture media with low serum DMEM (0.1%) to coordinate cell cycle and eliminate interfering exogenous cell signals resulting from the serum. Cells were fixed and stained for β-catenin. Images of cell pairs and their corresponding post deflections (δ) were captured by a Nikon Eclipse Ti inverted microscope using a 40X objective.

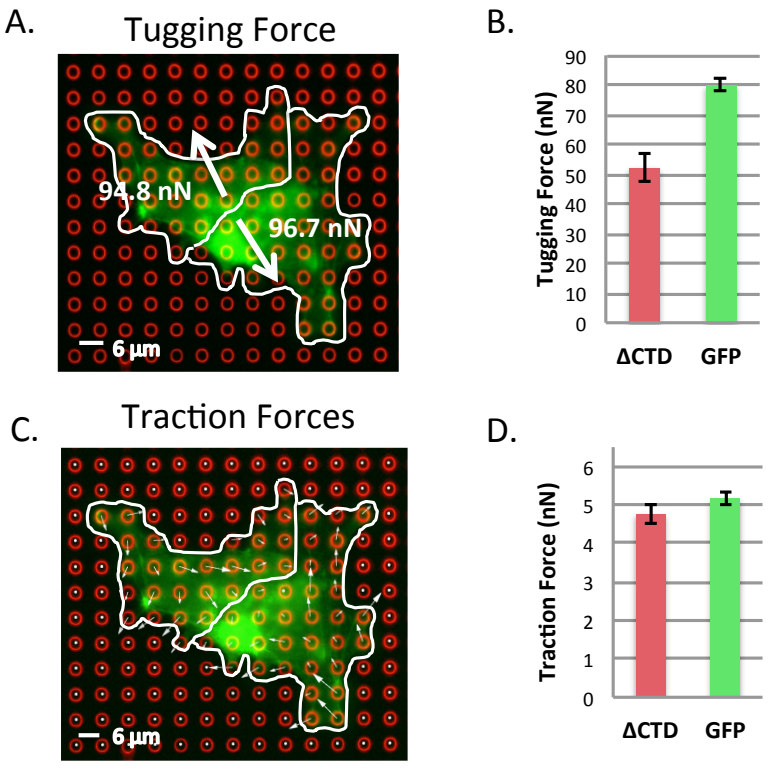


**Figure 3.2 MID1ΔCTD cells exert less force than GFP control cells.** **A.** Image of a pair of GFP control cells and tugging force generated by each cell. **B.** MID1ΔCTD cells had lower mean tugging value than controls (mean difference 27.9, 95% CI: -40.2 to -15.7; $p<0.01$ where n=3). **C.** Image of paired GFP control cells and the traction force vectors generated at each post. **D.** Difference in traction force between MID1ΔCTD and GFP controls was neither meaningful nor significant (mean difference 0.07, CI-0.68 to 0.54, $p=0.814$ where n=3). Error bars represent standard error of the mean.

Post deflections were measured and used to calculate cell forces at each post. For cell pairs in mechanical equilibrium, the magnitude of the traction forces should sum to zero. Thus the sum of the traction forces underneath a cell is balanced by the sum of the traction forces underneath its paired cell, and the tugging force is determined by the mean of the absolute value of the traction force generated by the paired cells (Figure 3.2A). In three replicate experiments, the average tugging force for paired MID1ΔCTD cells measured to be 52.1 ± 4.5 nN while GFP control cells exerted 80.0 ± 1.9 nN, and this difference was statistically meaningful (Figure 3.2B). Thus MID1ΔCTD cells exerted less tugging force than control cells expressing a wild type MID1 with a mean difference of 27.9 nN at a 95% confidence interval of -40.2 to -15.7 nN.

Decrease in tugging force suggests weakened cell-cell adhesion

The decreased tugging force observed in MID1ΔCTD cells may reflect both changes at the cell-ECM interface as well as altered cell-cell adhesion. It is expected that MID1ΔCTD cells would have less force at adhesions formed at the laminin-cell interface, given cell adhesion assays showed that MID1ΔCTDs adhere less well on laminin and polarized MID1ΔCTD cells showed irregular staining for focal adhesion kinase, a marker for cellular adhesion to its ECM (Huang and Cox, unpublished data). At the same time, it is also likely that tugging forces in MID1ΔCTD cells are weakened by defects in cell-cell adhesion. Not only has it been found that polarized MID1ΔCTD cells displayed disorganized E-cadherin staining, an indication that cell-cell adhesion is abnormal (Huang and Cox, unpublished data), but also, in Xenopus

knockdown of both MID1 and MID2 (akin to expression of dominant negative MID1ΔCTD) showed a significant decrease in expression of the functioning cell-cell adhesion markers, C-cadherin, ZO-1, and β-catenin (Suzuki et al., 2010). In looking at traction forces, a measure of cell-ECM adhesion, the average traction force for MID1ΔCTD cells was 4.8 ± 0.3 nN per post, which was not statistically different than the traction force generated by GFP control cells, which averaged 5.2 ± 0.2 nN per post (Figure 3.2D). Since traction forces were similar in magnitude for MID1ΔCTD and GFP control cells it suggests that cell-ECM adhesion did not contribute significantly to the diminished tugging force of MID1ΔCTD cells or the MID1 complex does not contribute significantly to cell-basement membrane stability.

Tugging Force Relative to Spread Area

Tugging force relative to cell spread-area was also evaluated. It has been shown that cells with smaller spread areas exhibit less overall force (Han et al., 2012). Because MID1ΔCTD cells tend to be smaller than GFP control cells, tugging force relative to cell spread areas were compared to evaluate if the smaller size of MID1ΔCTD cells contributed to the diminished tugging force that was observed (Figure 3.3). For all cell pairs, tugging force increased in proportion to spread area at a slope that was not statistically different in MID1ΔCTD versus control cells (p-0.738) (Figure 3.3). However, when comparing cell pairs of similar sizes, MID1ΔCTD cells exhibited less tugging force than that of control cells. Thus, although MID1ΔCTD cells are in general smaller than GFP control cells, the size difference does not fully account for the decrease in tugging force. These results

indicate that defects in cell-cell adhesion in MID1ΔCTD cells contribute to the observed decrease in tugging force.

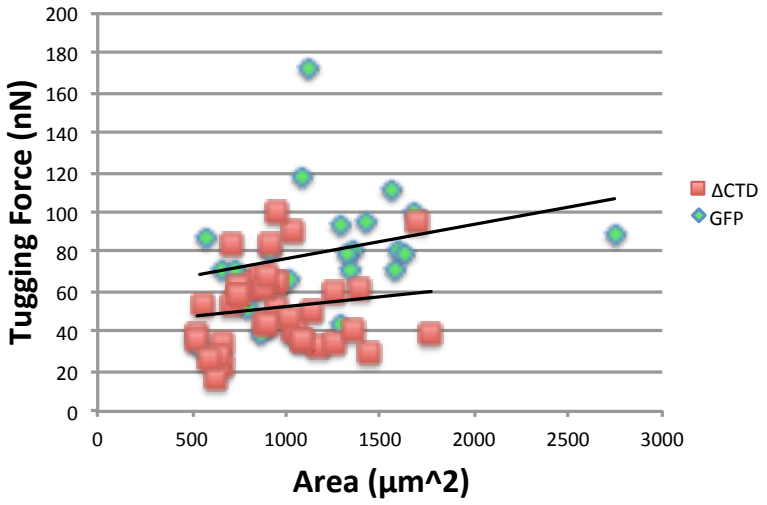


**Figure 3.3 Comparing Tugging Force versus Cell Size.** For both MID1ΔCTD and GFP cell pairs, tugging force increases with increased spread area at slopes that are not statistically different (p=0.738 where n=3). Further, for any given area, the elevation of lines shows that MID1ΔCTD cells exert less tugging force than control cells.

Force/Junction Length

In endothelial cells, where spread area is confined to a bowtie pattern, cell pairs form larger cell-cell junctions when tugging force is increased (Liu et al., 2010). At the same time, MDCK epithelial cells grown without constraints, showed no correlation between junction size and force (Maruthamuthu et al., 2011). In this study, cell-cell junctions were stained using an antibody against β-catenin, and junction length was measured along cell-cell contacts as indicated by staining.

When comparing the tugging force per junction length, MID1ΔCTD cells and GFP control cells both showed that as force increased, junction length also increased, and moreover, there was no difference in the amount of force per length of junction for MID1ΔCTD cells versus control cells (fig 3.4A). However, the average junction length for MID1ΔCTD cells was smaller than that of GFP control cells (25.5 ± 8.7 μm versus 35.8 ± 12.3 μm respectively) (fig 3.4B). These results indicate that weaker cell-cell tugging forces in MID1ΔCTD cells as compared to control cells results primarily from shorter cell-cell junctions.

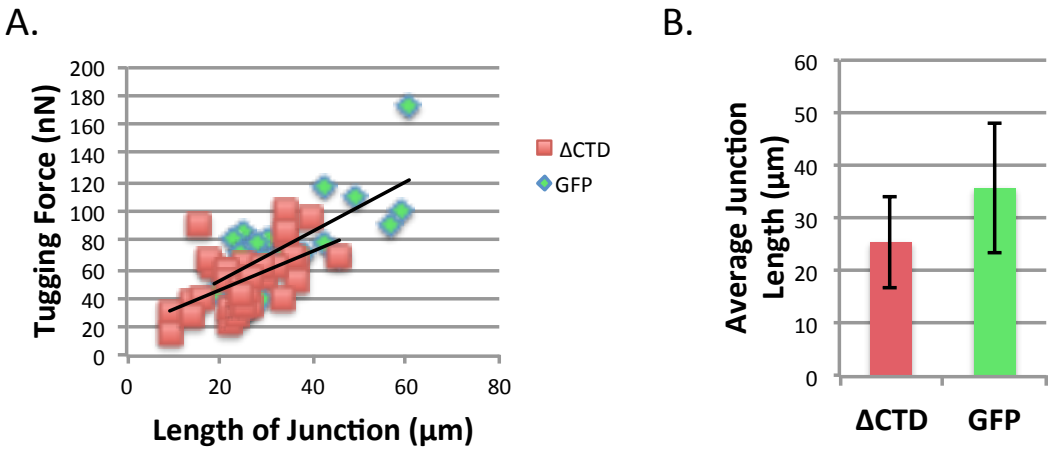


**Figure 3.4 Tugging Force and Junction Length.** **A.** For both MID1ΔCTD and GFP controls, the tugging force increased in direct proportion to length of cell-cell contacts at rates which did not differ significantly ($p=0.810$ where $n=3$). **B.** GFP-MID1ΔCTD cells averaged smaller cell-cell junctions compared to GFP controls with a mean difference of 10.24 μm, 95% CI: -15.3 to -5.2; $p<0.01$ where $n=3$.

**Discussion**

Mutant MID1 cells generate less tugging force.

Our initial studies indicate that MID1ΔCTD cells generate only ~65% as much tugging force as GFP control cells. These forces seem appropriate relative to previously reported cell-cell forces. In a dual pipette assay, E-cadherin adhesions required about 20 nN - 200 nN of force to separate cells depending on duration of adhesion (i.e. 30 seconds and 1 hour respectively) (Chu et al., 2004). Also in a study using microposts to look at migration of MDCK cells plated on fibronectin, the leading edge of cells generated around 2-3 nN of force (du Roure et al., 2005). While our studies show that our MDCK cells generated a slightly higher force per post (4-6 nN) than those reported by du Roure *et al*., our experiment was performed on posts with a stiffer spring constant (38.38 nN/μm) than that used by du Roure *et al*. (21.8 nN/μm). It has been demonstrated on microposts that average force is directly proportional to substrate stiffness (Han et al., 2012), thus the forces generated in our study are appropriate in scale, to those observed in MDCK migration assays (du Roure et al., 2005).

While the consequence of this decrease in force is not yet known, forces that have been reported to elicit cellular responses important in development are on scale with the difference in tugging forces (27.9 ± 4.9 nN) between the mutant, MID1ΔCTD cells and the GFP control cells. Weber *et al*. showed that application of 1.5 nN of force by 22.9 μm magnetic beads with C-cadherin could generate enough force on Xenopus mesodermal cells to elicit a morphological response. In the developing Drosophilia embryos, stomodeal cells experiencing 60 +/- 20 nN of force

stimulate the expression of the early embryo pattering gene, Twist (Desprat et al., 2008).

Shorter cell-cell junctions contributed to decreased force in mutant cells

When comparing the cell traction forces, which provide a measure of cell-laminin adhesion, MID1ΔCTD cells showed slightly less force that control cells, but at a level that was not statistically significant, indicating that in MID1ΔCTD cells, forces at cell-cell junctions, not cell-ECM adhesions, were responsible for the decrease in force. Previously Suzuki *et al*. found that in neuroepithelial cells, when MID1 and MID2 were knocked down by morpholinos, cells showed decreased expression of the junctional components, zonula occludins-1, β-catenin, and C-cadherin. Given that formation of adherens junctions depends on generation of tugging forces and moreover adherens junction size grows with increasing tugging force (Liu et al., 2010), it might be expected that MID1ΔCTD cells would exhibit smaller adherens junctions than control cells. Thus when cell junction length was measured, it was found that while force per junction length in mutant versus control cells was the same, the average length of cell-cell junctions in MID1ΔCTD cells was smaller than those of control cells. This indicates that decreased tugging force in MID1ΔCTD cells results from shorter cell-cell contact lengths. This was in contrast to work done by Maruthamuthu et al, which showed that in unconstrained MDCK cells tugging force was independent of cell-cell contact length, but instead grew in porportion to cell-ECM traction force (Maruthamuthu et al., 2011). At the same time, work by Liu et al showed a direct correlation between tugging force and

adherens junction size in endothelial cells confined to a bowtie pattern, leading Maruthamuthu et al. to propose that cell confinements determine whether junction size depended on tugging force or cell-ECM traction force ( Liu et al., 2010; Maruthamuthu et al., 2011). However, work presented here showed an interdependence of tugging force and junction length in unconstrained MDCK cells. A possibility that may account for this observation is that differences in ECM substrate can impact cellular response. Experiments in this chapter analyzed forces in cells plated on laminin whereas Maruthamuthu et al. utilized cells plated on collagen and fibronectin (Maruthamuthu et al., 2011). Both high confinement conditions and laminin, leading to an activation of Rac1, are required for the proper polarization of epithelial cells (Rodríguez-Fraticelli et al., 2012; Yu et al., 2005). Moreover, cells in low confinement are contractile and form large actin stress fibers and focal adhesions (Rodríguez-Fraticelli & Martín-Belmonte, 2013). These studies suggest that a cell's environmental context (high confinement/laminin or low confinement) may dictate whether or not cell tugging forces depend on junction size.

Possible linkage of MID1 to regulators of cell-cell junctions

It has been shown that cell-cell adhesion formed by cadherins play a central role in mechanotransduction (Ganz et al., 2006; Ladoux et al., 2010; le Duc et al., 2010; Plestant et al., 2014; Yonemura et al., 2010). These studies show that when MID1 is mutated, tugging forces at cell-cell adhesions are reduced, but how exactly MID1 regulates cell-cell adhesion remains unclear. However, Chapter 2 of this thesis identifies an interesting possibility; when overexpressed in 293T cells, MID1

is able to immunoprecipitate PLEKHA5, PLEKHA7 as well as p120 catenin, regulators of cell-cell adhesion. While at the same time, colocalization of MID1 with these proteins was not observed (fig 2.1 C and D), and suggests that these interactions may be indirect (possibly through endogenous MID2) and/or perhaps limited to the small microtubule fraction that is not visible by immunocytochemistry. Regardless of whether MID1 interactions are direct or indirect, it is reasonable to speculate that shorter cell-cell junctions leading to less tugging force in mutant MID1 cells may result from its association with these regulators of cell-cell adhesion. Whether MID1 functions as an E3 ubiquitin ligase to regulate the ubiquitination and possible degradation of PLEKHA5, PLEKHA7, and p120 or whether MID1 can regulate the phosphorylation of PLEKHA7 and p120 through their association with the phosphatase PP2A remains to be seen.

Future applications: Using microposts to evaluate role of MID2

Moreover, as the role of MID2 in cell adhesion emerges, characterizing its unique role - especially functions that are independent of MID1 - is difficult because the MID1 and MID2 proteins are so closely linked to one another through both direct binding as heterodimers and their overlapping cellular functions in the cell. For this reason, a knockdown of MID2 may not result in overt phenotypic changes because MID1 may likely compensate for its loss. As a result, standard assays that provide qualitative data such as migration assays, cell adhesion assays, and staining of cell adhesion proteins may not reveal the specific role of MID2 in cell adhesion. The work in this chapter indicates that future work utilizing micropost technology

may allow us to discriminate cell adhesion changes when either MID1 or MID2 is lost by knockdown or using a dominant-negative construct. Such an approach should allow testing to determine how various factors such as Alpha4/PP2Ac and PLEKHA5/PLEKHA7 rescue the observed changes in force.

## Chapter4: MID1 Knockout model of XLOS using CRISPR/Cas9

### Introduction

The aim of this chapter is to generate an in vitro model of X-linked Opitz syndrome that will clarify the role of MID1 in the cell. X-linked Opitz syndrome (XLOS) is caused by mutations in the Midline-1 (*MID1*) gene, which lead to loss of protein function (Cox et al., 2000). Although, mutations in *MID1* that result in XLOS occur throughout the length of the gene, a high percentage of the mutations occur in the C-terminal domain (Fontanella et al., 2008). Both point and insertion mutations have been identified in the C-terminal domain of MID1, some of which lead to early truncations (Fontanella et al., 2008). While the type of mutation found in the C-terminus varies, the phenotypic consequence of MID1 mutations in the C-terminus is the same; *MID1* mutations in the C-terminus disrupt the normal distribution of MID1 along the microtubules and instead it form aggregates in the cytoplasm (Cainarca et al., 1999; Cox et al., 2000; S Schweiger et al., 1999; Short & Cox, 2006). Cells overexpressing fluorescently labeled C-terminal deletions of MID1 not only form aggregates, like those seen in some patient cells, but also, mutant MID1 recruits endogenous MID1 to the ectopic aggregates (Cainarca et al., 1999; Cox et al., 2000; S Schweiger et al., 1999; Short & Cox, 2006). Furthermore, evidence supports the notion that aberrant cytoplasmic clumps of MID1 result in the loss of its E3 ubiquitin ligase activity on the microtubules (Du et al., 2013; Liu et al., 2001; Trockenbacher et al., 2001). MID1 is believed to be involved in the ubiquitination of the catalytic subunit of the cellular phosphatase PP2A (PP2Ac), and accordingly, these cells showed higher levels of hypophosphorylated proteins that are associated

with microtubules. (Trockenbacher et al., 2001). Although MID1 does not directly bind to PP2Ac, its regulation of PP2Ac is presumed to be mediated through Alpha4, a binding partner of MID1 and known regulator of PP2A (Short et al., 2002; Trockenbacher et al., 2001). This trimeric complex has also been shown to regulate the phosphorylation of MID1 which is shown to affect MID1 association to the microtubules (Liu et al., 2001).

Current *in vitro* model of XLOS-overexpression of dominant negative MID1ΔCTD

An *in vitro* model of XLOS in epithelial cells stably overexpressing a GFP-tagged, C-terminal deletion of MID1 (MID1ΔCTD) illuminates an even broader scope of the cellular role of MID1. MID1ΔCTD cell lines exhibit elevated levels of Alpha4, supporting biochemical studies that demonstrate MID1 E3 ubiquitin ligase activity also targets Alpha4 for degradation (Du et al., 2013; Du et al., 2014). Additionally, MID1ΔCTD stable cell lines display disrupted cell migration, possibly a reflection of the abnormal cell-cell and weakened cell-extracellular matrix adhesion displayed by these cells (Huang and Cox, unpublished data).

Considerations of existing *in vitro* model of XLOS

While this model has provided valuable insight into MID1 function (Du et al. 2013; Huang and Cox, unpublished), overexpression of dominant negative MID1ΔCTD in cells presents with the following considerations: 1. ) Although, C-terminal deletions are reported XLOS patient mutations, overexpression of MID1ΔCTD, itself, does not faithfully reproduce naturally occurring MID1 protein

levels represented in XLOS. 2.) MID1ΔCTD binds to endogenous MID2, presumably affecting MID2 function (Short et al., 2002), and although this may also occur in XLOS patient mutations, this model does not allow us to identify a role for MID2 in the cell that is independent of MID1. 3.) Protein overexpression itself may produce other unforeseen consequences; in particular, since MID1ΔCTD maintains its protein binding domains, it would be expected to exert a dominant negative effect on all of its protein binding partners (MID1 itself, MID2, MIG12, and Alpha4/PP2Ac) at protein levels that are artificially high. 4.) Over time, MID1ΔCTD cells lose expression of the mutant protein, and as a result, experimental design as well as interpretation can be impacted. 5.) Overexpression of MID1ΔCTD shows variable protein expression levels, even within cells from the same cell passage number, and this too can contribute to experimental variability.

MID1 knockout model of XLOS using CRISPR/Cas9

To circumvent these complicating factors, CRISPR (clustered regularly interspaced short palindromic repeats)/Cas9 (CRISPR associated nuclease 9) technology was used to develop an in vitro *MID1* knockout model that more accurately portrays the MID1 phenotype in XLOS patient cells. While C-terminal, *MID1* mutations are more prevalent than mutations in other domains of *MID1*, mutations have been reported throughout the length of MID1 except for the RING finger (Fontanella et al., 2008). Like mutations in the C-terminal domain, which ultimately impacts MID1 function, mutations in other regions can also be detrimental to MID1 function. For example, a XLOS patient mutation leading to an

amino acid substitution in the B-box 1 domain, reduced MID1 binding to Alpha4 (Schweiger & Schneider, 2003). Additionally, whole gene deletions of MID1 have been described in three cases of XLOS (Fontanella et al., 2008). Thus, with the advent of CRISPR/Cas9 technology for targeted genome editing, we sought to generate a MID1 knockout cell line that would be more representative of the cellular context that exists in XLOS.

CRISPR/Cas9

The CRISPR/Cas9 system is part of the CRISPR Type II adaptive immune system that allows bacteria to recognize and target foreign nucleic acids for destruction, however, its recent introduction as a tool for targeted gene editing has transformed the way we study and understand disease. Cas9 is an endonuclease that can create DNA double strand breaks at sites specified by CRISPRs (Jinek et al., 2012). When DNA double strand breaks occur, they are repaired by homology directed repair, if donor sequence is available, or non-homologus end joining (NHEJ), where insertions and deletions can be introduced and lead to a premature termination codon (Ran et al., 2013). CRISPRs encode for RNA is that comprised of a trans-activating RNA and a guide RNA (Jinek et al., 2012). The trans-activating RNA binds to Cas9 and hybridizes with the guide RNA (Jinek et al., 2012) . The guide RNA directs this complex and Cas9 endonuclease activity to specific DNA sequences, which are complementary to the guide itself (Jinek et al., 2012). In recent years, groundbreaking studies have shown how CRISPR/Cas9 can be adapted to generate user-specified, genetic modifications of virtually any sequence in any organism,

making genetic engineering a simple and accessible process that has and will propel research forward in remarkable ways.

In this chapter, CRISPR/Cas9 technology was used to target and generate a double strand break in the first coding exon of MID1. Through NHEJ a double strand break in the DNA can be repaired to its original sequence, but often repair of the break introduces an insertion or deletion mutation (indel) (Ran et al., 2013). A consequence of indel mutations can be the introduction of an early termination codon, which can ultimately code for mRNA transcript that will be degraded by nonsense mediated decay or code for a non-functional protein. Using a MID1-targeted CRISPR/Cas9, this chapter describes the generation of MID1 knockout cell lines as well as the preliminary phenotypic characterization of these cells.

## Materials and Methods

### Cell culture

Madin Darby canine kidney cells (MDCK) were maintained in DMEM with sodium pyruvate (Cellgro) supplemented with 10% FBS (Cellgro), and 2 mM GlutaMax (Gibco). Cells were plated in vented flasks or dishes treated for tissue culture and cultured at 37˚C with 5% $CO_2$. To maintain cells in culture, cells were passaged every 2-3 days. To passage cells, medium was aspirated from cells and cells were washed with 1X PBS without calcium or magnesium. TrypLE Express (Life Technologies) was added to cell culture dishes to ensure coverage of cell monolayers. Cells were incubated at 37˚C until cells detached as observed using an inverted microscope. Detached cells were resuspended in pre-warmed complete

DMEM. Cells were pelleted by centrifugation at 200 g for 5 minutes. Cells were resuspended in complete DMEM and split to maintain lines. To freeze cell lines, cells were detached from plates as described above. Cells were pelleted by centrifugation (200 g, for 5 minutes) and resuspended in freezing media (95% Complete DMEM and 5% DMSO). Resuspended cells were alliquoted in cryovials and frozen overnight at -80˚C using a freezing container filled with isopropyl alcohol. For long-term cell storage, cryovials were transferred to liquid nitrogen.

Generation of MID1 knockout cells using CRISPR/Cas9

Online CRISPR design tools (http://tools.genome-engineering.org and http://www.e-crisp.org) were used to identify targets in the first coding exon of MID1. Potential target sequences were ranked for specificity and predicted off-target sites. From the results, the top ranking target site was used to generate oligonucleotides to be cloned into the sgRNA/Cas9 expression plasmid, pSpCas9(BB)-2A-GFP (Addgene plasmid ID: 48138), which is the expression construct published by Feng Zhang's group at MIT. Following their published protocol (Ran et al., 2013), custom oligos were ordered: MID1(134)bottom-5'AAACACGAGTCTGTGGAGTCCATC 3' and MID1(134) top- 5' CACCGATGGACTCCACAGACTCGT 3' (Eurofins). Oligos were diluted to 100 μM, phosphorylated then annealed. Annealed oligos were ligated into pSpCas9(BB)-2A-GFP, which had previously been digested with BbsI (NEB) and gel purified. The cloned plasmid was named pX458_MID1(134). pX458_MID1(134) was transformed into TOP 10 E.coli (Invitrogen) and grown on LB plates supplemented with

ampicillin. Colonies grown on plates were PCR screened for plasmids containing oligo-inserts by PCR amplification using a forward primer which anneals to the U6 promoter region of pSpCas9(BB)2A-GFP (U6Long-5'GGACTATCATATGCTTACCGTAACTTGAAAG 3') and the reverse primer which anneals to the sgRNA oligo (MID1(134)bottom). pX458_MID1(134) was then verified by sequencing from U6 promoter.

Sequence verified pX458_MID1(134) was transfected into MDCK cell lines using Polyjet reagent (Signagen) as directed by manufacturer. One day (24 hours) post-transfection, cells were detached, pelleted, and resuspended in FACS sorting media. GFP-positive, single cells were sorted into a 96-well plate (1 cell/well). Cells were incubated at 37˚C/5% $CO_2$ and cells media was replaced with fresh complete DMEM supplemented with penicillin-streptomycin every 3-5 day as needed. Each well of the 96 well-plate was monitored for cell growth and "clonal" appearance in which cells appeared to be radiating from a central point. Wells that appeared to be growing from multiple clones were eliminated. Cell clones were expanded for genotyping and maintenance.

Genotyping of MDCK cell clones

MDCK cell clones, which had previously been transfected with pX458_MID1(134), were expanded in a 6-well dish. When cells reached approximately 65-85% confluence, cells were detached using TrypLE and centrifuged at for 5 minutes X 250 g. Cell pellets were collected and genomic DNA was isolated from cells using DNeasy Blood and Tissue Kit (Qiagen). Genomic DNA

concentration was determined using UV spectrophotometer and diluted to 90 ng/mL. PCR amplification using a high fidelity polymerase was used to amplify MID1 genomic DNA in the region that is targeted by our MID1 CRISPR/Cas-9 expression plasmid, pX458_MID1(134). PCR products were submitted for sequencing through SimpleSeq (Eurofins, Operon) to determine effect of MID1 gene sequence that resulted from targeting by CRISPR/Cas-9.

RNA isolation and cDNA synthesis

RNA was isolated from cells grown in a 6-well dish to approximately 75-90% confluence. Cells were detached and pelleted by centrifugation for 5 minutes at 500 x g. To isolate RNA, cells were processed using SV Total RNA Isolation System (Promega). RNA concentration was determined using UV spectrophotometer (NanoDrop 1000, NanoDrop Technologies). RNA was stored at -80˚C for downstream applications. To generate cDNA, 1 µg RNA was reverse transcribed using High Capacity cDNA Reverse Transcription Kit (Applied Biosystems). cDNA was stored at -20˚C for subsequent applications.

Protein concentration determination

Protein concentrations were determined using Bradford reagent (BioRad). Bradford reagent was warmed to room temperature for 20 minutes prior to use. Protein standards were made from serial dilutions of BSA at 2 mg/mL and used at a range of 0.125 mg/mL to 2 mg/mL. Unknowns were diluted 1:10 in $H_2O$. Samples were mixed with Bradford reagent at a ratio 1:50 and plated in triplicate on a

microplate. Plate was incubated at room temperature for 20 minutes then absorbance was measured at 595 nm using a plate reader.

Western blot

Protein samples were prepared by diluting 20-30 µg cell lysate in Laemmli – SDS loading buffer. To denature protein, samples were heated at 95˚C for 5 minutes. Next, samples were loaded in wells of a SDS-PAGE gel and run in BupH Tris-HEPES-SDS running buffer (Pierce) at 87 V for 1 hour. Proteins were transferred onto PVDF membrane by wet transfer. After transfer, membranes were blocked for 1 hour at room temperature in 5% non-fat dried milk dissolved in TBS-T (w/v). After blocking, blots were incubated in primary antibody solution made up as directed by the antibody manufacturer. Rabbit anti-MID1(Bioworld) was diluted 1:1000. Mouse-anti-cMyc [9E10] (Abcam) was diluted 1:1000. After incubation with primary antibody, blots were washed 3X in TBS-T for 5 minutes/wash. Blots were then incubated with HRP-conjugated secondary antibody solution for 30 minutes at room temperature. Blots were next washed 3X in TBS-T for 10 minutes/wash and the signal was developed using a chemiluminescent reagent (West Pico from Pierce or Femto from Pierce diluted 1:5 in water). Chemiluminescence was detected through exposure to x-ray film.

Digital Western Blot using Protein Simple

Digital Western blot was performed using Simon (12-180 kDa) Master Kit (ProteinSimple, Santa Clara, CA). Western blot was performed as directd by manufacturer.

c-Myc-tagged immunoprecipitation and co-immunoprecipitation-

Cells overexpressing proteins tagged with c-Myc were immunoprecipitated using the Pierce c-Myc-tagged immunoprecipitation kit (Thermo Scientific), and immunoprecipitations were carried out as recommended by manufacturer. Briefly, cells overexpressing proteins tagged with c-Myc were rinsed in cold TBS and lysed using M-PER lysis buffer prepared with protease inhibitor (1 µL/100 µL lysis buffer). Lysis was allowed to proceed for 5 minutes on ice. Lysis reactions including cell debris were transferred to cold microcentrifuge tubes and centrifuged for 15 mins X 14,000 rpm at 4˚C. Supernatants were transferred to clean tubes. Protein concentrations were determined by Bradford assay and 300-500 µg total protein was combined with anti-c-Myc agarose beads in spin columns provided in the kit. Samples were incubated overnight at 4˚C with end-over-end mixing. Samples were pulse centrifuged and flow through was saved for analysis. Anti-c-Myc agarose beads and proteins bound to beads were retained in spin columns and washed 3X with cold TBS with 0.05% Tween-20. Proteins tagged with c-Myc and protein binding partners were eluted with 2X non-reducing sample buffer at 95˚C. After elution, 1.5 µL BME was added to each sample to denature proteins. Samples were

loaded and run onto 8-16% SDS page gels, transferred to PVDF membranes, and analyzed by western blot.

QPCR

Primers used in QPCR were validated to determine Ct value, slope, and efficiency. RNA was extracted from MDCK clonal cell lines and converted to cDNA to determine MID1 transcript levels relative to the housekeeping gene, 40S ribosomal protein 5S (RPS5). QPCR reactions were performed using SensiMix™ SYBR Low-ROX Kit (Bioline). All samples were run in duplicate, and each 20 µL reaction used 20 ng cDNA (assuming 100% RNA to cDNA conversion). MID1 primers were used at a final concentration of 250 nM while RPS5 was used at a final concentration of 400 nM (for primer sequences, see Table 1). Relative quantification analysis was performed using the $2^{-\Delta\Delta C_T}$ method (Livak & Schmittgen, 2001).

Immunocytochemistry

Cells were grown on #1.5 coverslips pre-treated as follows: Coverslips were acid washed and coated with poly-L-lysine (Sigma) overnight at 4˚ C with rocking. Coverslips were next washed 10X in $ddH_2O$ then rinsed in 100% ethanol and allowed to dry in a sterile incubator. Dried coverslips were stored at 4˚C for several months until needed. To prepare cells for imaging, coverslips were washed and fixed at RT for 10 minutes in 4% paraformaldehyde, 1% sucrose in PBS. Cells were permeabilized in 0.2% Triton-X-100 and blocked in 10% NGS at RT in humidifying chamber for 1 hour. rhodamine phalloidin (Cytoskeletal Inc.) was used to stain F-

actin at a concentration of 100 nM for 30 minutes. Cell nuclei were stained with DAPI (100 ng/mL diluted in PBS) for 5 minutes at RT in the dark. Coverslips were mounted on slides using Vectashield mounting medium with DAPI. Slides were imaged using a 40X oil immersion lens on Leica TCS SP5 Confocal System.

Cell adhesion assay on laminin-1

Natural mouse laminin-1 (Invitrogen) was diluted to 5.8 µg/mL in PBS. Fifty µL diluted laminin-1 was used per well of 96-well plate to coat the plate overnight at 4˚C. Uncoated wells were reserved for negative control wells. After incubation, wells were washed 2X in washing buffer (0.1% BSA in PBS, filter sterilized) and blocked with 150 µL blocking buffer (1% BSA in PBS, filter sterilized) at 37˚C for 60 minutes. While blocking, cells were serum starved in DMEM with 0.1% FBS for 30 minutes at 37˚C and 5% $CO_2$. After blocking, the plate was washed 1X in washing buffer and chilled on ice until cells were readied for plating. Cells were detached using TrypLE (Life Technologies) and resuspended in DMEM containing 10% FBS. Cells were pelleted by centrifugation for 5 minutes X 250 g. Cells were washed 1X in DMEM, 0.1% FBS, then re-suspended at a concentration of $4.0 \times 10^5$ cells/mL DMEM, 0.1% FBS. Cell clones were plated in triplicate using 50 µL of cells/well. Cells were incubated at 37˚C/5% $CO_2$ for 60 minutes. After incubation, cells were decanted and the plate was washed 3X in washing buffer with gentle shaking. Cells that remained on plate were fixed with 4% paraformaldehyde for 10 minutes at room temperature. Plate was washed and allowed to dry completely. Crystal Violet was used as a colorimetric readout of cells that remained attached to plate by adding 50 µL of

Crystal Violet (5 mg/mL in 2% EtOH) per well of a 96-well plate. The plate was incubated at RT for 30 minutes and read on a plate reader at 550 nm.

## Results

Generation of mutant MID1 cell lines

The goal of this chapter was to develop a MID1 knockout cell line, which reflects actual patient whole gene deletions identified in X-Linked Opitz syndrome (XLOS), to better understand how XLOS pathologies arise when MID1 is lost. Work by Huang et al highlights the importance of MID1 in regulating epithelial behavior using Madin Darby canine kidney epithelial cells that overexpress a GFP-labeled, dominant negative mutant MID1 protein (MID1ΔCTD) (Huang and Cox, unpublished). To generate our MID1 knockout lines, MDCKs stood out as an ideal candidate cell line. Not only has the effect of MID1ΔCTD overexpression in these lines been evaluated by Huang (Huang and Cox, unpublished), but also, compared to the MCF10A epithelial cell lines that were considered, maintenance of cell cultures and cell doubling time in MDCKs provided significant advantages. Before generating MID1 knockouts, the expression of *MID1* transcript in MDCK cells was validated by RT-PCR (Chapter 2, figure 2.2A).

To generate a MID1 knockout cell line, an sgRNA was designed to target the region of MID1 coding for residues 134-153 contained in the first coding exon of MID1 (MID1-134) (Figure 4.1A). The MID1 sgRNA target sequence was designed using the CRISPR design tool E-CRISP (ecrisp.org), which ranks potential sgRNA sequences by accounting for specificity and potential off targets (Heigwer et al.,

2014). MID1-134 was next cloned into pSpCas9(BB)-2A-GFP, an GFP-expression cassette that contains dual promoters to express the custom designed sgRNA as well as the Cas9 endonuclease (Ran et al., 2013). This expression plasmid was then transfected into MDCK cells. DNA cleavage of the MID1 target region by CRISPR/Cas9 was verified using a T7 endonuclease assay. To generate clonal stable cell lines, transfected cells that were GFP positive, indicating expression of MID1-134 sgRNA/Cas9, were sorted into single wells of a 96-well plate and expanded. From clonal cell cultures, genomic DNA was isolated, amplified, and sequenced for MID1 mutations in the region targeted by MID1-134 sgRNA/Cas9. Two of the 10 clones were found to have no MID1 mutations and were maintained as "wild-type" controls. These clones were termed MID1-WT 1.4 and MID1-WT 1.5 (Figure 4.1B). One of 10 clones (MID1ΔRING 1.3) resulted in an in-frame, 21 bp deletion that codes for amino acid residues 46-52 of the MID1 RING domain (Figure 4.1C). Two of the 10 clones sequenced showed noisy sequencing results indicating clones were heterozygous or that the DNA isolated was non-clonal and represented sequence from more than one clone (not shown). Five out of ten clones sequenced possessed the same genetic modification. In these clones, an adenine was inserted at position 137, and this frame shift mutation lead to an early termination codon 292 base pairs 5' of the exon splice junction (Figure 4.1D). Early termination codons located at least ~50-54 bp 5' of an exon splice junction are expected to elicit the cell's nonsense mediated decay (NMD) pathway, which eliminates transcripts with premature stop codons (Silva & Romão, 2009; Winter et al., 2004). Thus it was expected that the MID1 transcript generated from these 5 clones would be degraded

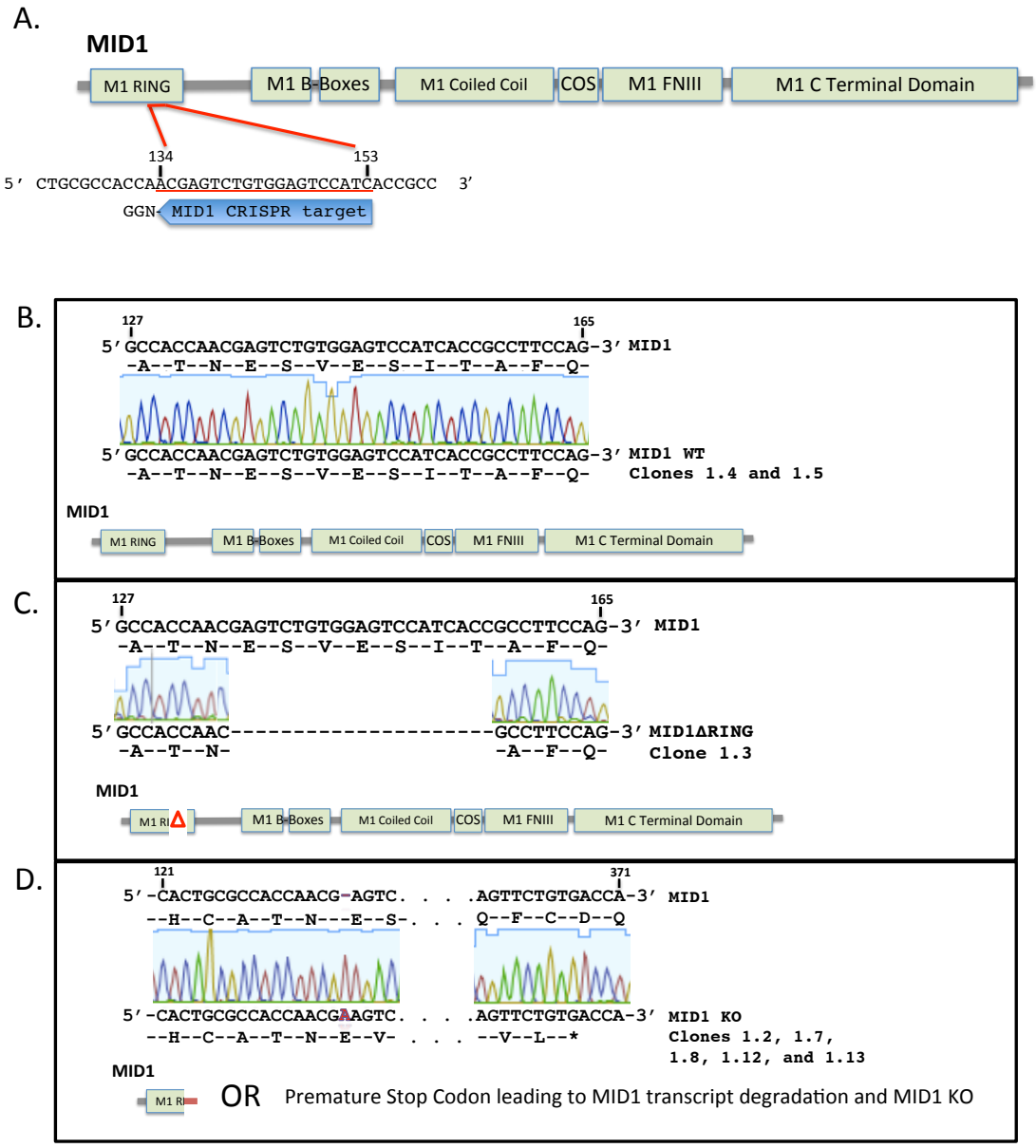


**Figure 4.1 MID1-134 sgRNA/Cas9 Targets MID1 RING domain to generate different cell clones. A.** Schematic diagram MID1 protein domains highlighting region of MID1 RING domain targeted by MID1-134 sgRNA/Cas9 **B.** Sequencing result from 2 clones that resulted in no mutation (MID1 WT 1.4 and MID1 WT 1.5) **C.** Sequencing result from 1 clone resulting in an inframe, 21 bp deletion (MID1ΔRING 1.3) **D.** Sequencing result of 5 clones possessing 1 bp (A) insertion leading to a premature stop codon (MID1 KO 1.2, MID1 KO 1.7, MID1 KO 1.8, MID1 KO 1.12, and MID1 KO 1.13).

by the cell's NMD pathway and therefore represent a MID1 knockout phenotype. The five clones (MID1 KO 1.2, MID1 KO 1.7, MID1 KO 1.8, MID1 KO 1.12, and MID1 KO 1.13) were therefore named according to their expected phenotype and clone number.

Validation of MID1 knockout by Western blot and QPCR

Western blots and QPCR were used to determine if clones represented true knockouts. Initially by western blot, when probing for MID1, MID1 was detected in cell lysates from human embryonic kidney 293T cells but not in MDCK cell lysate. This suggested the possibility that the antibody, which had been shown to have reactivity to human, mouse, and rat, but not dog, did not detect canine MID1. Alternatively, it meant that either MID1 was not present in MDCK cells, or MID1 levels were too low to detect by this method. The antibody used in the blot was generated against a synthetic peptide corresponding to amino acids 71-120 of human MID1. Given that human and canine MID1 share 100% amino acid identity in this region, it was expected that this antibody would detect MID1 in MDCK cells. Also, given that MID1 transcripts are detected in MDCK cells, it seemed likely that MID1 was present but in low levels. To concentrate MID1 in cell lysates, cell cultures were expanded to 85% confluence in 10 cm dishes. Cells were then transfected to overexpress the MID1 binding protein, Alpha4 (tagged with Myc), and afterwards, MID1 was co-immunoprecipitated with Myc-Alpha4. Using this technique, MID1 was detected in MDCK cell lysates as well as in the wild type control, MID1 WT 1.4, but not in cell clones with early MID1 truncations (MID1 KO

1.2, MID1 KO 1.7, MID1 KO 1.8, MID1 KO 1.12, and MID1 KO 1.13), indicating that MID1 knockout cell lines had successfully been generated (Figure 4.2A).

A.

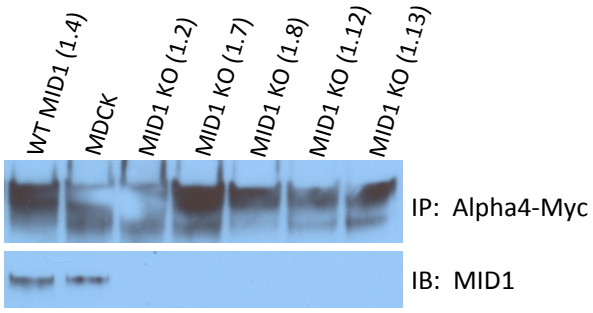


B.

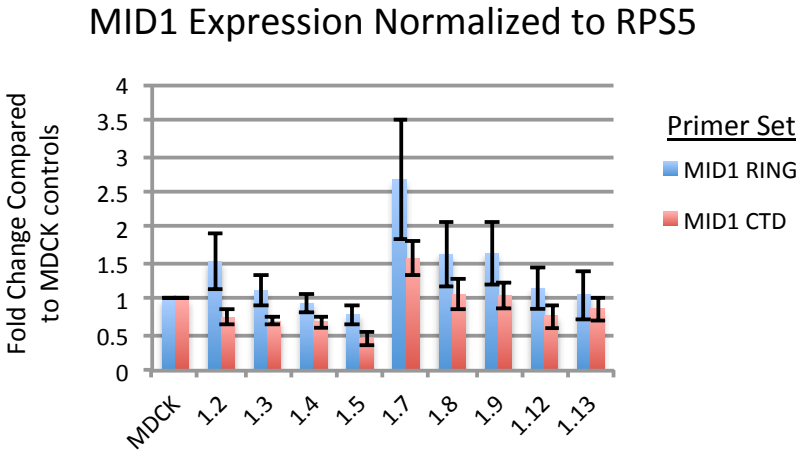


**Figure 4.2 MID1 protein not detected in MID1 KO clones, but MID1 transcript levels vary depending on clone.** **A.** Immunoprecipitation of C-myc from cell lysates derived from transfections using Myc-tagged Alpha4 (a known MID1 binding partner) show absence of MID1 in MID1 KO clones **B.** QPCR from 3 different experiments with duplicate runs for each sample shows that MID1 transcript is present at levels similar to or higher than MDCK control cells depending on cell clone. Error bars represent standard deviation of the mean.

QPCR was also used to analyze *MID1* transcript levels. Eukaryotic cells use nonsense mediated mRNA decay as a surveillance system to eliminate transcripts harboring mutations that would otherwise code for truncated proteins (Silva & Romão, 2009) and it is believed that MID1 transcripts harboring premature stop codons can elicit this pathway (Winter et al., 2004). Thus, it was expected that MID1 knockout lines, generated from an early MID1 termination codon, would have reduced MID1 transcript levels. However, this was not the case. MID1 transcripts were quantified using two sets of primer pairs. One primer pair (MID1 RING) amplifies the 5' end surrounding the MID1 knockout region, and one pair (MID1 CTD) amplifies exon 7/8 at the 3' end. For clones MID1ΔRING 1.3, MID1 WT 1.4, MID1 WT 1.5, MID1 KO 1.12, and MID1 KO 1.13, levels of *MID1* transcripts, relative to the housekeeping gene RPS5, were comparable to MDCK control cells (Figure 4.2B). Clones MID1 KO 1.2, MID1 KO 1.8 and MID1 KO 1.9 showed approximately 1.5 fold increase over MDCK control cells in MID1 transcript levels using the primer pair, MID1 RING, while they showed similar levels of transcript, relative to controls, using the primer pair MID1CTD (Figure 4.2B). Clone MID1 KO 1.7 showed a ~2.5-fold and ~1.5 fold increase in transcript levels relative to controls using primers MID1RING and MID1CTD respectively (Figure 4.2B). In summary, depending on the cell clone, QPCR results indicated the persistence of MID1 mRNA at similar or higher levels relative to MDCK controls.

Phenotypic Characterization of MID1 knockouts.

Initial characterizations of MID1 knockout cell lines show an inconsistent phenotypic presentation. To assay functional consequences of MID1 knockouts, protein levels of alpha4 and PP2Ac were quantified. MID1 acts as an E3 ubiquitin ligase to target alpha4 and PP2Ac for degradation (Du et al., 2013; Liu et al., 2011; Trockenbacher et al., 2001), so it would be expected that knockout of MID1 would result in increased levels of both alpha4 as well as PP2Ac. However, in initial immunoblot studies of knockout and control lines, this was not the case. In general, alpha4 levels relative to β-actin varied depending on the clone (Figure 4.3A). While MID1 knockout clones, 1.8 and 1.7, showed levels of alpha4 protein that were comparable to that of controls, MID1 knockout clone 1.2 showed approximately a four-fold increase in alpha4 over that of control cells (Figure 4.3A), although this increase may in part be attributed to the low intensity of B-actin loading control of this sample, which may have resulted from a processing artifact, and in support of this, our controls also did not show expected levels of alpha4; MID1ΔCTD control cell lines A4 and D5 did not show elevated levels of alpha4 as compared to wild-type MID1, GFP control cells (D5 GFP) (Figure4.3A). Unlike alpha4 quantification, quantification of PP2Ac was done using digital western blot, which eliminates developing errors and thus makes quantification more accurate. PP2Ac levels as determined by digital western blot found varying protein levels (relative to β-actin) that was not dependent on MID1 phenotype (Figure 4.3B). Contrary to expectations, in general PP2Ac levels were slightly lower in MID1 knockout clones as compared to control lines, with exception of the control overexpressing GFP (previously

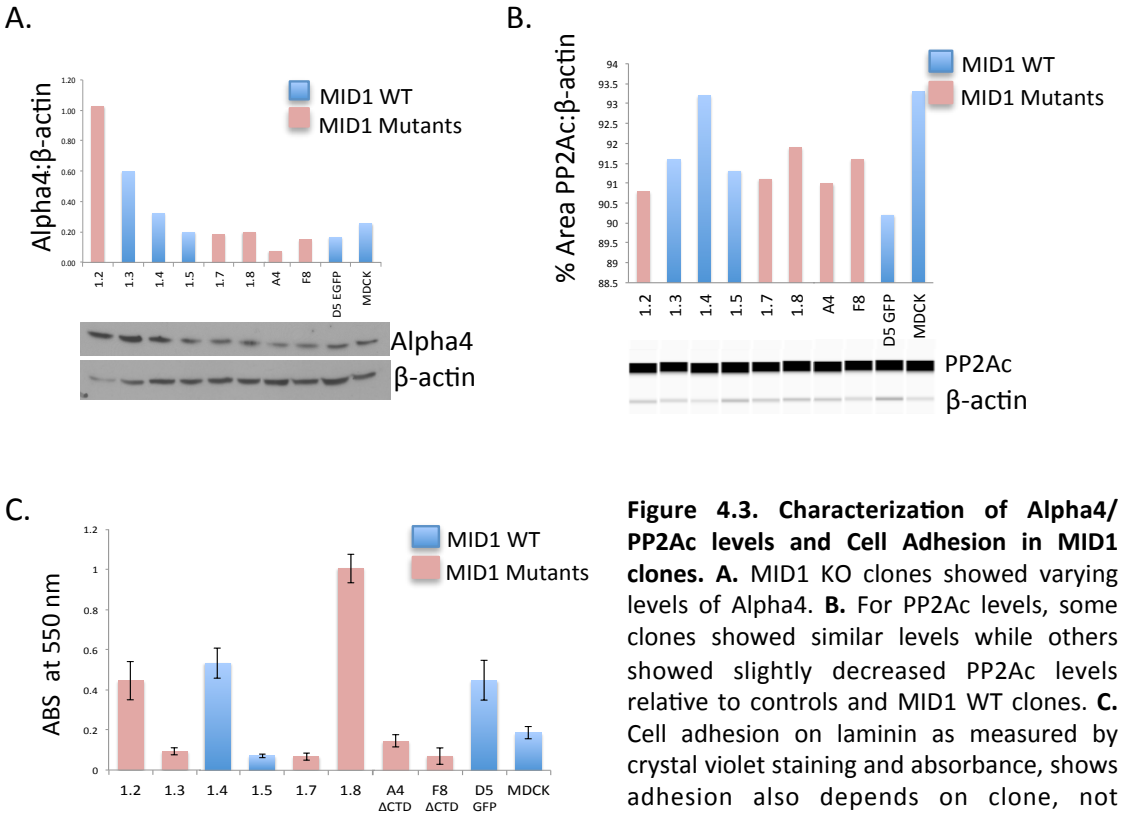


**Figure 4.3. Characterization of Alpha4/ PP2Ac levels and Cell Adhesion in MID1 clones. A.** MID1 KO clones showed varying levels of Alpha4. **B.** For PP2Ac levels, some clones showed similar levels while others showed slightly decreased PP2Ac levels relative to controls and MID1 WT clones. **C.** Cell adhesion on laminin as measured by crystal violet staining and absorbance, shows adhesion also depends on clone, not genotype.

generated by Huang and Cox, unpublished). When comparing PP2Ac levels between controls MID1ΔCTD A4 and MID1ΔCTD F8 to D5 GFP controls, PP2Ac levels are approximately double in MID1 mutants. However, in wild-type MDCK cells, which were used to derive all cell clones, PP2Ac levels are approximately 2X higher than that of the D5-GFP wild-type controls, suggesting that the differences in PP2Ac levels observed here might be insignificant.

Cell-ECM adhesion of the MID1 knockout cell lines was also tested. Work by Huang and Cox, indicates that MDCK cells overexpressing MID1ΔCTD show delayed adhesion to the extracellular matrix protein, laminin (Huang and Cox, unpublished).

To test cell adhesion to laminin using the MID1 knockout lines, serum depleted knockout and control cell lines were plated into wells of a 96-well dish, which was precoated with laminin. Each cell line tested was plated in triplicate using 2.0 X $10^4$ cells per well. After allowing cells to adhere for 60 minutes, unattached cells were washed from plates. Cells that remained attached to laminin-coated wells were quantified by crystal violet staining. Unlike cells overexpressing MID1ΔCTD (A4 and F8) which show decreased adhesion as compared to GFP controls, both MID1 knockout and control lines showed varying adhesion to laminin that was dependent on clone rather than MID1 phenotype (Figure 4.3C). Additionally, when comparing MDCK controls, which represent the non-clonal cell populations used to derive the MID1-targeted CRISPR/Cas9 cell clones as well as the overexpression cell clones (MID1ΔCTD and GFP controls, generated by Huang and Cox, unpublished), it can be seen that MDCK cell controls show adhesion levels to laminin that are more similar to MID1ΔCTD mutant cells than they are to GFP control cells. One possibility that may account for this observation is that heterogeneity within the original MDCK cell population contributes to the variability in cell phenotype seen in clonal cell lines.

Adhesion to laminin ECM was not the only assay to demonstrate that MID1 knockout clones do not reproduce the cellular phenotype characterized by cell lines overexpressing MID1ΔCTD. In polarized, MDCK cells, overexpressed MID1ΔCTD cells show increased intensity of actin staining at the basal membranes of mutant cells as compared to control cells overexpressing GFP alone (Huang and Cox, unpublished). To evaluate actin fiber formation relative to control lines, GFP positive MDCK control cell lines generated by Huang and Cox were mixed and plated

with our MID1 knockout cell lines, which were no longer GFP positive (Huang and Cox, unpublished data). Cells were seeded at a high density and cultured for two days. Afterwards, cells were fixed and F-actin was labeled with fluorescently conjugated rhoadamine phalloidin. Images of F-actin were captured by confocal microscopy. For each image, pixel intensity was determined on a line drawn orthogonal to the direction of actin fibers and across the width of a cell (drawn in yellow, Figure 4.4). Unexpectedly, MID1 KO cell clone did not show differences in actin over GFP control cells, as measured by pixel intensity across the cell. Likewise, MID1 WT and MDCK cells also showed similar actin staining as compared to GFP control cells. Unexpectedly, F8-MID1ΔCTD cells showed slightly decreased levels of actin staining relative to MDCK control cells (Figure 4.4). While this may seem contrary to previous work done by Huang and Cox that showed increased actin fiber formation in MID1ΔCTD cells, work done in these studies did not look at actin formation in polarized cells. Work as done by Huang and Cox looked at actin stress fiber formation in the basal domain of polarized cells (Huang and Cox, unpublished data), where signaling events associated with apico-basal polarity are known to impact actin polymerization (O'Brien et al., 2001; Yu et al., 2005), where as work shown here was in non-polarized cells.

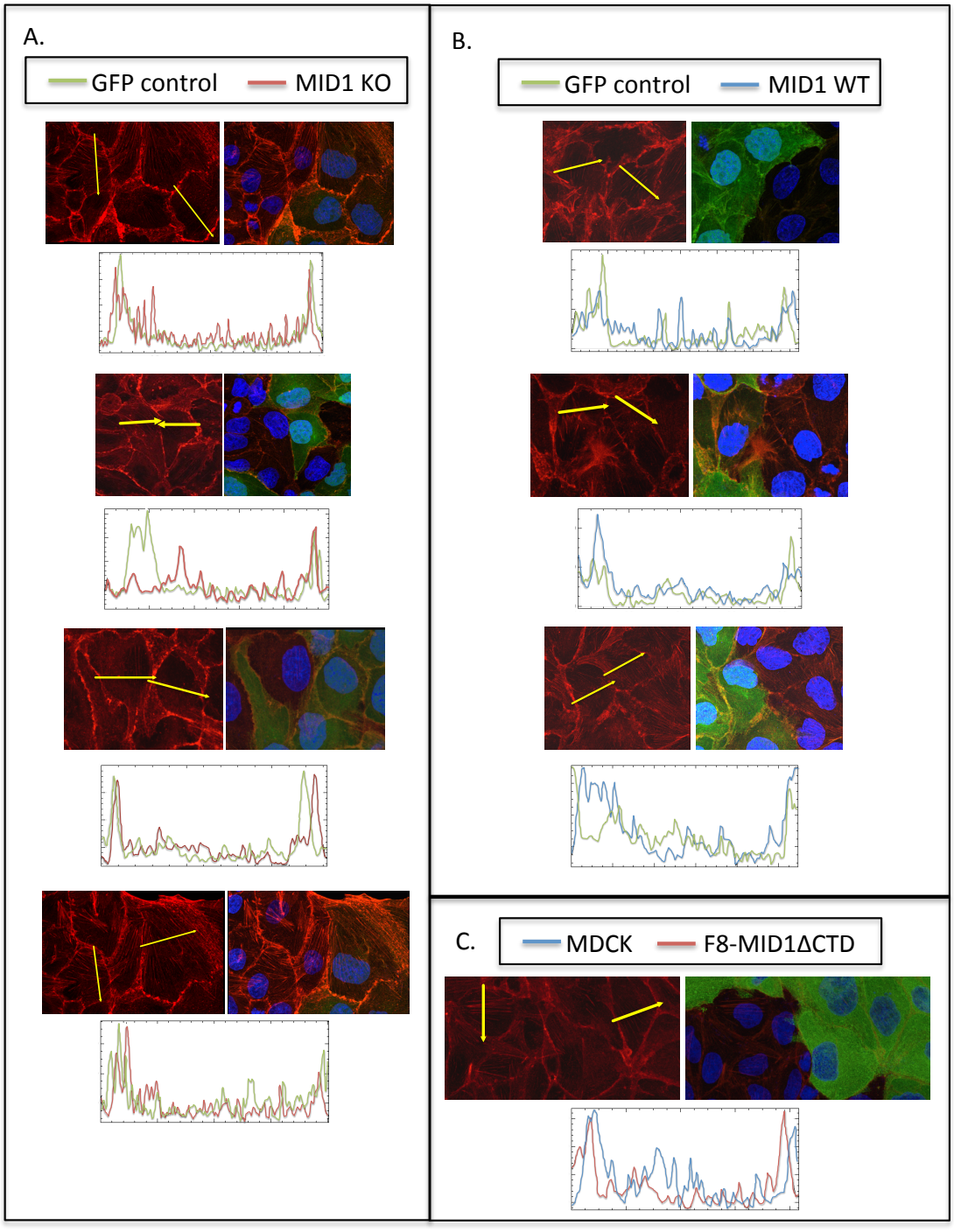


**Figure 4.4 Actin staining in non-polarized MID1 clones. A.** Relative to GFP control cells, actin staining of MID1 KO clones showed comparable pixel intensity along a line drawn orthogonal to fiber direction. **B.** Relative to GFP control cells, MID1 WT and MDCK cells also showed similar pixel intensity of actin staining. **C.** Mutant F8-MID1ΔCTD cells showed slightly higher pixel intensity of actin staining relative to MDCK control cells.

## Discussion

Knockout of MID1 in cell clones but transcripts persist

In this chapter, CRISPR/Cas9 technology was used to knockout MID1 in MDCK cells, and thereby, generate an *in vitro* model of X-linked Opitz syndrome, which is reflective of XLOS patients that have been identified with whole gene deletions of MID1 (Fontanella et al., 2008). By western blot, MID1 could not be detected in any of the MID1-134 CRISPR/Cas9 modified cell lines carrying an early termination codon. However, when quantifying MID1 transcript levels relative to controls by QPCR, there was no significant difference in MID1 transcript levels as compared to control cells. Although the rules governing how transcripts are identified and eliminated by nonsense mediated decay (NMD) mechanisms are not fully understood, in general, transcripts will be degraded by NMD if a stop codon is present at least 50 -54 nucleotides upstream of an exon-exon junction (Silva & Romão, 2009). Since MID1-134 CRISPR/Cas9 generated a frameshift mutation that leads to an early termination codon 292 base pairs from the exon-exon junction, it was expected that this transcript would be susceptible to degradation by NMD. However, MID1 knockouts and control lines had comparable levels of transcript.

A number of factors may account for the persistence of MID1 transcripts despite the introduction of a premature termination codon. Transcript levels of MID1 were less abundant than those of the housekeeping gene RPS5, thus small differences in transcript levels of MID1 would be less striking due to the high expression of RPS5 mRNA. Additionally, in MID1, multiple promoters, alternative splicing, and alternative translation have been found to regulate MID1 transcription

and translation (Winter et al., 2004). Importantly, some alternative splice variants of MID1 that introduce premature termination codons, both at the N-terminus and C-terminus, are not eliminated by nonsense mediated decay (Winter et al., 2004). Instead, transcripts, which include alternative start codons or splicing variants that introduce new poly (A+) 3' tails, are translated to produce truncated MID1 proteins (Winter et al., 2004). These mechanisms of MID1 regulation have been shown to be tissue specific and developmentally dependent (Landry & Mager, 2002; Winter et al., 2007). While transcript stability in MDCK cells has not yet been explored, MID1 transcriptional regulation has been shown to be conserved across species (Landry & Mager, 2002; Winter et al., 2007) and thus it is reasonable to assume that regulation of MID1 in MDCKs can be subject to transcriptional regulation through alternative promoter regions and alternative splicing, which may influence transcript survival.

Implications of non-degraded transcripts

With the persistence of MID1 transcript in our cell lines, it was important to consider that within the first coding exon of MID1, a second in-frame ATG codon exists at amino acid residue 111 that could potentially act as an alternative initiation codon. Should this transcript be translated, it would generate a N-terminally-truncated MID1 that might not be detected by our MID1 antibody since it would code for only 10 of the 50 amino acid residues used to generate the MID1 antibody. Yet another important consideration is the possibility that the mutant MID1 transcript is translated from its original initiation codon and produces a peptide with unknown consequences.

Phenotypic variability not dependent on genotype

Despite the unknown consequence of MID1 mutant transcript detected in our cell lines, preliminary characterization of our MID1 knockout clones was performed. In assays used to evaluate our cell clones, MID1 genotype did not correlate with phenotype. For example, despite the fact that all MID1 knockout clones possess the same mutation, their adhesion to laminin varied widely. This may be an indication that heterogeneity exists in the MDCK cell line itself and these differences become evident when clonal lines are generated. Work by Yongzhao Huang in the Cox lab supports this possibility. Huang also used MDCK cells to stably express GFP and MID1ΔCTD. In doing so, she found that cell clones varied in size and contributed to phenotypic variation (personal communication). As mentioned, we also cannot rule out that the heterogenity observed in our cell clones may reflect the MID1 transcript persistence and subsequent translation as well as unknown CRISPR/Cas9 off target effects.

Regardless of the heterogeneity of MDCK cells themselves and despite the persistence of MID1 transcript in our knockout clones, it would still be reasonable to expect that our MID1 clones would show increased levels of alpha4/PP2Ac relative to controls. Specifically expression of either a knockout MID1 cell line or an N-terminally truncated MID1, which is missing its critical E3 ubiquitin ligase RING domain, would still be able to bind alpha4/PP2Ac but would be predicted to lose its ability to ubiquitinate and target either of its substrates (alpha4 or PP2Ac) for degradation. However when alpha4 and PP2Ac levels were quantified by western blot, varying levels of alpha4 and PP2Ac were detected in controls and knockouts

with some clones showing similar levels of alpha4 and PP2Ac regardless of MID1 genotype. A number of explanations may account for these observations: 1.) MID1 is thought to regulate alpha4/PP2Ac at the microtubules, and any change to alpha4/PP2Ac levels in our MID1 knockouts might be obscured by the fact that the microtubule pool of alpha4/PP2Ac only accounts for a fraction of the total cellular levels of alpha4/PP2Ac. 2.) As mentioned previously, initial alpha4 quantification may reflect processing errors as evidenced by a weak β-actin band for sample 1.2 as well as no effect observed when comparing alpha4 levels in MID1ΔCTD controls A4 and F8 to D5-GFP controls. 3.) In addition, previous work that showed alpha4 levels increased in the presence of mutant MID1, did so using overexpressed, dominant-negative MID1ΔCTD. Because MID1 is a strong binding partner of alpha4, overexpression of MID1ΔCTD itself, may oversaturate alpha4 binding and possibly prevent its interaction with other regulators. This would ultimately lead to increased alpha4 levels. Unlike a protein overexpression model, this scenario does not occur with MID1 knockouts. 4.) Although previous work supported a hypothesis that PP2A activity increases in fibroblast from XLOS patient cells as a result of the inability of mutant MID1 to target PP2Ac for degradation (Trockenbacher et al., 2001), work by Du *et al*. indicates PP2Ac ubiquitination by MID1 actually decreases in the presence of alpha4. This suggests that MID1 mutations would result in increased levels of alpha4, but not necessarily PP2Ac. Moreover, it was suggested that increased levels of alpha4 could serve a protective role for PP2Ac (Du et al., 2014). 5.) Lastly, alpha4 and PP2Ac levels were quantified relative to β-actin, however, recent work by Huang and Cox shows that actin levels increase in cell lines

overexpressing dominant negative MID1ΔCTD (Huang and Cox, unpublished data), thus, should actin levels increase in MID1 knockouts, it would skew relative quantifications of alpha4 and PP2Ac to appear less than expected.

Conclusions and future work

In conclusion, CRISPR/Cas9 was successfully used to introduce a frameshift mutation in the first coding exon of MID1, which caused an early termination codon. Despite this, we saw persistent levels of MID1 transcript, indicating that this XLOS model requires further modification and characterization. Future work may identify multiple MID1 targets for CRISPR/Cas9 as well as targeting of CRISPR/Cas9 to the 5'UTR of MID1 and thereby decrease the likelihood of transcript survival. Alternatively, CRISPR/Cas9 could be used to generate MID1 mutations that have been identified in XLOS to study specific patient mutations. Additionally, initial phenotypic characterizations indicate that the MDCK cell lines may have heterogeneity that contributes to the differences in cellular responses. Future work could eliminate this possibility by generating and using a clonal line of MDCK as a starting point. Despite technical challenges faced in this chapter, this work highlights how a MID1 knockout model of XLOS may show subtle cellular changes that may be inaccurately portrayed by overexpression models of XLOS.

## Chapter 5: Conclusions

The broad goal of this thesis was to illuminate how MID1 mutations impact cell adhesion. To do so, protein interactions of the MID1 paralog and binding partner, MID2 were studied. Micropost technology was also utilized to measure cell forces in mutant MID1 cell lines. Lastly, to overcome some of the limitations of the existing *in vitro* model of XLOS, a MID1 knock out cell line using CRISPR/Cas9 technology was generated.

In Aim 1, MID2 binding partners, PLEKHA5 and PLEKHA7, were shown to connect the MID1/MID2 complex to regulators of cell-cell adhesion. Work presented here shows the emergence of a cellular role for MID2, which unlike MID1, was found to bind PLEKHA7, a close family member to the previously identified MID2 binding partner, PLEKHA5 (Zou, 2004). While PLEKHA7 has been linked to the regulation of cell-cell adhesion at apical adherens junctions (Meng et al., 2008) as well as the maturation of tight junctions (Kurita et al., 2013; Pulimeno et al., 2011), it was shown here that the largely uncharacterized protein PLEKHA5 also binds proteins involved in the regulation of cell-cell junctions. Through yeast-two hybrid assays PLEKHA5 was shown to interact with TP53BP2 and Siah2, both of which are linked to epithelial cell adhesion and turnover of cell junctions (Cong et al, 2012; Kim et al, 2013). Through immunoprecipitations of Myc-tagged PLEKHA5, it was found that p120 co-immunoprecipitates with this protein complex. Moreover, when immunoprecipitating either MID1 or MID2, p120 is also pulled down, which indicates that p120 is part of the MID1/MID2 protein complex. Significantly, p120

catenin is a well-characterized protein that is perhaps best known for its binding and stabilization of the cell-cell adhesion protein, E-cadherin (Yap, 1998). Additionally, it was confirmed that the RING and coiled-coil domain of MID2 were necessary for its interaction with PLEKHA5. These findings raise the possibility that these interactions may have regulatory consequences such as the targeting of MID2 E3 ubiquitin ligase activity or the guidance of PP2A phosphatase activity. These studies also showed that MID2 overexpression, like that of MID1 can decrease alpha4 levels *in vitro*. Thus, while the functional significance of these interactions remains undefined, this work suggests that MID1 mutations that impact its function and localization, but maintain its binding with MID2, will act in a dominant negative manner to disrupt MID2 interactions with PLEKHA5, PLEKHA7, and alpha4 (Figure 5.1).

In Aim 2, cell traction and cell tugging forces were measured in cells, overexpressing a dominant negative MID1 mutation, MID1ΔCTD. While cell adhesion to the laminin ECM at the micropost tips showed insignificant differences in traction force between mutant and control cells, MID1 mutant cells showed less tugging force than control cells at their cell-cell juctions. The decrease in tugging force by mutant cells was not a consequence of cell size, but rather the decrease in force resulted from shorter cell-cell junctions that were formed by mutant cells as compared to controls.

In Aim3, introduction of a premature stop codon in the first coding exon of MID1 produced MID1 knockout cell lines as measured by lack of MID1 by western

blot. However using RT-PCR, MID1 transcripts were detected in clones harboring premature stop codons, which were expected to be degraded by nonsense mediated decay mechanisms. Although the MID1 knockout cell lines all possessed the identical insertion mutation that resulted in a premature stop codon, they displayed different cellular pheonotypes. Variation between clones may be a reflection of CRISPR/Cas9 off target effects, differential transcriptional and translational regulation between cell clones, and/or indicate that heterogeneity exists within the cell line used to generate the clones. Thus future strategies should address some of these confounding results by generating a clonal population of cells prior to genetic modification. Additionally, designing and testing multiple gene targets for the CRISPR/Cas9 may help ensure that true knockouts exist at both the protein and transcript level.

Concluding remarks

The studies presented in this thesis provide insight into the molecular interactions that are affected by MID1 mutations, which ultimately give rise to the pathologies that define X-linked Opitz syndrome (XLOS). XLOS is caused by loss of MID1 function (Cox et al., 2000) and recent studies highlight that in epithelial cells, when MID1 function is lost, cells display aberrant cell adhesion (Huang and Cox, unpublished data; Suzuki et al., 2010), but how MID1 mutations lead to adhesion defects is unknown. In this thesis, cell adhesion forces are quantified in non-polarized MDCK epithelial cells to show that when MID1 function is disrupted, cells exert less force at their cell-cell junctions, not their cell-ECM junctions. When measuring cell-cell contact length using an antibody against β-catenin, which binds

the cytoplasmic domain of E-cadherin to mark cell-cell junctions, it was found that MID1 mutant cells formed shorter junctions. E-cadherin stability and adhesiveness is modulated by a number of factors in the cell such as phospho-regulation of its catenin binding partners (such as p120 and β-catenin), local regulation of the actin cytoskeleton, activation of signaling GTPases, and lateral clustering of E-cadherin, all of which to an extent are interdependent (Gumbiner, 2005; Nelson, 2008; Yap et al., 1998). While it is not yet known why MID1 loss of function resulted in shortened cell-cell junctions, it was found that MID1 as well as the MID1 binding partner, MID2, interact with proteins known to regulate the formation and stability of cell-cell junctions. Thus future work might be directed at exploring the MID effect on stability of these protein interactions, possibly through the role of MID1 as an E3 ubiquitin ligase or phosphorylation activity through MID1 association to the alpha4/PP2Ac complex. In summary, this thesis identifies that the MID1/MID2 protein complex includes regulators of cell-cell adhesion, and moreover, mutations in MID1 can impact the ability of cell-cell junctions to form and generate appropriate levels of cellular tugging force, a known mechanism by which cells can sense and respond to tension to drive processes such as morphogenesis.

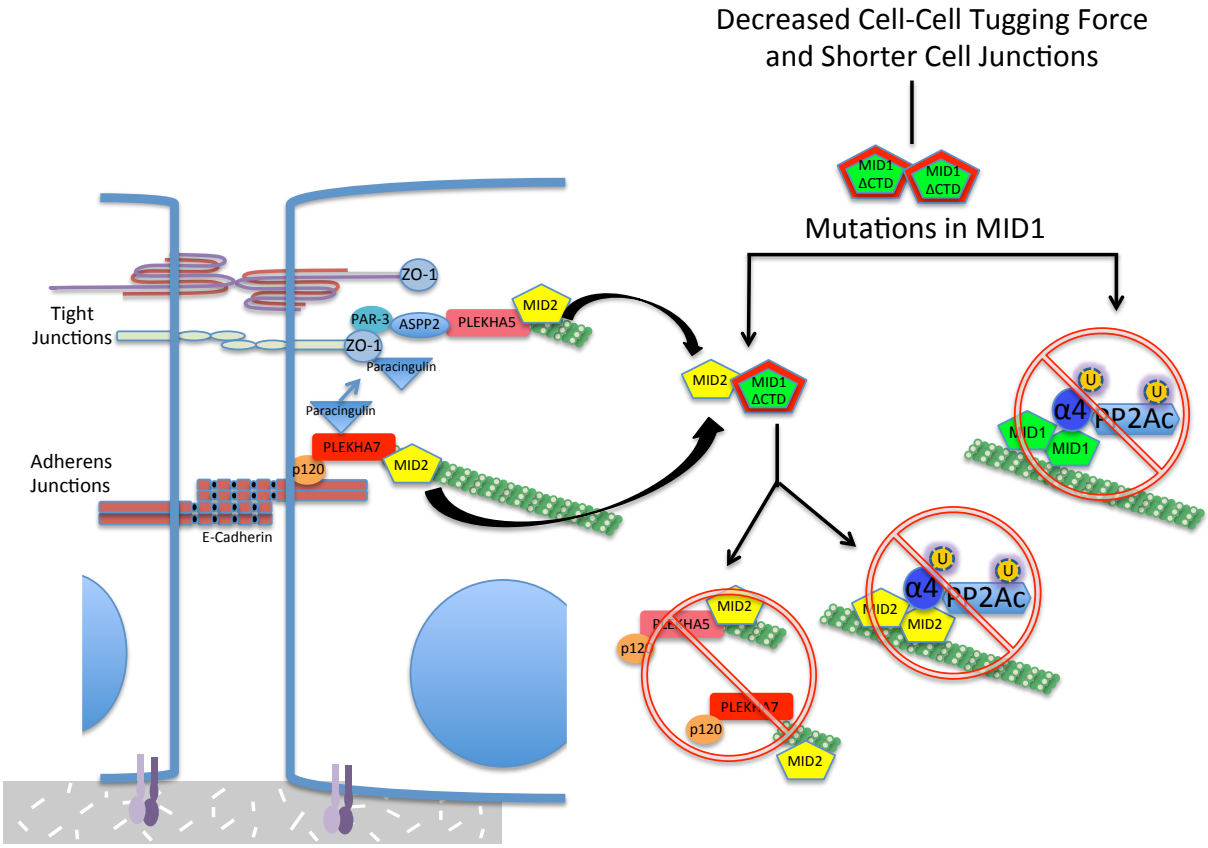


**Figure 5.1 Proposed Model for Contributions to Cell Adhesion Defects in XLOS**. Smaller cell-cell tugging force and shorter cell-cell junctions in MID1ΔCTD cells are influenced by MID2 interactions (PLEKHA5, PLEKHA7, p120 catenin, and alpha4/ PP2Ac) as well as the known role of MID1-alpha4 and PP2Ac complex.

## References


Berti, C., Fontanella, B., Ferrentino, R., & Meroni, G. (2004). Mig12, a novel Opitz syndrome gene product partner, is expressed in the embryonic ventral midline and co-operates with Mid1 to bundle and stabilize microtubules. *BMC Cell Biol*, *5*, 9. http://doi.org/10.1186/1471-2121-5-9

Boding, L., Hansen, A. K., Meroni, G., Johansen, B. B., Braunstein, T. H., Bonefeld, C. M., Geisler, C. (2014). Midline 1 directs lytic granule exocytosis and cytotoxicity of mouse killer T cells. *European Journal of Immunology*, *44*(10), 3109–3118. http://doi.org/10.1002/eji.201344388

Boding, L., Hansen, A. K., Meroni, G., Levring, T. B., Woetmann, A., Ødum, N., … Geisler, C. (2015). MID2 can substitute for MID1 and control exocytosis of lytic granules in cytotoxic T cells. *APMIS : Acta Pathologica, Microbiologica, et Immunologica Scandinavica*. http://doi.org/10.1111/apm.12402

Boding, L., Hansen, A. K., Nielsen, M. M., Meroni, G., Braunstein, T. H., Woetmann, A., … Geisler, C. (2014). Midline 1 controls polarization and migration of murine cytotoxic T cells. *Immunity, Inflammation and Disease*, *2*(4), 262–71. http://doi.org/10.1002/iid3.44

Buchner, G., Montini, E., Andolfi, G., Quaderi, N., Cainarca, S., Messali, S., … Franco, B. (1999). MID2, a homologue of the Opitz syndrome gene MID1: similarities in subcellular localization and differences in expression during development. *Hum Mol Genet*, *8*(8), 1397–1407. Retrieved from http://www.ncbi.nlm.nih.gov/pubmed/10400986

Cainarca, S., Messali, S., Ballabio, A., & Meroni, G. (1999). Functional characterization of the Opitz syndrome gene product (midin): Evidence for homodimerization and association with microtubules throughout the cell cycle. *Human Molecular Genetics*, *8*(8), 1387–1396. http://doi.org/10.1093/hmg/8.8.1387

Chen, C. S., Tan, J., & Tien, J. (2004). Mechanotransduction at cell-matrix and cell-cell contacts. *Annual Review of Biomedical Engineering*, *6*, 275–302. http://doi.org/10.1146/annurev.bioeng.6.040803.140040

Cox, T. C., Allen, L. R., Cox, L. L., Hopwood, B., Goodwin, B., Haan, E., & Suthers, G. K. (2000). New mutations in MID1 provide support for loss of function as the cause of X-linked Opitz syndrome. *Hum Mol Genet*, *9*(17), 2553–2562. Retrieved from http://www.ncbi.nlm.nih.gov/pubmed/11030761

De Falco, F., Cainarca, S., Andolfi, G., Ferrentino, R., Berti, C., Rodriguez Criado, G., … Meroni, G. (2003). X-linked Opitz syndrome: novel mutations in the MID1 gene and redefinition of the clinical spectrum. *Am J Med Genet A*, *120A*(2), 222–228. http://doi.org/10.1002/ajmg.a.10265

Du, H., Huang, Y., Zaghlula, M., Walters, E., Cox, T. C., & Massiah, M. A. (2013). The MID1 E3 ligase catalyzes the polyubiquitination of Alpha4 (alpha4), a regulatory subunit of protein phosphatase 2A (PP2A): novel insights into MID1-mediated regulation of PP2A. *J Biol Chem*, *288*(29), 21341–21350. http://doi.org/10.1074/jbc.M113.481093

Du, H., Huang, Y., Zaghlula, M., Walters, E., Cox, T. C., & Massiah, M. a. (2013). The MID1 E3 ligase catalyzes the polyubiquitination of alpha4 (α4), a regulatory subunit of protein phosphatase 2A (PP2A): Novel insights into MID1-mediated regulation of PP2A. *Journal of Biological Chemistry*, *288*(29), 21341–21350. http://doi.org/10.1074/jbc.M113.481093

Du, H., Wu, K., Didoronkute, A., Levy, M. V. a., Todi, N., Shchelokova, A., & Massiah, M. a. (2014). MID1 Catalyzes the Ubiquitination of Protein Phosphatase 2A and Mutations within Its Bbox1 Domain Disrupt Polyubiquitination of Alpha4 but Not of PP2Ac. *PLoS ONE*, *9*(9), e107428. http://doi.org/10.1371/journal.pone.0107428

Engler, A. J., Sen, S., Sweeney, H. L., & Discher, D. E. (2006). Matrix elasticity directs stem cell lineage specification. *Cell*, *126*(4), 677–89. http://doi.org/10.1016/j.cell.2006.06.044

Etienne-Manneville, S. (2014). Neighborly relations during collective migration. *Current Opinion in Cell Biology*, *30*(1), 51–59. http://doi.org/10.1016/j.ceb.2014.06.004

Eyckmans, J., Boudou, T., Yu, X., & Chen, C. S. (2011). A hitchhiker's guide to mechanobiology. *Dev Cell*, *21*(1), 35–47. http://doi.org/10.1016/j.devcel.2011.06.015

Farge, E. (2011). Mechanotransduction in Development. *Curr Top Dev Biol*, 95(8), (pp. 243–265).

Fontanella, B., Russolillo, G., & Meroni, G. (2008). MID1 mutations in patients with X-linked Opitz G/BBB syndrome. *Hum Mutat*, *29*(5), 584–594. http://doi.org/10.1002/humu.20706

Ganz, A., Lambert, M., Saez, A., Silberzan, P., Buguin, A., Mege, R. M., & Ladoux, B. (2006). Traction forces exerted through N-cadherin contacts. *Biol Cell*, *98*(12), 721–730. http://doi.org/10.1042/BC20060039

Gaudenz, K., Roessler, E., Quaderi, N., Franco, B., Feldman, G., Gasser, D. L., … Muenke, M. (1998). Opitz G/BBB syndrome in Xp22: mutations in the MID1 gene cluster in the carboxy-terminal domain. *Am J Hum Genet*, *63*(3), 703–710. Retrieved from http://www.ncbi.nlm.nih.gov/pubmed/9718340

Geetha, T. S., Michealraj, K. A., Kabra, M., Kaur, G., Juyal, R. C., & Thelma, B. K. (2014). Targeted Deep Resequencing Identifies MID2 Mutation for X-Linked Intellectual Disability with Varied Disease Severity in a Large Kindred from India. *Human Mutation*, *35*(1), 41–44. http://doi.org/10.1002/humu.22453

Geiger, B., Bershadsky, A., Pankov, R., Yamada, K. M., & Correspondence, B. G. (2001). Transmembrane extracellular matrix– cytoskeleton crosstalk. *Nature Reviews. Molecular Cell Biology*, *2*(November), 793–805. http://doi.org/10.1038/35099066

Gomez, G. a., McLachlan, R. W., & Yap, A. S. (2011). Productive tension: Force-sensing and homeostasis of cell-cell junctions. *Trends in Cell Biology*, *21*(9), 499–505. http://doi.org/10.1016/j.tcb.2011.05.006

Goody, M. F., & Henry, C. a. (2010). Dynamic interactions between cells and their extracellular matrix mediate embryonic development. *Molecular Reproduction and Development*, *77*(6), 475–488. http://doi.org/10.1002/mrd.21157

Granata, A., & Quaderi, N. A. (2003). The Opitz syndrome gene MID1 is essential for establishing asymmetric gene expression in Hensen's node. *Dev Biol*, *258*(2), 397–405. Retrieved from http://www.ncbi.nlm.nih.gov/pubmed/12798296

Granata, A., Savery, D., Hazan, J., Cheung, B. M. F., Lumsden, A., & Quaderi, N. a. (2005). Evidence of functional redundancy between MID proteins: Implications for the presentation of Opitz syndrome. *Developmental Biology*, *277*(2), 417–424. http://doi.org/10.1016/j.ydbio.2004.09.036

Gumbiner, B. M. (2005). Regulation of cadherin-mediated adhesion in morphogenesis. *Nature Reviews. Molecular Cell Biology*, *6*(8), 622–634. http://doi.org/10.1038/nrm1699

Han, S. J., Bielawski, K. S., Ting, L. H., Rodriguez, M. L., & Sniadecki, N. J. (2012). Decoupling substrate stiffness, spread area, and micropost density: a close spatial relationship between traction forces and focal adhesions. *Biophys J*, *103*(4), 640–648. http://doi.org/10.1016/j.bpj.2012.07.023

Han, X., Du, H., & Massiah, M. A. (2011). Detection and characterization of the in vitro e3 ligase activity of the human MID1 protein. *J Mol Biol*, *407*(4), 505–520. http://doi.org/10.1016/j.jmb.2011.01.048

Heigwer, F., Kerr, G., & Boutros, M. (2014). E-CRISP: fast CRISPR target site identification. *Nature Methods*, *11*(2), 122–123. http://doi.org/10.1038/nmeth.2812

Hoffman, B. D., Grashoff, C., & Schwartz, M. A. (2011). Dynamic molecular processes mediate cellular mechanotransduction. *Nature*, *475*(7356), 316–323. http://doi.org/10.1038/nature10316

House, C.M., Frew, I.J., Huang, H., Wiche, G., Traficante, N., Nice, E., Catimel, B., & Bowtell, D.D.L. (2003). A binding motif for Siah ubiquitin ligase. *PNAS,* 100(6), 3101-3106.

Huang Cox T.C., Y. (n.d.). The function of MID1 in regulation of epitehlial cell adhesion. Implications in craniofacial morphogenesis.

Jilaveanu, L. B., Parisi, F., Barr, M. L., Zito, C. R., Cruz-Munoz, W., Kerbel, R. S., … Kluger, H. M. (2014). PLEKHA5 as a Biomarker and Potential Mediator of Melanoma Brain Metastasis. *Clinical Cancer Research*, *21*(9), 2138–2147. http://doi.org/10.1158/1078-0432.CCR-14-0861

Jinek, M., Chylinski, K., Fonfara, I., Hauer, M., Doudna, J. A., & Charpentier, E. (2012). A Programmable Dual-RNA-Guided DNA Endonuclease in Adaptive Bacterial Immunity. *Science*. http://doi.org/10.1126/science.1225829

Keil, R., Schulz, J., & Hatzfeld, M. (2013). P0071/PKP4, a multifunctional protein coordinating cell adhesion with cytoskeletal organization. *Biological Chemistry*, *394*(8), 1005–1017. http://doi.org/10.1515/hsz-2013-0114

Kim, H., Claps, G., Möller, a, Bowtell, D., Lu, X., & Ronai, Z. a. (2013). Siah2 regulates tight junction integrity and cell polarity through control of ASPP2 stability. *Oncogene*, (January), 1–7. http://doi.org/10.1038/onc.2013.149

Krämer, O. H., Stauber, R. H., Bug, G., Hartkamp, J., & Knauer, S. K. (2012). SIAH proteins: Critical roles in leukemogenesis. *Leukemia*, (October 2012), 792–802. http://doi.org/10.1038/leu.2012.284

Kruszka, P., Li, D., Harr, M. H., Wilson, N. R., Swarr, D., Elizabeth, M., … Donna, M. (2015). Mutations in SPECC1L, encoding sperm antigen with calponin homology and coiled-coil domains 1-like, are found in some cases of autosomal Opitz G/BBB syndrome, *52*(2), 104–110. http://doi.org/10.1136/jmedgenet-2014-102677.Mutations

Kurita, S., Yamada, T., Rikitsu, E., Ikeda, W., & Takai, Y. (2013). Binding between the Junctional Proteins Afadin and PLEKHA7 and Implication in the Formation of Adherens Junction in Epithelial Cells. *J Biol Chem*, *288*(41), 29356–29368. http://doi.org/10.1074/jbc.M113.453464

Ladoux, B., Anon, E., Lambert, M., Rabodzey, A., Hersen, P., Buguin, A., … Mège, R. M. (2010). Strength dependence of cadherin-mediated adhesions. *Biophysical Journal*, *98*(4), 534–542. http://doi.org/10.1016/j.bpj.2009.10.044

Lander, E.S., Linton, L.M., Birren, B., Nusbaum, C., Zody M.C., & Baldwin J. (2001). Initial sequencing and analysis of the human genome. *Nature,* 409, 860-921.

Landry, J. R., & Mager, D. L. (2002). Widely spaced alternative promoters, conserved between human and rodent, control expression of the opitz syndrome gene MID1. *Genomics*, *80*(5), 499–508. http://doi.org/10.1016/S0888-7543(02)96863-1

Le Duc, Q., Shi, Q., Blonk, I., Sonnenberg, A., Wang, N., Leckband, D., & de Rooij, J. (2010). Vinculin potentiates E-cadherin mechanosensing and is recruited to actin-anchored sites within adherens junctions in a myosin II-dependent manner. *J Cell Biol*, *189*(7), 1107–1115. http://doi.org/10.1083/jcb.201001149

Leckband, D. E., le Duc, Q., Wang, N., & de Rooij, J. (2011). Mechanotransduction at cadherin-mediated adhesions. *Current Opinion in Cell Biology*, *23*(5), 523–530. http://doi.org/10.1016/j.ceb.2011.08.003

Lemmon, M. A., Ferguson, K. M., & Abrams, C. S. (2002). Pleckstrin homology domains and the cytoskeleton. *FEBS Lett*, *513*(1), 71–76. Retrieved from http://www.ncbi.nlm.nih.gov/pubmed/11911883

Liu, E., Knutzen, C. A., Krauss, S., Schweiger, S., & Chiang, G. G. (2011). Control of mTORC1 signaling by the Opitz syndrome protein MID1. *Proc Natl Acad Sci U S A*, *108*(21), 8680–8685. http://doi.org/10.1073/pnas.1100131108

Liu, J., Prickett, T. D., Elliott, E., Meroni, G., & Brautigan, D. L. (2001). Phosphorylation and microtubule association of the Opitz syndrome protein mid-1 is regulated by protein phosphatase 2A via binding to the regulatory subunit alpha 4. *Proc Natl Acad Sci U S A*, *98*(12), 6650–6655. http://doi.org/10.1073/pnas.111154698

Liu, Z., Tan, J. L., Cohen, D. M., Yang, M. T., Sniadecki, N. J., Ruiz, S. A., … Chen, C. S. (2010). Mechanical tugging force regulates the size of cell-cell junctions. *Proc Natl Acad Sci U S A*, *107*(22), 9944–9949. http://doi.org/10.1073/pnas.0914547107

Livak, K. J., & Schmittgen, T. D. (2001). Analysis of relative gene expression data using real-time quantitative PCR and the 2(-Delta Delta C(T)) Method. *Methods (San Diego, Calif.)*, *25*(4), 402–408. http://doi.org/10.1006/meth.2001.1262

Maruthamuthu, V., Sabass, B., Schwarz, U. S., & Gardel, M. L. (2011). Cell-ECM traction force modulates endogenous tension at cell-cell contacts. *Proc Natl Acad Sci U S A*, *108*(12), 4708–4713. http://doi.org/10.1073/pnas.1011123108

McBeath, R., Pirone, D. M., Nelson, C. M., Bhadriraju, K., & Chen, C. S. (2004). Cell Shape, Cytoskeletal Tension, and RhoA Regulate Stem Cell Lineage

Commitment. *Developmental Cell*, *6*(4), 483–495. http://doi.org/10.1016/S1534-5807(04)00075-9

Meng, W., Mushika, Y., Ichii, T., & Takeichi, M. (2008). Anchorage of microtubule minus ends to adherens junctions regulates epithelial cell-cell contacts. *Cell*, *135*(5), 948–959. http://doi.org/10.1016/j.cell.2008.09.040

Meroni, G. (2004). X-linked Opitz G/BBB Syndrome. In: *GeneReviews* at GeneTests Medical Genetics Information Resource (database online). Copyright, University of Washington, Seattle. 1997-2013. Available at http://www.genetests.org.

Migliore, C., Athanasakis, E., Dahoun, S., Wonkam, A., Lees, M., Calabrese, O., … Meroni, G. (2013). Complex rearrangement of the exon 6 genomic region among Opitz G/BBB Syndrome MID1 alterations. *European Journal of Medical Genetics*, *56*(8), 404–410. http://doi.org/10.1016/j.ejmg.2013.05.009

Nabokina, S. M., Subramanian, V. S., & Said, H. M. (2011). Association of PDZ-containing protein PDZD11 with the human sodium-dependent multivitamin transporter. *American Journal of Physiology. Gastrointestinal and Liver Physiology*, *300*(4), G561–G567. http://doi.org/10.1152/ajpgi.00530.2010

Nelson, W. J. (2008). Regulation of cell-cell adhesion by the cadherin-catenin complex. *Biochem Soc Trans*, *36*(Pt 2), 149–155. http://doi.org/10.1042/BST0360149

O'Brien, L. E., Jou, T. S., Pollack, a L., Zhang, Q., Hansen, S. H., Yurchenco, P., & Mostov, K. E. (2001). Rac1 orientates epithelial apical polarity through effects on basolateral laminin assembly. *Nature Cell Biology*, *3*(9), 831–838. http://doi.org/10.1038/ncb0901-831

Pacheco-Alvarez, D., Solórzano-Vargas, R. S., & Del Río, A. L. (2002). Biotin in metabolism and its relationship to human disease. *Archives of Medical Research*, *33*(5), 439–447. http://doi.org/10.1016/S0188-4409(02)00399-5

Perry, J., Short, K. M., Romer, J. T., Swift, S., Cox, T. C., & Ashworth, A. (1999). FXY2/MID2, a gene related to the X-linked Opitz syndrome gene FXY/MID1, maps to Xq22 and encodes a FNIII domain-containing protein that associates with microtubules. *Genomics*, *62*(3), 385–394. http://doi.org/10.1006/geno.1999.6043

Pinson, L., Auge, J., Audollent, S., Mattei, G., Etchevers, H., Gigarel, N., Razavi, F., Lacombe, D., Odent, S., Merrer, M.L., Amiel, J., Munnich, A., Meroni, G., Lyonnet, S., Vekemans, M., & Attie-Bitach, T (2004). Embryonic expression of the human MID1 gene and its mutations in Opitz syndrome. Journal of Medical Genetics, 41, 381-386.

Plestant, C., Strale, P.-O., Seddiki, R., Nguyen, E., Ladoux, B., & Mège, R.-M. (2014). Adhesive interactions of N-cadherin limit the recruitment of microtubules to cell-cell contacts through organization of actomyosin. *Journal of Cell Science*, *127*(Pt 8), 1660–71. http://doi.org/10.1242/jcs.131284

Pulimeno, P., Paschoud, S., & Citi, S. (2011). A role for ZO-1 and PLEKHA7 in recruiting paracingulin to tight and adherens junctions of epithelial cells. *J Biol Chem*, *286*(19), 16743–16750. http://doi.org/10.1074/jbc.M111.230862

Qi, J., Kim, H., Scortegagna, M., & Ronai, Z. (2013). Regulators and Effectors of Siah Ubiquitin Ligases. *Cell Biochemistry and Biophysics*, *67*(1), 15–24. http://doi.org/10.1007/s12013-013-9636-2

Quaderi, N. A., Schweiger, S., Gaudenz, K., Franco, B., Rugarli, E. I., Berger, W., … Ballabio, A. (1997). Opitz G/BBB syndrome, a defect of midline development, is due to mutations in a new RING finger gene on Xp22. *Nat Genet*, *17*(3), 285–291. http://doi.org/10.1038/ng1197-285

Ran, F. A., Hsu, P. D., Wright, J., Agarwala, V., Scott, D. A., & Zhang, F. (2013). Genome engineering using the CRISPR-Cas9 system. *Nat. Protocols*, *8*(11), 2281–2308. http://doi.org/10.1038/nprot.2013.143\rhttp://www.nature.com/nprot/journal/v8/n11/abs/nprot.2013.143.html#supplementary-information

Robin, N. H., Feldman, G. J., Aronson, A. L., Mitchell, H. F., Weksberg, R., Leonard, C. O., … Muenke, M. (1995). Opitz syndrome is genetically heterogeneous, with one locus on Xp22, and a second locus on 22q11.2. *Nat Genet*, *11*(4), 459–461. Retrieved from http://dx.doi.org/10.1038/ng1295-459

Rodríguez-Fraticelli, A. E., Auzan, M., Alonso, M. a., Bornens, M., & Martín-Belmonte, F. (2012). Cell confinement controls centrosome positioning and lumen initiation during epithelial morphogenesis. *Journal of Cell Biology*, *198*(6), 1011–1023. http://doi.org/10.1083/jcb.201203075

Rodríguez-Fraticelli, A. E., & Martín-Belmonte, F. (2013). Mechanical control of epithelial lumen formation. *Small GTPases*, *4*(2), 136–40. http://doi.org/10.4161/sgtp.24303

Saadi, I., Fowzan, S. A., Stephen, S. G., Goessling, W., Cavallesco, R., Turbe-Doan, A., … Maas, R. L. (2011). Deficiency of the cytoskeletal protein SPECC1L leads to oblique facial clefting. *American Journal of Human Genetics*, *89*(1), 44–55. http://doi.org/10.1016/j.ajhg.2011.05.023

Scheffzek, K., & Welti S. (2012). Pleckstrin homology (PH) like domains-versatile modules in protein-protein interaction platforms. *FEBS Lett* 586(17), 2662-2673.

Schwartz, M. a., & DeSimone, D. W. (2008). Cell adhesion receptors in mechanotransduction. *Current Opinion in Cell Biology*, *20*(5), 551–556. http://doi.org/10.1016/j.ceb.2008.05.005

Schweiger, S., Foerster, J., Lehmann, T., Suckow, V., Muller, Y. A., Walter, G., … Ropers, H. H. (1999). The Opitz syndrome gene product, MID1, associates with microtubules. *Proc Natl Acad Sci U S A*, *96*(6), 2794–2799. Retrieved from http://www.ncbi.nlm.nih.gov/pubmed/10077590

Schweiger, S., & Schneider, R. (2003). The MID1/PP2A complex: A key to the pathogenesis of Opitz BBB/G syndrome. *BioEssays*, *25*(4), 356–366. http://doi.org/10.1002/bies.10256

Short, K. M., & Cox, T. C. (2006). Subclassification of the RBCC/TRIM superfamily reveals a novel motif necessary for microtubule binding. *J Biol Chem*, *281*(13), 8970–8980. http://doi.org/10.1074/jbc.M512755200

Short, K. M., Hopwood, B., Yi, Z., & Cox, T. C. (2002). MID1 and MID2 homo- and heterodimerise to tether the rapamycin-sensitive PP2A regulatory subunit, alpha 4, to microtubules: implications for the clinical variability of X-linked Opitz GBBB syndrome and other developmental disorders. *BMC Cell Biol*, *3*, 1. Retrieved from http://www.ncbi.nlm.nih.gov/pubmed/11806752

Silva, A. L., & Romão, L. (2009). The mammalian nonsense-mediated mRNA decay pathway: To decay or not to decay! Which players make the decision? *FEBS Letters*, *583*(3), 499–505. http://doi.org/10.1016/j.febslet.2008.12.058

Smutny, M., & Yap, A. S. (2010). Neighborly relations: cadherins and mechanotransduction. *J Cell Biol*, *189*(7), 1075–1077. http://doi.org/10.1083/jcb.201005151

So, J., Suckow, V., Kijas, Z., Kalscheuer, V., Moser, B., Winter, J., … Schweiger, S. (2005). Mild phenotypes in a series of patients with Opitz GBBB syndrome with MID1 mutations. *Am J Med Genet A*, *132A*(1), 1–7. http://doi.org/10.1002/ajmg.a.30407

Suzuki, M., Hara, Y., Takagi, C., Yamamoto, T. S., & Ueno, N. (2010). MID1 and MID2 are required for Xenopus neural tube closure through the regulation of microtubule organization. *Development*, *137*(14), 2329–2339. http://doi.org/10.1242/dev.048769

Tan, J. L., Tien, J., Pirone, D. M., Gray, D. S., Bhadriraju, K., & Chen, C. S. (2003). Cells lying on a bed of microneedles: an approach to isolate mechanical force. *Proc*

*Natl Acad Sci U S A*, *100*(4), 1484–1489. http://doi.org/10.1073/pnas.0235407100

Trockenbacher, A., Suckow, V., Foerster, J., Winter, J., Krauss, S., Ropers, H. H., … Schweiger, S. (2001). MID1, mutated in Opitz syndrome, encodes an ubiquitin ligase that targets phosphatase 2A for degradation. *Nat Genet*, *29*(3), 287–294. http://doi.org/10.1038/ng762

Watkins, G. R., Wang, N., Mazalouskas, M. D., Gomez, R. J., Guthrie, C. R., Kraemer, B. C., … Wadzinski, B. E. (2012). Monoubiquitination promotes calpain cleavage of the protein phosphatase 2A (PP2A) regulatory subunit alpha4, altering PP2A stability and microtubule-associated protein phosphorylation. *J Biol Chem*, *287*(29), 24207–24215. http://doi.org/10.1074/jbc.M112.368613

Winter, J., Kunath, M., Roepcke, S., Krause, S., Schneider, R., & Schweiger, S. (2007). Alternative polyadenylation signals and promoters act in concert to control tissue-specific expression of the Opitz Syndrome gene MID1. *BMC Molecular Biology*, *8*, 105. http://doi.org/10.1186/1471-2199-8-105

Winter, J., Lehmann, T., Krauß, S., Trockenbacher, A., Kijas, Z., Foerster, J., … Schweiger, S. (2004). Regulation of the MID1 protein function is fine-tuned by a complex pattern of alternative splicing. *Human Genetics*, *114*(6), 541–552. http://doi.org/10.1007/s00439-004-1114-x

Yap, A. S., Niessen, C. M., & Gumbiner, B. M. (1998). The juxtamembrane region of the cadherin cytoplasmic tail supports lateral clustering, adhesive strengthening, and interaction with p120ctn. *J Cell Biol*, *141*(3), 779–789. Retrieved from http://www.ncbi.nlm.nih.gov/pubmed/9566976

Yonemura, S., Wada, Y., Watanabe, T., Nagafuchi, A., & Shibata, M. (2010). alpha-Catenin as a tension transducer that induces adherens junction development. *Nat Cell Biol*, *12*(6), 533–542. http://doi.org/10.1038/ncb2055

Yu, W., Datta, A., Leroy, P., O'Brien, L. E., Mak, G., Jou, T.-S., … Zegers, M. M. P. (2005). Beta1-integrin orients epithelial polarity via Rac1 and laminin. *Molecular Biology of the Cell*, *16*(2), 433–445. http://doi.org/10.1091/mbc.E04-05-0435

Zou, Y. (2004). Investigation into the cellular function of Opitz Syndrome gene MID1 and its homologue MID2. *University of Adelaide, Graduate Thesis, Cox Lab*.